# Evolution of Mutation Rates in Asexual Populations

A Thesis

Submitted for the Degree of

DOCTOR OF PHILOSOPHY

IN THE FACULTY OF SCIENCE

by

ANANTHU JAMES


THEORETICAL SCIENCES UNIT
JAWAHARLAL NEHRU CENTRE FOR ADVANCED SCIENTIFIC RESEARCH
(A Deemed University)
Bangalore – 560 064

July 2017

*To The Living World*

# DECLARATION

I hereby declare that the matter embodied in the thesis entitled "**Evolution of Mutation Rates in Asexual Populations**" is the result of investigations carried out by me at the Theoretical Sciences Unit, Jawaharlal Nehru Centre for Advanced Scientific Research, Bangalore, India under the supervision of **Prof. Kavita Jain**, and that it has not been submitted elsewhere for the award of any degree or diploma.

In keeping with the general practice in reporting scientific observations, due acknowledgement has been made whenever the work described is based on the findings of other investigators.

**Ananthu James**

# CERTIFICATE

I hereby certify that the matter embodied in this thesis entitled "**Evolution of Mutation Rates in Asexual Populations**" has been carried out by **Mr. Ananthu James** at the Theoretical Sciences Unit, Jawaharlal Nehru Centre for Advanced Scientific Research, Bangalore, India under my supervision and that it has not been submitted elsewhere for the award of any degree or diploma.

**Prof. Kavita Jain**
( Research Supervisor)

# Acknowledgements

First of all, I express my gratitude to my Ph. D. advisor Prof. Kavita Jain for her support throughout my academic life as a Ph. D. student. I am really grateful to her for giving me enough freedom to explore and learn things the way I wanted and letting me publish a single author paper, which resulted in improving my confidence substantially.

I got benefited a lot by attending various schools, conferences, and seminars at institutes like IISc, ICTS and NCBS in Bangalore. Apart from that, I am happy for getting the opportunity to participate in PopGroup49, held in Edinburgh.

I would like to thank Council of Scientific and Industrial Research (CSIR) for the funding during my first five years of Ph. D. life.

I remember the quote "Nothing in biology makes sense except in the light of evolution" by Theodosius Dobzhansky in one of my Biology textbooks in school. The concept of biological evolution as well as the mathematical aspects of genetics have been fascinating to me since my school days. I am fortunate to have come across the theory of evolution in my school curriculum.

As an undergraduate student in Physics, I got the opportunity to do summer research as part of the Kishore Vaigyanik Protsahan Yojana (KVPY) fellowship. This was a turning point in my life which made me realize that research is actually very much enjoyable. Moreover, I acknowledge Prof. Vincent Mathew who would encourage me during my undergraduate days and with whom and I did two projects.

At JNCASR, I have spent more than five years as a Ph. D. student. I thank my institute for providing all the necessary facilities and funds. I acknowledge Prof. Amitabh Joshi, Prof. Shobhana Narasimhan, Prof. Subir K. Das, Prof. Swapan K. Pati, Prof. Umesh V.

Waghmare, Prof. Vidhyadhiraja N. S., Dr. T. N. C. Vidya, Prof. Srikanth Sastry, Dr. Meher K. Prakash, and Prof. Meheboob Alam for the courses they have offered and the interactions with them. I also thank Dr. Mukund Thattai from NCBS who was the external examiner of my comprehensive viva.

I acknowledge my labmates Sarada, Priyanka, Sona, Jyoti, Tanmoy, and Archana for their help and support. I am deeply thankful to Priyanka and Sona for their help in various academic and non-academic things. I was part of various committees in JNC. I thank all the committee members who worked with me. I express my special thanks to the cultural forum Dhwani, in which I worked for more than two years screening documentaries on topics such as society, politics, history, science etc. Playing and watching football, photography, and most importantly, trekking have been my hobbies during my Ph. D. life. I went trekking to many places in South India, mainly Western Ghats, with Bangalore Mountaineering Club (BMC). I extend my gratitude to Nikhil, Sonia, and Kanchan for organizing some trips and treks from JNC. Moreover, I am thankful to those who used to play football and (rarely) badminton with me. Further, I thank my batchmates and friends Anjali, Chakri, Meha, Sharmila, and Vinay with whom I used to spend my time during the first one or two years, especially during the coursework. I extend my thanks to Nandu for the intellectual conversations and Vybhav for the inspiring discussions about the history of science.

I am greatly indebted to Jyoti for her motivation and support, who joined my lab four years after me. The interactions with her helped me to understand her research area, coalescent theory. Apart from her, I am very much happy to have a cousin, whom I call Monu, who would always encourage me for anything creative and rebellious and accompanied me on so many trips. In addition, I am glad to have spent two years at IIT Madras, where I met my friends Siddharth and Varghese whom I appreciate for their positive mentality and never-say-die attitude.

I am pleased to have a family which is relatively liberal and rational for the society they live in. I am thankful to them for motivating me to pursue basic science instead of professional courses. I also recall that it was my mother who insisted me to apply to institutes in

India for Ph. D. when I was only interested in doing a Ph. D. from abroad. I also thank my brother for all sorts of discussions varying from academics to football and philosophy.

I do appreciate the help and support I received from all the academic and non-academic staff in JNC including the hostel staff, Dhanvantri staff, library staff, and canteen staff. Finally, I thank Rajesh Ranjan from Engineering Mechanics Unit for help with the thesis template in the current format, without whom the thesis writing would have been much harder.

# Synopsis

The living world exists in the present form because of the evolutionary processes that have been going on since the origin of life on earth. Mutations that are random changes in the genetic material of a cell or an organism are one of the main drivers of the evolutionary process. Mutations are classified as beneficial, deleterious, or neutral, respectively depending on whether they increase, decrease, or do not alter the reproductive ability or fitness of an organism. Early studies on the mutation rates led to the important conclusion that like many other traits, the mutation rate is also subject to evolution [1]. Since then, there have been various experimental as well as theoretical studies on the evolution of mutation rates [2, 3].

These studies suggest that in adapting populations, mutators (the alleles or individuals with higher mutation rates than the wild type) are favored [4, 3]. Although there are experimental evidences [5, 6] indicating that the lower mutation rate increases in frequency in adapted mutator populations, this phenomenon has been very less theoretically explored [7, 3]. Our aim in this thesis is to fill this gap and gain an insight into the process of reduction of the mutation rate. The thesis is divided into five chapters. The details of each chapter are given below.

In Chapter 1, we first provide an introduction to the evolutionary forces viz., selection, mutation, and random genetic drift in our study. The class of fitness landscapes used are single-peaked in which magnitude epistasis can be tuned [8]. We also describe the Wright-Fisher process to deal with finite populations and discuss the branching process formalism [9] to understand the chances of fixation of a beneficial allele in a large population.

In Chapter 2, we study the role of selection and random genetic drift in the evolution of mutation rates [10]. Using a multitype branching process, we first derive analytical expressions for the fixation probability of a rare nonmutator in a large mutator population when the fitness landscape is non-epistatic. Throughout this analysis, we assume that the

mutator is strong i.e., its mutation rate is much larger than that of the nonmutator. Using a drift-barrier argument [11, 7], we show that the minimum mutation rate is inversely proportional to the population size when selection is strong [7] but decays much faster when selection is weak [10]. We also discuss how our results relate to the experimental observations of [6].

In Chapter 3, we consider a more general scenario of the case studied in Chapter 2 [12]. Here, we analytically calculate the fixation probability of a rare nonmutator when the mutation rate of the nonmutator can be comparable to that of the mutator. Our analytical expressions reveal that the fixation probability can be a decreasing or increasing function of the background mutation rate depending on the strength of selection and mutation rate of the nonmutator. In fact, the decreasing trend is counterintuitive and it is discussed in detail.

In Chapter 4, we examine the role of the epistatic fitness interactions on the fixation of a nonmutator in an adapted mutator background [13]. We find that the fixation probability increases with the interaction strength and a critical value of the epistasis parameter exists beyond which the fixation probability is a nonmonotonic function of the mutation rate of the mutator population.

Finally, in Chapter 5, we summarize our results and discuss some open questions.

# List of publications

- *Fixation probability of rare nonmutator and evolution of mutation rates,* Ananthu James and Kavita Jain, ***Ecol. Evol.*** 6, 755–764 (2016).
- *Role of epistasis on the fixation probability of a non-mutator in an adapted asexual population*, Ananthu James, ***J. Theor. Biol.*** 407, 225–237 (2016).
- *Fixation probability of a nonmutator in a large population of asexual mutators,* Kavita Jain and Ananthu James, ***arXiv:1705.00153***.

# Table of contents

# List of figures

# Chapter 1

# Introduction

## 1.1 Theoretical population genetics and modeling evolution

The term "evolution" in the context of biology refers to the collective changes in the features of a population over a period of time [15]. Population genetics provides a framework to understand the processes and mechanisms by which evolutionary changes occur [16]. The main goal of theoretical population genetics is to gain an insight into how the interactions between the forces of mutation, natural selection, random genetic drift, and population structure result in the variations amongst the individuals of a population by formulating the problem into a workable mathematical model [17]. Since the inclusion of all the complexities that are part of the actual biological systems is not possible in a mathematical model, simplifications, which do not significantly alter the details of the real system, but using which a further mathematical progress can be achieved, are required.

In this thesis, the evolutionary forces are considered to be not changing with time. Moreover, we model mutation and selection as simple processes [17, 18], though in reality, more complex scenarios are possible for the mutation rate of an organism as well as the selection acting on it. It will be seen in the subsequent Chapters that despite the simplifications in our models, we encounter mathematically challenging problems. However, a mathematical approach is very helpful in obtaining quantitative predictions as well as a deep understanding of the mechanism behind the evolutionary processes [19]. The two sentences

taken from the classic book [20] by R. A. Fisher emphasize the importance of developing a mathematical framework in evolution: "I believe no one will be surprised that a large number of the points considered (here) demand a far fuller, more rigorous, and more comprehensive treatment. It seems impossible that full justice should be done to the field in this way, until there is built up a tradition of mathematical work devoted to biological problems, comparable to the researches upon which a mathematical physicist can draw in the resolution of special difficulties.". A survey conducted by Otto and Day [19] demonstrates that the use of mathematical models is becoming extensively common in the articles published in biological journals. This Chapter is dedicated to describing the way we model the action of the various evolutionary forces.

## 1.2 Evolutionary forces

The major evolutionary forces that are encountered in our study are discussed in this Section. In addition to that, we describe how they are being modeled.

### 1.2.1 Natural selection

The genetic sequence or genome of an organism stores all the heritable information. In our study, we consider haploid asexual individuals and model the genome using a binary sequence of length $L$, corresponding to which $2^L$ combinations are possible. If we assume that each site in the sequence represents a base pair, the minimum length of the sequence could be few thousands of base pairs, based on the data from natural populations [21, 22]. The resulting number of sequences exceeds $10^{300}$. In order to avoid the complexities in dealing with such astronomically large numbers, we make rather simple assumptions, that are given below, using which we can proceed further.

The fitness of an individual denotes its survival ability in a specific environment. In our model, fitness is assumed to be proportional to the probability of reproduction. The representation of the fitness values corresponding to all the possible genetic sequences is known as a fitness landscape [23]. The schematic representation of a typical fitness landscape can

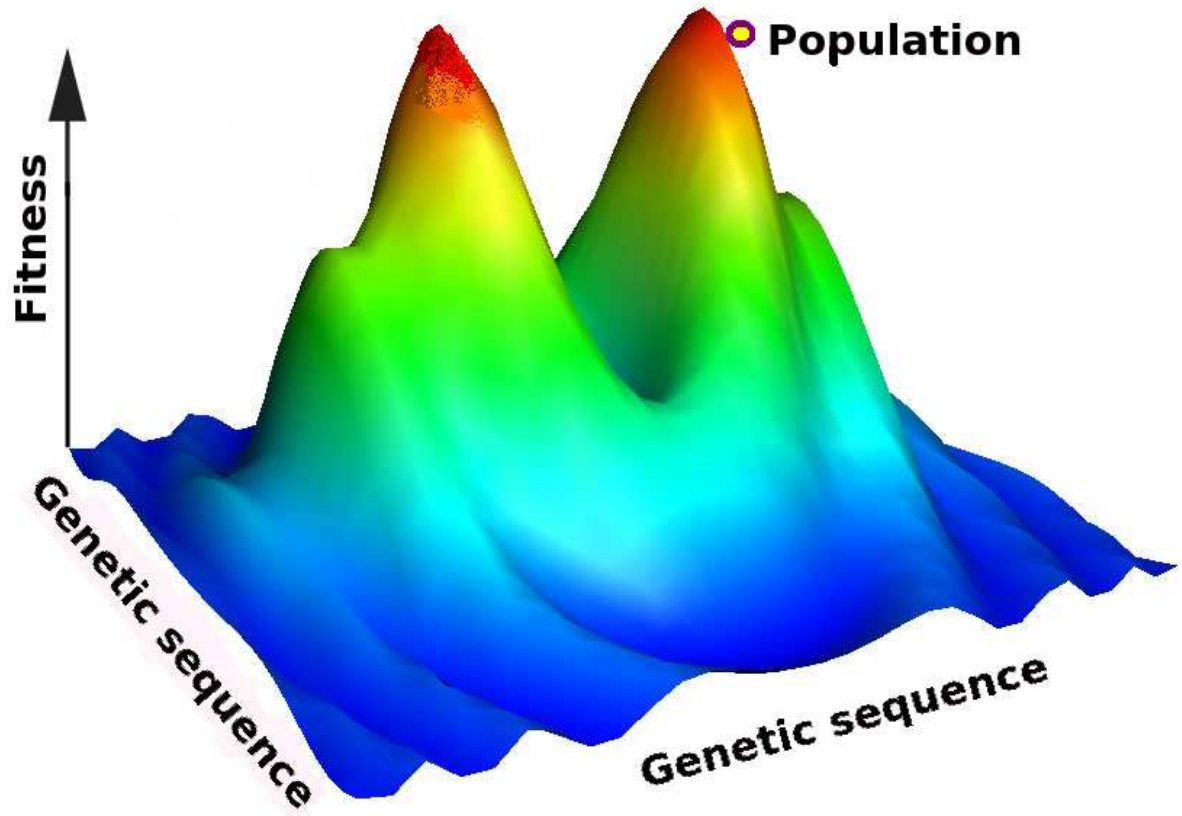


Fig. 1.1 Schematic diagram showing the position of an adapted population (shown using the circle) on a fitness landscape. (*Ref: http://evolutionarysystemsbiology.org/intro/)*

be seen in Fig. 1.1. An adapted population will be close to a local fitness peak as shown here. If we consider that the population does not accumulate any large effect mutations so as to move away from its nearest fitness peak, we can effectively restrict ourselves to a single-peak fitness landscape, with the population close to its peak. (However, such simplifications are not always possible. To know more about how to generate the more complicated and realistic fitness landscapes, one can refer to [18].) Due to the inconvenience associated with considering all the possible configurations of the genome, we consider a fitness function [8]

$$W(k) = (1-s)^{k^{\alpha}} \tag{1.1}$$

which depends only on the total number $k \geq 0$ of a particular allele (mutation) carried by the genome, but not on their locations. Here, the genome is taken to be infinitely long ($L \to \infty$). In (1.1), $s$ represents the selection coefficient (also see the last paragraph of this

Subsection), whereas $\alpha$ stands for the epistasis parameter. The latter is a measure of the degree of interactions between the mutations in the genome. In fact, a fitness landscape of the form (1.1) with $\alpha = 0.46$ has been observed experimentally as well [24].

The value of the interaction strength $\alpha$ can be tuned. The case $\alpha = 1$ indicates a non-epistatic or multiplicative fitness landscape, in which the interactions among the mutations are absent. Moreover, the effect of each mutation on the fitness is the same. For any other value of $\alpha$, the effect of a mutation on the fitness is determined by the number of mutations already present in the genome. In Chapters 2 and 3, we have studied a non-epistatic fitness landscape, while in Chapter 4, we have considered an epistatic fitness landscape.

The individuals that are more suited to the environment will reproduce more and increase in number. In this way, the force of natural selection acts on the variation in fitness among the organisms and tries to reduce it. When all the individuals in the population become the descendants of a beneficial allele, that allele is said to have attained *fixation*.

### 1.2.2 Mutation

The random changes in the genetic material of an individual are termed as mutations. Errors in DNA (genetic material) replication or physical damage to DNA can lead to mutations [25]. Mutations are classified mainly on the basis of the following: 1) the type of change they cause to the genome [25], and 2) their effect on the fitness of an organism. In asexual organisms, mutations are the only source of de novo variation. We learn from experiments [26] that the number of beneficial mutations is very small relative to the deleterious ones. Moreover, in an adapted population (as shown in Fig. 1.1), there is no room for the beneficial mutations to act, assuming that the environment does not change during the period of study. As a result, any mutation that improves the fitness of the best genotype has been neglected. However, we include the rare compensatory mutations [10, 27, 12], which oppose the build-up of detrimental mutations at a rate much smaller than that of the deleterious mutations, but do not increase the fitness of the best genotype. The deleterious and compensatory mutations, respectively increase and decrease the value of $k$ in (1.1).

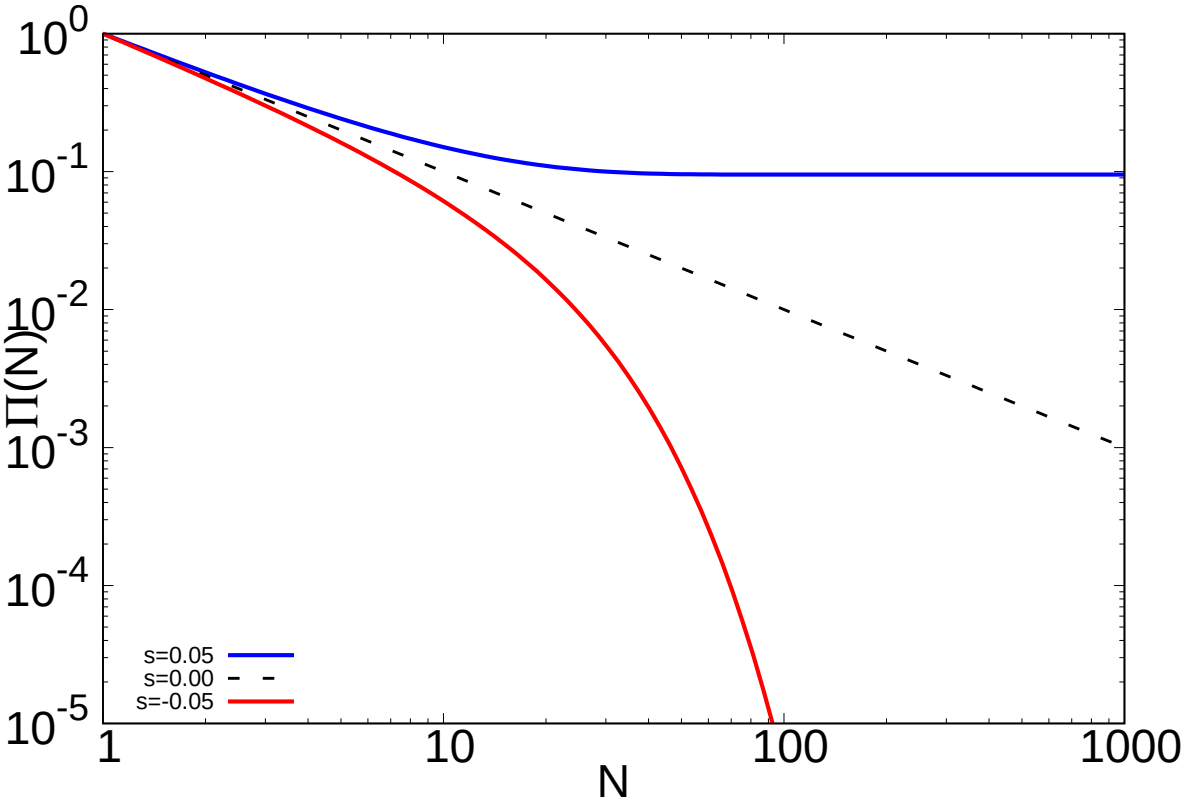


Fig. 1.2 The fixation probability of an individual carrying a beneficial ($s = 0.05$), deleterious ($s = -0.05$), or neutral ($s = 0.00$) mutation as a function of the population size. The lines show (1.2).

In our model, the accumulation of mutations lowers the reproductive ability of an individual, as one can clearly see from (1.1). Due to this, the population will be shifted away from the fitness peak. On the other hand, selection keeps the population closer to the peak. When the force of selection balances that of mutation, a *steady state* can be established. In this steady state, also known as the *mutation-selection balance*, the mean fitness of the population as well as the population frequencies corresponding to all the genotypes (refer to Section 1.3.1) become time independent. In later parts of the thesis, we will see that the concept of steady state is very helpful in deriving relatively simple analytical expressions.

### 1.2.3 Random genetic drift

Real populations are finite in size. Moreover, reproduction is a stochastic process. Even if an individual carries a beneficial (deleterious) mutation, it may fail (manage) to reproduce. Owing to their non-zero probabilities, these unlikely events can repeat and eventually lead to the extinction (fixation) of the beneficial (deleterious) allele. However, such improbable occurrences have a higher likelihood of happening in small populations. This can be seen in Fig. 1.2 in which the expression [28]

$$\Pi(N) = (1 - e^{-2s})/(1 - e^{-2sN}) \tag{1.2}$$

is plotted for the fixation probability $\Pi(N)$ of a mutant with a selective advantage $s$ in a population of size $N$. For a deleterious mutation, $s$ is a negative number, and hence, $\Pi(N) \sim e^{-2sN}$. In the case of a neutral mutation, $s \to 0$, $Ns \ll 1$, due to which, $\Pi(N) = 1/N$. In the limit $N \to \infty$, $\Pi(N) \sim 0$ for both the deleterious and neutral mutants, whereas $\Pi(N) = 2s$ for a beneficial mutant.

## 1.3 Models and methods

Here, our aim is to incorporate the effect of the evolutionary forces, namely, selection, mutation, and genetic drift that have been discussed till now into mathematical models.

### 1.3.1 Deterministic models

The stochastic effects due to the fluctuations in the population vanish in the limit $N \to \infty$ and one develops deterministic theories for the evolution of the various genotypes under the action of mutation and selection, as well as for the fixation of a beneficial mutant.

The deterministic fraction $p(k, t+1)$ of the population carrying $k$ mutations in generation $t+1$ is related to the population fractions in the previous generation according to the expression [29]

$$p(k, t+1) = \frac{\sum_j M(k \leftarrow j)\, W(j)\, p(j, t)}{\overline{W}(t)}\,, \tag{1.3}$$

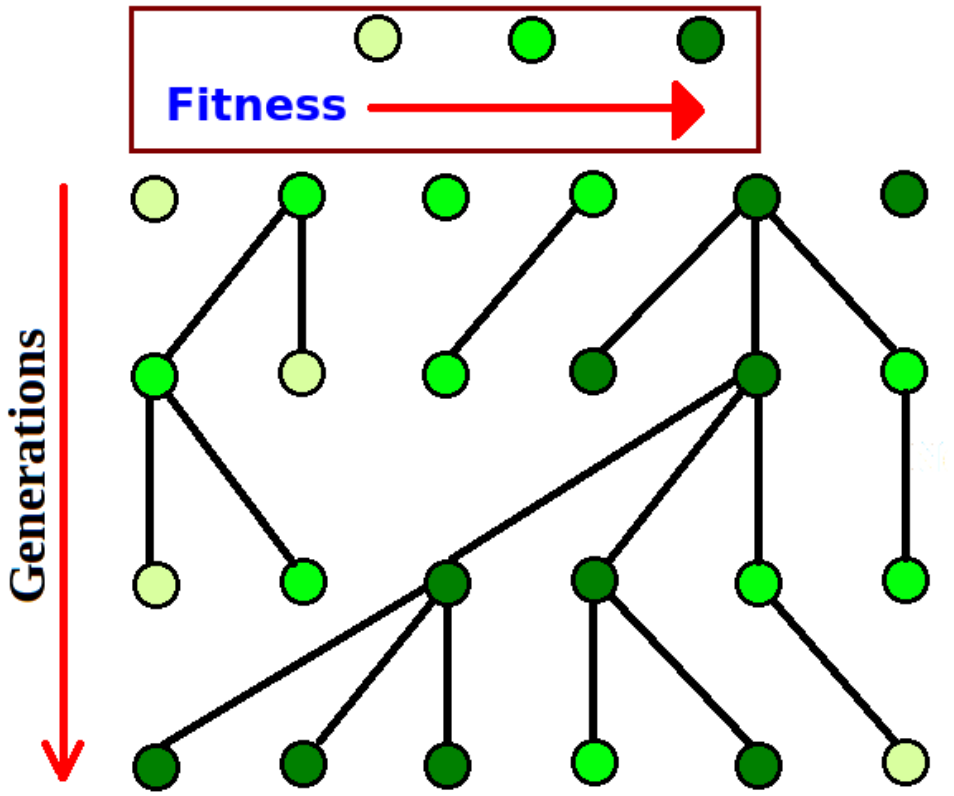


Fig. 1.3 Schematic diagram showing Wright-Fisher process for a population size $N = 6$. The darker the shade of green, the higher the fitness is.

where the fitness $W(j)$ is given by (1.1), and $M(k \leftarrow j)$ is the probability with which number of mutations changes from $j$ to $k$. The mean fitness $\overline{W}(t)$ of the population is $\overline{W}(t) = \sum_j p(j,t)\ W(j)$. The steady state ($t \to \infty$) solution to (1.3) has been utilized in the coming Chapters.

### 1.3.2 Wright-Fisher process

Unlike Section 1.3.1, here we consider a finite population of constant size $N$ that evolves according to a Wright-Fisher process. The generations are discrete and non-overlapping. In every generation, corresponding to each individual, an individual in the previous generation is assigned as the parent, with a probability proportional to its fitness. The parent can undergo mutations during the process of passing the genes to its offspring. According to Wright-Fisher process, the probability $P_k(n,t)$ of an individual having the fitness $W(k)$

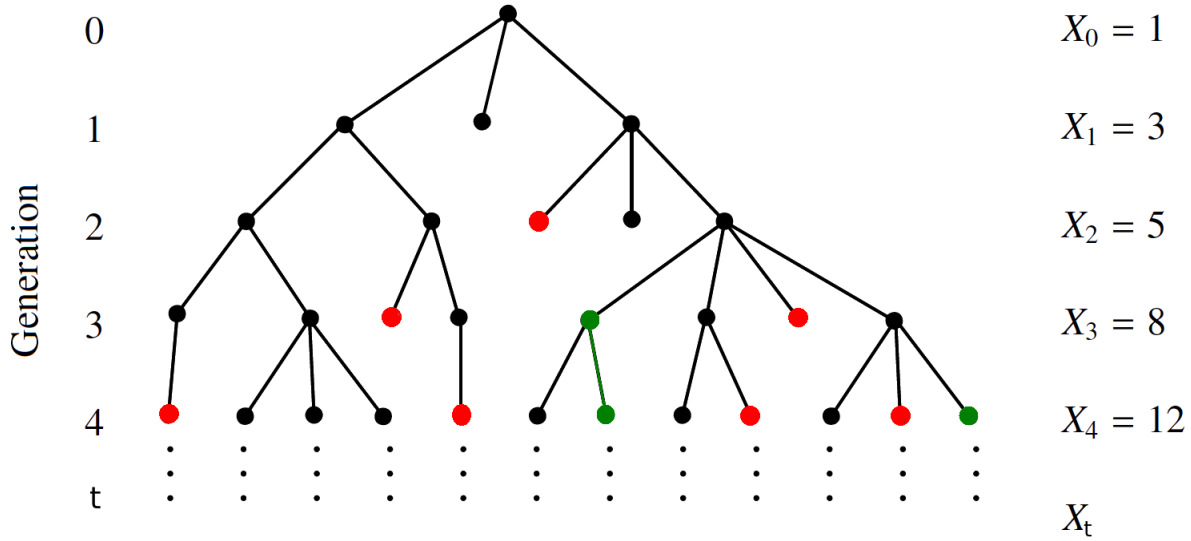


Fig. 1.4 Schematic diagram showing a multitype branching process. Here, $X_t$ represents the number of descendants of the mutant in generation $t$. The different colors indicate the fact that during reproduction, one type can give rise to different types.

in generation $t$ to give birth to $n$ offspring in the next generation, assuming that mutations do not occur, can be expressed using a Binomial distribution as shown below:

$$P_k(n,t) = \binom{N}{n} \left(\frac{W(k)}{N\overline{W}(t)}\right)^n \left(1 - \frac{W(k)}{N\overline{W}(t)}\right)^{N-n}. \tag{1.4}$$

An example for Wright-Fisher process is shown in Fig. 1.3. In order to incorporate the stochastic behavior of finite populations [25], Wright-Fisher method has been implemented in our simulations, which will be discussed in the succeeding Chapters.

### 1.3.3 Branching process formalism for the fixation probability of a beneficial mutant

The branching processes [9, 30] are applicable to a wide variety of problems ranging from nuclear physics to population genetics [31]. One main assumption, which the branching process relies on is that the probability of reproduction of each individual is independent of the other individuals in the population [31]. This method is useful in determining the probability of eventual extinction (fixation) of a mutant which has an advantage over the

rest of the individuals in the population [31, 32]. Therefore, it can be employed to examine the fate of a mutant having a low mutation rate arising in an adapted population which is undergoing mutations at a high rate.

In our thesis, each genotype can undergo mutations during the reproduction. To account for this, we use a multitype branching process here as discussed later [32]. Fig. 1.4 shows the schematic representation of a multitype branching process.

## 1.4 The main goals and overview of the thesis

In this thesis, we want to address the question how mutation rates evolve in an adapted asexual population. Because harmful mutations play a major role in well-adapted populations, a reduction in the mutation rate is advantageous here. There have been various experiments [33, 5, 34, 6] in which such a reduction in mutation rate has been observed. But, barring a computational work [35] that showed the possibility of decline in the mutation rate and a recent analytical study [7] conducted for the special case in which all the mutations are assumed to be lethal, a theoretical understanding is largely missing.

We study the role of the factors viz., drift, selection, compensatory mutations, epistasis, and mutation rates of the invader as well as the resident population on the fixation probability of the nonmutator (invader).

In Chapter 2 [10], we calculate the chances of a rare nonmutator to reach fixation in a strong mutator background [4, 36], in which the nonmutator has a negligible mutation rate compared to that of the mutator background. This calculation reveals that the dependence of the lower bound of the mutation rate on the population size can be different from the prediction by the existing theory [7]. Moreover, the probability of occurrence of the compensatory mutations has been taken into account. We find that the nonmutator can be favored due to compensatory mutations if the selection is milder than the background mutation rate [10]. However, as laboratory experiments [34, 6] show that the mutator and nonmutator can have comparable mutation rates, in Chapter 3, we analyze the case in which mutator is weak [12]. Here, we find that the nonmutator can experience a disadvantage in

a high mutation rate background when the mutation rates exceed the selection and make predictions regarding the behavior of the advantage associated with the nonmutator (in the presence of compensatory mutations) as a function of the mutation rates of the invader as well as the resident population [12].

All the above studies have considered the very simple fitness landscape in which the mutations do not interact with each other ($\alpha = 1$ in (1.1)). However, such a situation may not be realistic. In order to take this into account, in Chapter 4, we investigate the impact of epistatic interactions ($\alpha \neq 1$) on the fixation of a nonmutator [13]. Interestingly, the presence of a critical value of the epistasis parameter, below which the fixation probability manifests a nonmonotonic trend as a function of the background mutation rate, is found here [13].

Our main findings are summarized in Chapter 5. In addition to that, some open questions are discussed here.

# Chapter 2

# Fixation of a nonmutator in a strong mutator background

## 2.1 Introduction

In this Chapter, our purpose is to understand the role of selection and random genetic drift in the evolution of mutation rates when the effect of each mutation is the same [10]. Moreover, we examine the impact of compensatory mutations on the fixation of a rare mutant having a negligible mutation rate relative to that of the background [10].

Because most mutations are deleterious, the mutation rate cannot be too high; in fact, in an infinitely large population, for a broad class of fitness functions, an error threshold has been shown to exist above which the deleterious effects of mutation cannot be compensated by selection [37, 29]. The mutation rate is not zero either [2], and it has been argued that the stochastic fluctuations in a finite population limit the evolution of mutation rates below a certain level since in small enough populations, the advantage gained by lowering the mutation rate cannot compensate the effect of random genetic drift [11]. Empirical data for organisms with widely different effective population size shows a negative correlation between the deleterious mutation rate and the population size [22], and some quantitative insight into this relationship has been obtained by treating all deleterious mu-

tations to be lethal [7]. However, this is clearly an extreme scenario, and it is important to ask how the deleterious mutation rate evolves when mutations are only weakly deleterious.

Many theoretical and experimental investigations have also shown that in an adapting asexual population, a mutator allele causing a higher mutation rate than that of the nonmutator can get fixed (see a recent review by [3]). Since the mutators produce not only deleterious but also beneficial mutations at a higher rate than the nonmutators, the mutator allele can hitchhike to fixation with favorable mutations [38, 35]. However, once the population has reached a high fitness level, high mutation rates are detrimental since most mutations will now be deleterious, and in such a situation, the mutation rate is expected to decrease [39]. Indeed, in some experiments [33, 5, 34, 40, 6], the mutation rate of an adapted population carrying a mutator allele has been seen to decrease and the time to fixation has been measured, but a theoretical understanding of this time scale is missing.

To address the issues discussed above, we study the fate of a rare nonmutator in a large asexual population of mutators using a multitype branching process [9]. An important difference between the previous works on mutator hitchhiking [35, 41–43] and our study is that here the mutator population is assumed to be at mutation-selection equilibrium and is therefore not under positive selection. However, compensatory mutations that alleviate the effect of deleterious mutations are included in our model. We find that when only deleterious mutations are present, a nonmutator can get fixed with a probability that increases with the deleterious mutation rate of the mutator. Compensatory mutations in the mutator population are expected to decrease the fixation probability of the nonmutator, and we find that this intuition is indeed correct when deleterious mutations in the mutator are effectively lethal. But, surprisingly, when the deleterious mutations are mildly harmful, the fixation probability is found to initially increase and then decrease as the rate of compensatory mutations increases. Our study thus identifies the conditions under which the spread of nonmutators is suppressed in the absence of positive selection, and complements earlier works in which a mutator hitchhikes with beneficial mutations to fixation [35, 41–43].

Using our results for the fixation probability and a drift-barrier argument which states that the advantage offered by a decrease in the deleterious mutation rate is limited by random genetic drift in a finite population [11], we find that the deleterious mutation rate decreases with increasing population size in accordance with experimental data [22]. However, unlike the previous theoretical work by Lynch [7] that treats the deleterious mutations to be effectively lethal, here we consider both strongly and weakly deleterious mutations, and not only reproduce the result by Lynch [7], but also find a new scaling law in the latter case. We also use the results for the fixation probability to find the time to lower the mutation rate in an adapted population of mutators, and compare our theoretical results with recent experiments [34, 6].

## 2.2 Model and methods

We consider an asexual population in which the fitness of an individual with $k$ deleterious mutations is given by $W(k) = (1-s)^k$, where the selection coefficient $0 < s < 1$. A deleterious mutation is allowed to occur at a rate $V_d$ and a compensatory one at a rate $V_b < V_d$ (see Appendix A.1 for details). We are interested in the fate of a nonmutator that arises in this population and whose total mutation rate is smaller than that of the mutator. In a sufficiently large population of mutators in which stochastic fluctuations due to genetic drift may be ignored, this can be addressed using a branching process [9], as described below.

The fixation probability $\pi(k,t)$ of a single copy of a nonmutator allele with fitness $W(k)$ present at generation $t$ changes according to [32]

$$1-\pi(k,t) = \exp\left[-\frac{W(k)}{\overline{W}(t)}\sum_{k'} M(k\to k')\pi(k',t+1)\right], \tag{2.1}$$

where $\overline{W}(t) = \sum_{k=0}^{\infty} W(k)\,p(k,t)$ is the average fitness of the mutator population and $p(k,t)$ is the mutator frequency. The above equation expresses the fact that a single copy of the rare allele in the fitness class $k$ whose offspring distribution is Poisson with mean $W(k)/\overline{W}(t)$ will be lost eventually if each of its offspring, which may undergo mutations with probabil-

ity $M(k \to k')$, do not survive. (Note that as explained in Section 1.3.2, throughout the thesis, the simulations are done assuming that the offspring are Binomially distributed. However, it is possible to convert the Binomial distribution in (1.4) to a Poisson when $N \to \infty$ and $\frac{W(k)}{N\overline{W}(t)} \to 0$. In branching process formalism, this approximation offers some advantages in calculation, as you can see in Section 4.2.2.) Here we consider strong mutators whose mutation rate is much higher than that of the nonmutator [4, 36], and therefore neglect the mutation rate of the latter in most of the following discussion (however, see Fig. 2.1). We also assume that the mutator population is at mutation-selection equilibrium as is likely to be the case in large populations that have been evolving for a long time in a constant environment. As a result, the probability $\pi(k,t)$ becomes time-independent. These considerations lead to a relatively simpler, but still highly nonlinear equation given by

$$1 - \pi(k) = \exp\left[-\frac{W(k)\,\pi(k)}{\overline{W}}\right] . \tag{2.2}$$

The above expression, of course, reduces to the well known single-locus equation [44, 45] when the nonmutator can be present in only one genetic background, but here we are dealing with a multitype branching process since a nonmutator can arise in any fitness class.

The total fixation probability is obtained on summing over all genetic backgrounds [32],

$$\Pi = \sum_{k=0}^{\infty} p(k)\,\pi(k) , \tag{2.3}$$

where the probability that a nonmutator arises in a background of $k$ deleterious mutations is given by the mutator frequency $p(k)$ in the stationary state.

Although the steady state frequency $p(k)$ in the absence of compensatory mutations that mitigate the effect of deleterious mutations is known exactly [46, 47], the corresponding solution with nonzero $V_b$ is not known. We therefore compute the mutator frequency numerically for nonzero $V_b$ using (A.1) given in Appendix A.1, and use these results in (2.2) to find the fixation probability for arbitrary $V_b$. To make analytical progress, we use a perturbation theory in which the effect of the small dimensionless parameter $V_b/s$ can be studied

by expanding the quantities of interest in a power series in $V_b/s$, and write

$$\pi(k) = \sum_{n=0}^{\infty} \left(\frac{V_b}{s}\right)^n \pi_n(k) \ , \ p(k) = \sum_{n=0}^{\infty} \left(\frac{V_b}{s}\right)^n p_n(k) \ . \tag{2.4}$$

The terms $\pi_0(k)$ and $p_0(k)$ corresponding to $n = 0$ in the above expansion give the results in the absence of compensatory mutations, and in Appendix A.1, we calculate the stationary state fraction $p(k)$ to linear order in $V_b/s$.

## 2.3 Results

### 2.3.1 Fixation probability

**In the absence of compensatory mutations:** We first consider the case when $V_b = 0$. Taking the logarithm on both sides of (2.2), and expanding the left hand side (LHS) up to $\pi_0^2(k)$, we find that either $\pi_0(k) = 0$, or

$$\pi_0(k) = 2\left(\frac{W(k)}{\overline{W_0}} - 1\right) \approx 2s(\bar{k}_0 - k) \ , \tag{2.5}$$

where the average fitness $\overline{W_0} = e^{-V_d}$ and the average number of deleterious mutations $\bar{k}_0 = V_d/s$ [46, 47]. The last expression on the right hand side (RHS) of (2.5) is obtained by expanding the exponentials as the parameters $V_d$ and $s$ are small. Since the fixation probability must not be negative, the expression (2.5) is valid when $k < \lfloor \bar{k}_0 \rfloor$, and the solution $\pi_0(k) = 0$ holds otherwise. Here $\lfloor x \rfloor$ denotes the largest integer less than or equal to $x$. More generally, a nonmutator can get fixed if its fitness $W(k) \approx e^{-sk}$ is larger than the average fitness $e^{-s\bar{k}}$ of the mutator population, or $k < \lfloor \bar{k} \rfloor$, $\bar{k}$ being the average number of deleterious mutations [32].

Equation (2.5) shows that the fixation probability $\pi_0(k)$ decreases as the number of deleterious mutations increase, as one would intuitively expect. However, the probability $p_0(k)$ that a nonmutator would arise in a background with $k < \bar{k}_0$ deleterious mutations increases. On summing over the backgrounds in which a nonmutator can arise, as explained in Ap-

pendix A.2, we find that the total fixation probability falls in two distinct regimes defined by whether $V_d$ is below or above $s$:

$$\Pi_0 = \sum_{k=0}^{\lfloor \bar{k}_0 \rfloor} \pi_0(k)\, p_0(k) = \begin{cases} 2V_d\,, & V_d \ll s \\ \sqrt{\frac{2sV_d}{\pi}}\,, & V_d \gg s\,. \end{cases} \tag{2.6}$$

For $\bar{k}_0 \ll 1$, since a mutation is costly, it can be treated as effectively lethal [48]. In this situation, the advantage conferred by the nonmutator is simply given by $1 - e^{-V_d} \approx V_d$ and the classical result for the single locus problem gives the fixation probability to be $2V_d$ [44, 45]. For $\bar{k}_0 \gg 1$, the total fixation probability apparently receives contribution from $\bar{k}_0$ genetic backgrounds, but merely $\sqrt{\bar{k}_0}$ genetic backgrounds are actually relevant because the Poisson-distributed frequency $p_0(k)$ has a substantial weight for fitness classes that lie within a width $\sqrt{\bar{k}_0}$ of the mean (also, see Appendix A.2). Equation (2.6) shows that for fixed $s$, the nonmutator is more likely to be fixed when $V_d$ is large. But, for a given $V_d$, the fixation probability initially increases with the selection coefficient and then saturates to $2V_d$. In Fig. 2.1, the analytical results above are compared with those obtained by numerically iterating (2.2) and (2.1) when the mutation rate of the nonmutator is zero and $V_d/50$ respectively, and we see a good agreement in both cases.

**Including compensatory mutations:** We now study how compensatory mutations in the mutator population affect the fixation probability of the nonmutator. Figure 2.2 shows that when $\bar{k}_0 \ll 1$, the fixation probability decreases with $V_b$, but for $\bar{k}_0 \gg 1$, it changes *non-monotonically*: it first increases and then decreases with increasing $V_b$. To understand this behavior, consider the change $\delta\Pi = \Pi - \Pi_0$ in the fixation probability due to compensatory mutations which is simply given by

$$\delta\Pi = \sum_{k=0}^{\lfloor \bar{k} \rfloor} p_0(k)\delta\pi(k) + \pi_0(k)\delta p(k) + \delta p(k)\delta\pi(k)\,. \tag{2.7}$$

When $V_b$ is nonzero, the change in the fixation probability $\delta\pi(k) = \pi(k) - \pi_0(k)$ and the mutator frequency $\delta p(k) = p(k) - p_0(k)$ behave in a qualitatively different manner. With

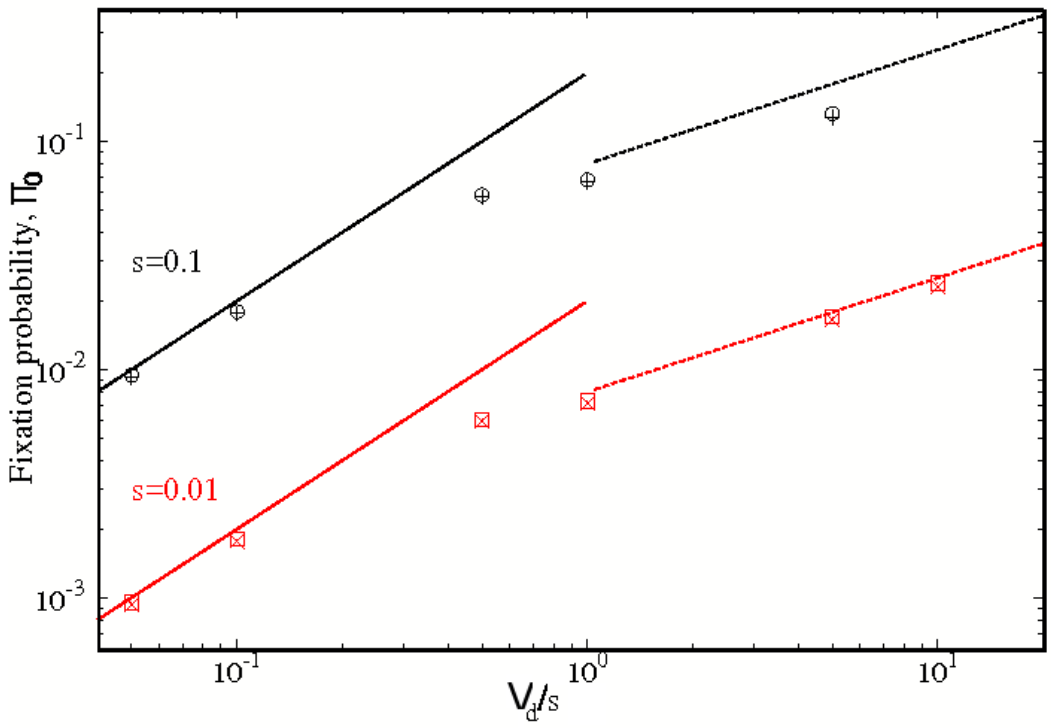


Fig. 2.1 Dependence of the fixation probability obtained using a multitype branching process on the deleterious mutation rate $V_d$ for two values of the selection coefficient $s$ and compensatory mutation rate $V_b = 0$. The points are obtained by numerically solving (2.2) when the mutation rate of the nonmutator is zero (the circles and squares), and the stationary state solution of (2.1) when the nonmutator's mutation rate is 50 times lower than that of the mutator ($+, \times$). The lines show the analytical result (2.6).

increasing $V_b$, the average *fitness* of the mutator population increases which, by virtue of (2.2), decreases the fixation probability of the nonmutator, *i.e.* $\delta\pi(k) < 0$. However, since the *frequency* of individuals with less deleterious mutations increases when $V_b$ is nonzero, the change in the mutator fraction $\delta p(k) > 0$ (refer to Fig. 2.3 as well as the paragraphs below to know more details). Thus the change in the total fixation probability given by (2.7) receives both positive and negative contributions, and it is not obvious which one of these factors would have a larger effect.

To address this question, we calculate the fixation probability for small $V_b/s$ as described below. Substituting (2.4) in the expression (2.7) for $\delta\Pi$, and neglecting terms of order $(V_b/s)^2$

and higher, we find that $\delta\Pi \approx (V_b/s)\Pi_1$, where

$$\Pi_1 = \sum_{k=0}^{\lfloor \bar{k}_0 \rfloor} p_0(k)\pi_1(k) + p_1(k)\pi_0(k) \, . \tag{2.8}$$

The contribution $\pi_1(k)$ is calculated in Appendix A.3, and we find that

$$\pi_1(k) \approx -2s\bar{k}_0(1-\pi_0(k)) \, , \; k < \lfloor \bar{k}_0 \rfloor \, , \tag{2.9}$$

which is negative, as expected. An expression for the fraction $p_1(k)$ is obtained in Appendix A.1, and its behavior is shown in Fig. 2.3 for small and large $\bar{k}_0$. For small $\bar{k}_0$, the frequency $p_0(k)$ is close to one in the zeroth fitness class and zero elsewhere. But the correction $p_1(k)$ is negligible in all the fitness classes. For large $\bar{k}_0$, the contribution $p_1(k)$ is significantly different from zero in many fitness classes and can be approximated by

$$p_1(k) = \bar{k}_0 p_0(k) \, \ln\left(\frac{\bar{k}_0}{k}\right) \, , \; k \gg 1 \, . \tag{2.10}$$

Thus, as claimed above, the fraction $p_1(k)$ is positive for $k < \bar{k}_0$ and negative for $k > \bar{k}_0$ (also, see Fig. 2.3).

When $V_d \ll s$, as already mentioned, the fraction $p_1(k)$ is negligible in all the fitness classes and $p_0(0) \approx 1$. Using these results in (2.8) and (2.9), we get $\pi_1 = -2s\bar{k}_0$, and thus

$$\frac{\delta\Pi}{\Pi_0} = -\frac{V_b}{s} \, , \; V_b < V_d < s. \tag{2.11}$$

This reduction in the fixation probability of the nonmutator when $V_b$ is nonzero is expected since the effect of compensatory mutation is to restore the mutators that have suffered lethal mutation to the zeroth mutation class thus enabling them to offer competition to the nonmutators.

When $V_d \gg s$, as shown in Appendix A.3, we can obtain a quantitative estimate of the initial increase in $\delta\Pi$ by calculating the sum on the RHS of (2.8) to obtain (A.14), and thence

$$\frac{\delta\Pi}{\Pi_0} = \frac{V_b}{2s}\ ,\ V_b < s < V_d\ . \tag{2.12}$$

Thus we find that for small $V_b$, the increase of the mutation frequency in fitness classes with fewer deleterious mutations dominates the increase in the mutator fitness resulting in positive $\delta\Pi$. However, for large $V_b$, the net change in the fixation probability is negative since the last term in the summand of (2.7), which is also negative, enters the picture. Since the maximum in $\delta\Pi$ occurs at large $V_b/s$, the perturbation theory described here cannot capture the eventual decrease in this parameter regime. A quantitative comparison of the results obtained by numerically solving (2.2) and (A.1) for arbitrary $V_b$ with the analytical results (2.11) and (2.12) for small $V_b/s$ is shown in Fig. 2.2, and we observe a good match when $V_b/s$ is small. For large $V_b/s$ and $V_d/s$, a fit to the numerical data shows that the fixation probability decreases linearly with $V_b$.

### 2.3.2 Evolution of mutation rates in finite populations

The drift-barrier hypothesis states that in a finite population, the beneficial effect of lower deleterious mutation rate can be outweighed by the stochastic effects of random genetic drift which limits the evolution of mutation rates [11]. In a finite population of size $N$, a mutation that decreases the deleterious mutation rate confers an indirect selective advantage and will spread through the population. However, as $V_d$ decreases, the fixation probability of such a mutant decreases until it reaches its neutral value $\Pi_{\rm neu} = 1/N$. Here we have calculated the fixation probability $\Pi_0$ neglecting stochastic fluctuations. The full fixation probability $\Pi$ that includes the neutral and the large population limit may be obtained as follows.

The fixation time for a mutator in a finite population of nonmutators when all mutations are deleterious has been calculated using a diffusion theory by Jain and Nagar [49], and shown to increase exponentially with the population size. The fixation probability

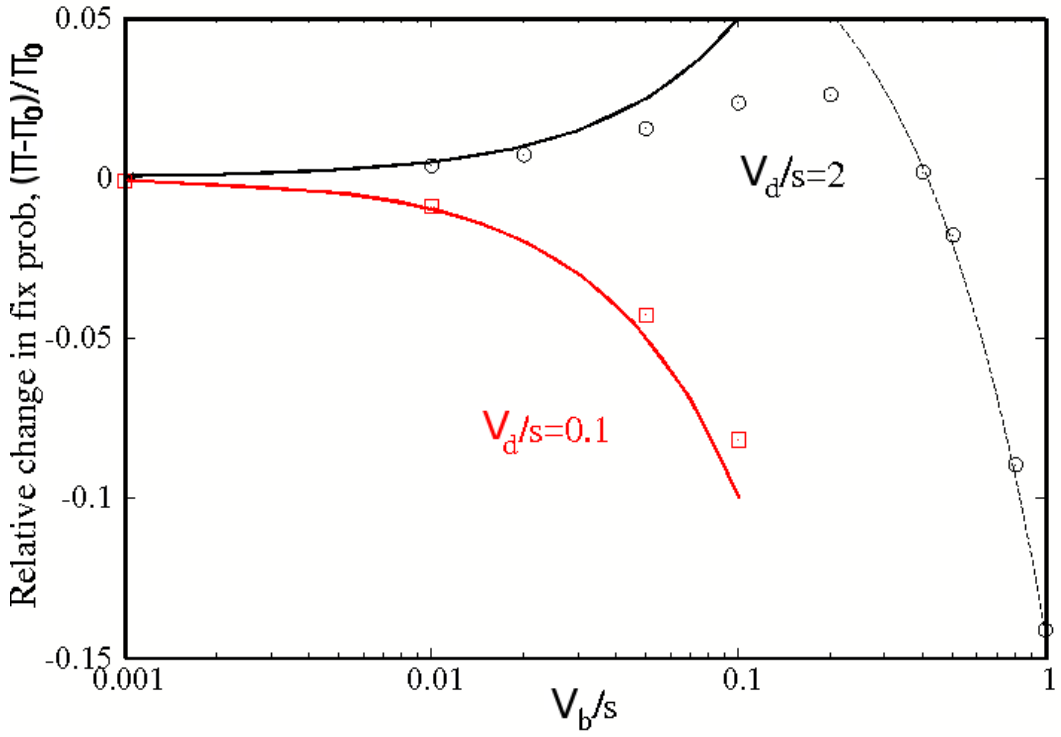


Fig. 2.2 Dependence of the fixation probability obtained using a multitype branching process on the compensatory mutation rate $V_b$ for two values of $V_d/s$. The points show the numerical solution of (2.2) and the lines show the analytical results (2.11) and (2.12). The broken curve for $V_b/s > 0.1$ is a linear fit, $0.1 - 0.24V_b/s$, to the numerical data. For $V_d/s = 0.1$, the ratio $V_b/s$ is also below 0.1 since $V_b$ is assumed to be smaller than $V_d$.

$\sim e^{-2NS}$ is thus exponentially small in the population size [50, 51], where we have identified the coefficient of population size in the exponent as a selection coefficient $2S$. (The discussion in Section 4.4.5 will be helpful in developing a better understanding, where the exact functional dependence of $S$ is shown.) This effective selection coefficient is found to match with the result (2.6) for the fixation probability $\Pi_0$ obtained here using a branching process. Although this is not a rigorous proof, these observations strongly suggest that the fixation probability of a nonmutator in a finite population of size $N$ is of the classical form [28]

$$\Pi = \frac{1 - e^{-2S}}{1 - e^{-2NS}}\,, \tag{2.13}$$

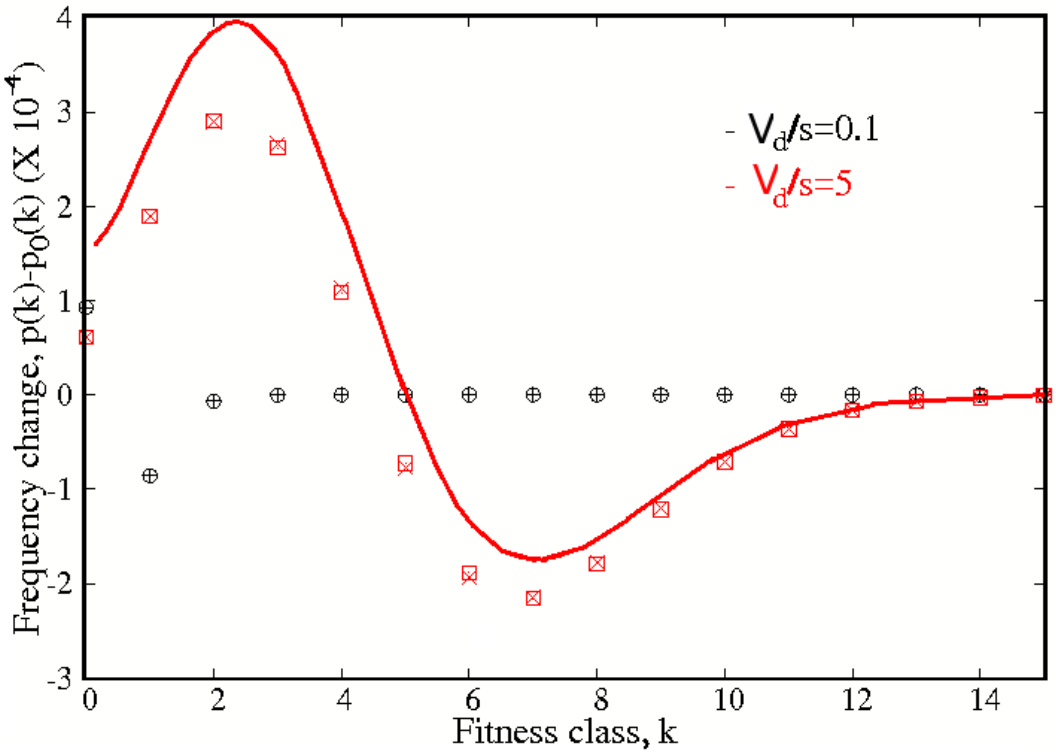


Fig. 2.3 Change in the mutator frequency when compensatory mutations are included, $\delta p(k) = p(k) - p_0(k)$ for $V_b = 10^{-4}$. The points (the circles and squares) are obtained by numerically iterating (A.1) and $(+, \times)$ show the perturbation theory result (A.7), and we observe a good agreement. The simple expression (2.10) for large $V_d/s$ is also shown (lines).

where $S = \Pi_0/2$. We also mention that the probability $2S$ depends on the difference in the deleterious mutation rate of the mutator and the nonmutator when the mutation rate of the nonmutator is nonzero [49], and has also been shown to be insensitive to the distribution of selective effects [43].

As described in Section 1.2.3, in (2.13), when $2NS \ll (\gg)\ 1$, $\Pi \sim 1/N$ $(2S)$. These two conditions respectively correspond to neutral regime and positive selection. Now, based on the argument in the above paragraph, by replacing $2S$ with $\Pi_0$, we can state that a crossover between positive selection and neutral regime occurs when $\Pi_0 \sim N^{-1}$. Now, using (2.6), we express $\Pi_0$ in terms of $s$ and $V_d$. This gives a lower bound on the mutation rates. We recall that the fixation probability $\Pi_0$ in (2.6) shows a transition when $V_d \sim s$, and at this mutation rate, the fixation probability $\Pi_0 \sim s$. This translates into a change in the behavior of $V_d$ when

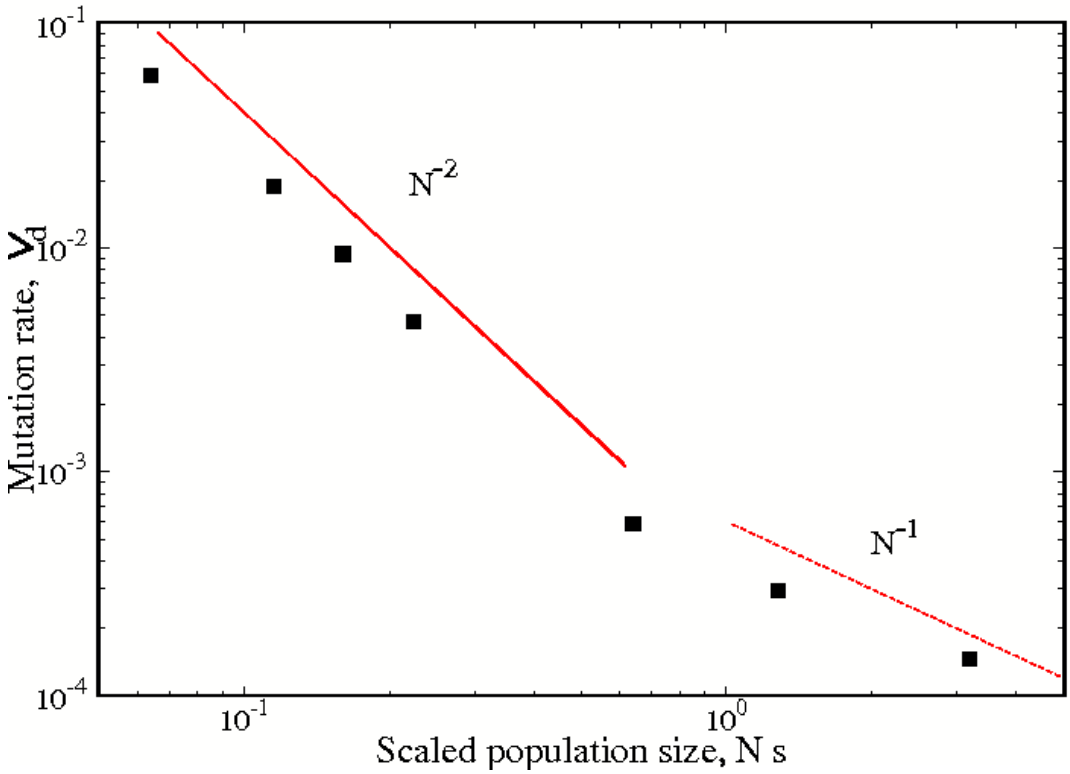


Fig. 2.4 Relationship between the deleterious mutation rate and the population size for selection coefficient $s = 0.0064$ when compensatory mutations are absent. The points are obtained by numerical simulations of a Wright-Fisher process, and the lines show the $N$-dependence in (2.14).

$Ns$ crosses one, and we have

$$V_d \sim \begin{cases} (sN^2)^{-1} \,, & Ns \ll 1 \\ N^{-1} \,, & Ns \gg 1 \,. \end{cases} \tag{2.14}$$

Thus in the weak selection regime ($Ns \ll 1$), the deleterious mutation rate depends on the selection coefficient, and decreases faster than when the selection is strong. Figure 2.4 shows the preliminary results of our numerical simulations for a finite size population of mutators with mutation rate $V_d$ in which nonmutators with mutation rate $V_d/2$ can arise with a certain probability. This population of nonmutators and mutators evolves via standard Wright-Fisher dynamics, and the time to fix the nonmutators is measured [49]. For a fixed $N$, the fixation time is found to increase as the mutation rate of the mutator is de-

creased until a minimum mutation rate is reached below which the fixation time remains constant. This lower bound, shown in Fig. 2.4, exhibits different scaling behavior in the weak and strong selection regimes, in accordance with (2.14).

## 2.4 Discussion

### 2.4.1 Fixation probability

A rare mutator arising in a population of nonmutators carries a higher load of deleterious mutations but offers indirect benefit by producing more beneficial mutations. The fixation probability of a rare mutator in a finite nonmutator population has been studied analytically [41, 42], and found to vary nonmonotonically with the mutation rate of the mutator. It has been shown that the fixation probability is of the classical form (2.13) where the effective selection coefficient $S$, when scaled by the selective advantage $s$ of a mutation, increases (decreases) when the ratio of mutation rate to selection coefficient is below (above) one. Here, we have studied a situation in which a nonmutator appears in a mutator population and is beneficial since it produces fewer deleterious mutations, and calculated its fixation probability $\Pi$ using a branching process. The mutator population is assumed to be at mutation-selection balance and therefore, by definition, selective sweeps resulting in the spread of favorable mutations are neglected. However, it is interesting to note that the scaled fixation probability of the nonmutator obtained here also changes its behavior when the deleterious mutation rate is of the order of the selection coefficient, see (2.6). Our work significantly extends the previous result by Lynch [7] as the deleterious effect of mutations is allowed to be mild here, and therefore we are dealing with a truly multilocus problem.

Compensatory mutations that alleviate the effect of deleterious mutations are found to have a surprising effect on the fixation probability of the nonmutator. Although they improve the fitness of the mutator population, it also means that the nonmutator can arise in a better genetic background where it has a better chance of fixation. Thus, compensatory mutations affect both the resident mutator population and the invading nonmutator allele in a positive manner. The effect of these two factors on the fixation probability of the

nonmutator is, however, opposite and can result in an unexpected increase in the fixation probability of the nonmutator when compensatory mutations are present. Here, we have shown analytically that this scenario is realized when the mutations are weakly deleterious and the compensatory mutation rate is small, as illustrated in Fig. 2.2. The increase in the fixation probability due to compensatory mutations can be quite high, but we do not have analytical estimates for this. An exact solution of (A.1) would, of course, pave the way for a better analytical understanding but is currently not available.

### 2.4.2 Fixation time

In a maladapted asexual population, the mutators can sweep the population since they facilitate rapid adaptation [3]. But as the population adapts and the supply of beneficial mutations diminishes, mutators have a detrimental effect on the population fitness and a mutation that lowers the mutation rate is favored. In bacteria *E. coli*, several genes (such as *mutT* and *mutY*) are involved in avoiding or repairing the errors that occur during the replication process, and defects in these genes can lead to the mutator phenotype [52]. But compensatory mutations in the defective error-repair machinery can reduce the mutation rate, at least, partially [6]. We therefore model this situation by assigning a probability $b$ with which mutators can convert into nonmutators due to a mutation in the proofreading or error-repair region. In *E.coli*, the conversion probability $f$ from nonmutator to mutators has been estimated to be $\sim 10^{-6}$ per bacterium per generation [53]. But the probability $b$ for the reverse mutation is not known, although one expects $b < f$, possibly because it is a gain-of-function mutation [6].

When the rate $Nb$ at which the nonmutators are produced from the mutators is small enough that the new alleles behave independently, the time taken to fix the nonmutator population is given by $T = (Nb\Pi)^{-1}$. (To know more about the fixation time, refer to Section 4.4.4.) In a long term evolution experiment on $E.coli$ by Wielgoss et al. [6], it has been found that the mutation rate decreases by about a factor two in a nearly adapted mutator population with a mutation rate 150 times that of the wildtype in two lineages. As the population size in the experiments by Wielgoss et al. has been estimated to be about $10^7$ [54], the

product $Nb$ can be at most ten which is not too large. We first note that in the experiment by Wielgoss et al. [6], the fixation time was longer in the lineage in which the mutation rate decreased by a smaller amount, in accordance with (2.6). To make a quantitative comparison, we consider the ratio of the times for the two lineages, as $T$ depends strongly on the probability $b$ which is not known experimentally. Using the data in Table 2 of the above mentioned article [6], we find the ratio of fixation time in *mutT mutY-L* background to that in *mutT mutY-E* background to be $9209/5157 \approx 1.8$. The theoretical formula (2.6), on replacing $V_d$ by the difference between the mutation rate of the nonmutator and mutator yields 1.5 (1.2) when mutations are assumed to be strongly (weakly) deleterious and the selection coefficient same in both lineages. Since (2.6) is obtained assuming that the mutators are strong whereas the mutation rates decreased merely by a factor two in the experiment, a more careful examination is needed. Solving (2.1) numerically in the stationary state, we find that the ratio is unaffected when the mutations are strongly deleterious. But, using the mutation rates in Table 2 of the article on the long term evolution experiment on $E.coli$ [6] and $s \sim 0.01$ yield the ratio to be about 4.5. Although the theoretical conclusions $(1.5-4.5)$ are in reasonable agreement with experiments, the above analysis suggests that the reversion probability $b$ may not be too small (*i.e.* $Nb \gtrsim 1$), and a more sophisticated theory that takes care of the interference between the nonmutators [55] may be required to obtain a closer match. We close this discussion by noting that in an experiment on *S. cerevisiae* in which the adapted population reduced its genome-wide mutation rate by almost a factor four in two of the experimental lines [34], the fixation time seems to increase with the mutation rate, in contradiction with the experiment by Wielgoss et al. [6] and the theory presented here.

### 2.4.3 Evolution of mutation rates

Experiments show that the mutation rate decays as $N^{-0.7}$ for prokaryotes and $N^{-0.9}$ for eukaryotes [22]. The population size and deleterious mutation rates are negatively correlated since deleterious mutations can get fixed in small populations due to stochastic fluctuations, but not in large populations where the genetic drift is ineffective [11]. Here, we have

shown that a reciprocal relationship between the population size and mutation rate holds for large populations, but for small populations, the deleterious mutation rate decreases much faster, see Fig. 2.4. This is in contrast to experimental results mentioned above where the data has been fitted assuming a *single* scaling law. In view of our theoretical results discussed above, a more careful analysis of experimental data is required.

While the evolution of deleterious mutation rate has received much attention, to the best of our knowledge, analogous theoretical predictions for the beneficial mutation rate are not available except a very recent study [56]. As large populations experience clonal interference [55] which results in the wastage of beneficial mutations, the rate of beneficial mutations is observed to be smaller in large populations in microbial experiments [57]. An understanding of the relationship between the population size and the rate of beneficial mutations would be an interesting avenue to explore. Other potential factors that can affect the correlation between the mutation rate and the population size include epistasis and recombination, among which how the former influences the fixation of a low mutation rate allele in an adapted population has been examined in detail in Chapter 4. Here, we have also ignored the cost of fidelity, and it remains to be seen how the results presented here are affected on including it [58–60]. A more detailed understanding of the mutation rates, both empirically and theoretically, remains a goal for the future.

# Chapter 3

# Fixation of a nonmutator in a weak mutator background

## 3.1 Introduction

In the last Chapter, we have studied the fate of a nonmutator in a strong mutator background. In the present Chapter, with the information obtained from some of the experiments [34, 6] that the mutation rate of the nonmutator can be as large as 60 per cent of that of the mutator, we undertake a more elaborate investigation on the process of nonmutator fixation considering both the deleterious and compensatory mutations as well as a non-zero mutation rate of the nonmutator [12].

Our analysis demonstrates that when the nonmutator can undergo mutations, the probability of its fixation can increase or decrease with the increase in the mutation rate of the resident population. The latter condition, which is counterintuitive, is fulfilled in the following cases: 1) the selection pressure exceeds the difference between the deleterious mutation rates, but the deleterious mutation rate of the mutator is greater than the selection, 2) the selection coefficient is smaller than the detrimental mutation rates, and the ratio between the mutation rate of the mutator and the selection coefficient outweighs the strength of the reduction in the mutation rate (this parameter gives the ratio of the mutation rate of the mutator to that of the nonmutator). Moreover, in the case of the nonmutators with

their mutation rates comparable to that of the mutators, the fixation probability behaves like a non-smooth function (of the ratio of the difference in mutation rates to selection coefficient), but its mean decays as the mutation rate of the background (selective cost) is increased (reduced).

The surprising role of the compensatory mutations in boosting the survival chances of the nonmutator has been already unraveled in Chapter 2 for the case in which the nonmutator remains in the same genetic background in which it appears. Our investigation in the present Chapter discloses that the presence of the compensatory mutations could turn out to be highly beneficial to the nonmutators if the mutation rates of both the invader and the resident population are higher than the selection coefficient. Moreover, we discuss the behavior of the advantage associated with the nonmutator as a function of the different parameters studied here.

## 3.2 Models and methods

A large asexual population of haploid individuals of size $N$ on a fitness landscape [8]

$$W(k) = (1-s)^k \tag{3.1}$$

has been considered here, where $0 < s < 1$ is the selection coefficient. Here, $k$ stands for the fitness class or the number of mutations carried by the genome of infinite length. The fitness function in (3.1) represents a multiplicative fitness landscape, and the effect of each mutation is the same. Moreover, (3.1) is applicable for a genome carrying infinite number of biallelic loci in which the fitness depends solely on the number of mutations, but not on their locations.

The simulations are done using the standard Wright-Fisher (W-F) process [61]. The population size remains a constant in each non-overlapping generation. Corresponding to each individual in a particular generation, the parent is chosen randomly. Now, the parent reproduces with a probability proportional to its fitness, and undergoes mutation.

In the absence of compensatory mutations, an asexual population of finite size can lose its least loaded class due to genetic drift [62]. This repeats, and the population keeps losing its fitness classes one by one. This process is called the Muller's ratchet [47, 63, 62]. In the case of a population that has a very small ratchet speed (very large inter-click time or the time to lose the least loaded class), a steady state due to the mutation-selection balance is possible [62]. In steady state, the population fractions corresponding to each genotype and the mean fitness of the population become time independent. In our model, we assume that a nonmutator with the mutation rate $U_d = V_d/\lambda$, where $\lambda > 1$, appears only after the mutator population having the mutation rate $V_d$ attains steady state [10, 13]. This is a valid assumption for the populations that have been evolving for large number of generations without environmental changes. In the simulations, the mutator population is initially considered to be in steady state. This assumption has been made by [13] in studying a similar problem. Corresponding to each set of parameters, we ensure that the population does not lose its least loaded fitness class for a period at least of the order of $20/s$ generations by observing the single run plots. A timescale of $10/s$ generations has been considered as the typical time for the population to attain steady state [32]. If the inter-click time to lose class 0 [62] does not exceed the time to reach steady state, we assume that the Muller's ratchet for the population operates rapidly. Hence, the simulation data is not given for such populations. However, to complement that, results valid for an infinite population, given in Section 2.2 have been obtained using *Wolfram mathematica* 9.0.1.0. (See the article by [62] to know more about the time to lose the least loaded class in a population.)

## 3.3 Results

### 3.3.1 When only deleterious mutations are present

We make use of the well known assumption that the probability of a genome to accumulate $i$ number of deleterious mutations is Poisson distributed with the mean being the mutation rate and the variable being $i$ [64]. Therefore, $M(k \to k+i) = e^{-U_d} \frac{(U_d)^i}{i!}$, where $U_d$ is the deleterious mutation rate of the nonmutator. (Note that the mutators also undergo mutations

| **The variation of $\Pi_0$ as $V_d$ increases** | | | | |
|---|---|---|---|---|
| Regime | $k_{max}$ | "Non-smooth" behavior by $\Pi_0$ | The condition and reference to the corresponding figure | $\Pi_0$ |
| I | 0 | absent | $\frac{V_d}{s} < 1$ (Figs. 3.2 & 3.3) | $\uparrow$ |
| | | | $\frac{V_d}{s} > 1$ (Fig. 3.2) | $\downarrow$ |
| II | $\lfloor \frac{V_d}{s} \rfloor$ or $\lfloor \frac{V_d}{s} \rfloor - 1$ | absent | always (Fig. 3.3) | $\uparrow$ |
| III | $\lfloor \left( \frac{V_d - U_d}{s} \right) \rfloor$ | present (Figs. 3.2 & 3.3) | $\frac{V_d}{s} < \lambda^2$ (Fig. 3.3) | $\uparrow$ |
| | | | $\frac{V_d}{s} > \lambda^2$ (Fig. 3.3) | $\downarrow$ |

Table 3.1 Summary of the main results in Section 3.3.1. The symbols $\uparrow$ and $\downarrow$ represent increase and decrease, respectively.

according to this expression, but with $U_d$ being replaced by $V_d$.) Hence, the population fraction $p_0(k)$ takes the form of a Poisson distribution [46] with the mean being $V_d/s$ as given below:

$$p_0(k) = e^{-V_d/s} \frac{(V_d/s)^k}{k!} . \tag{3.2}$$

Consequently, in steady state, (2.1) will become

$$1 - \pi_0(k) = e^{-\left[ \frac{(1-s)^k}{e^{-V_d}} \sum_i e^{-U_d} \frac{(U_d)^i}{i!} \pi_0(i+k) \right]} \tag{3.3}$$

since the steady state fitness $\overline{W}_0$ of the mutator population is $e^{-V_d}$ [65]. Assuming that the nonmutator accumulates at most one mutation in each generation, we can convert (3.3) to write

$$1 - \pi_0(k) = \exp\left[ -e^{V_d - sk} \left( (1 - U_d)\pi_0(k) + U_d \pi_0(k+1) \right) \right] . \tag{3.4}$$

The above expression is useful in obtaining an analytical solution to $\pi_0(k)$ which can be a fast decreasing function of $k$ as shown in Fig. 3.1.

If a nonmutator arising with $k$ detrimental mutations escapes drift and manages to reach fixation, the steady state fitness of the resulting population is $e^{-U_d}(1-s)^k$. Since $\overline{W}_0 = e^{-V_d}$, the condition for the nonmutator population to become established is $e^{-U_d}(1-s)^k > e^{-V_d}$ [10, 13]. Therefore, the maximum number of mutations the nonmutator can carry so as to have a selective advantage over the mutator population and hence, possess a

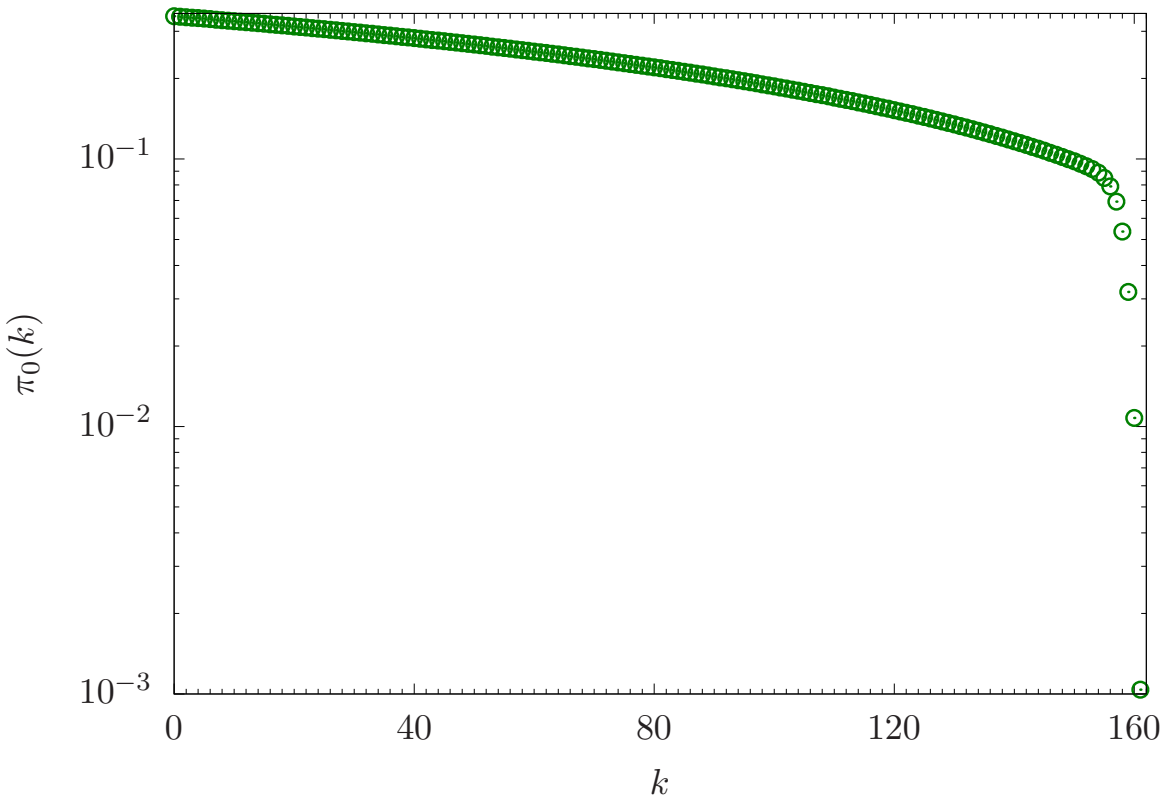


Fig. 3.1 Fixation probability $\pi_0(k)$ as a function of $k$ when only deleterious mutations are present. The symbols represent the solution to (3.3) using *Wolfram mathematica* 9.0.1.0. The parameters are $\lambda = 5$, $V_d = 0.202$, and $s = 10^{-3}$.

non-zero probability to get fixed in an infinite population is

$$k_{max} = \lfloor (V_d - U_d)/s \rfloor \,. \tag{3.5}$$

Here, $\lfloor x \rfloor$ is the maximum integer value less than or equal to $x$. Based on the value of the upper bound $k_{max}$ of deleterious mutations the nonmutator can carry in order to be considered for fixation, three different regimes are possible here (see Table 3.1). The trend shown by $\Pi_0$ as a function of $V_d$ is summarized in Table 3.1 for all the three regimes. The explanation for the nonmonotonic trend exhibited by $\Pi_0$ is given in the following paragraph.

The high mutation rate is a disadvantageous trait; hence a nonmutator carrying a given number of mutations will be highly beneficial in the background which has a large $V_d$ value. On the other hand, $\pi_0(k)$ in (3.2) is a decreasing function of $V_d$ for $k < V_d/s$. The intuitive

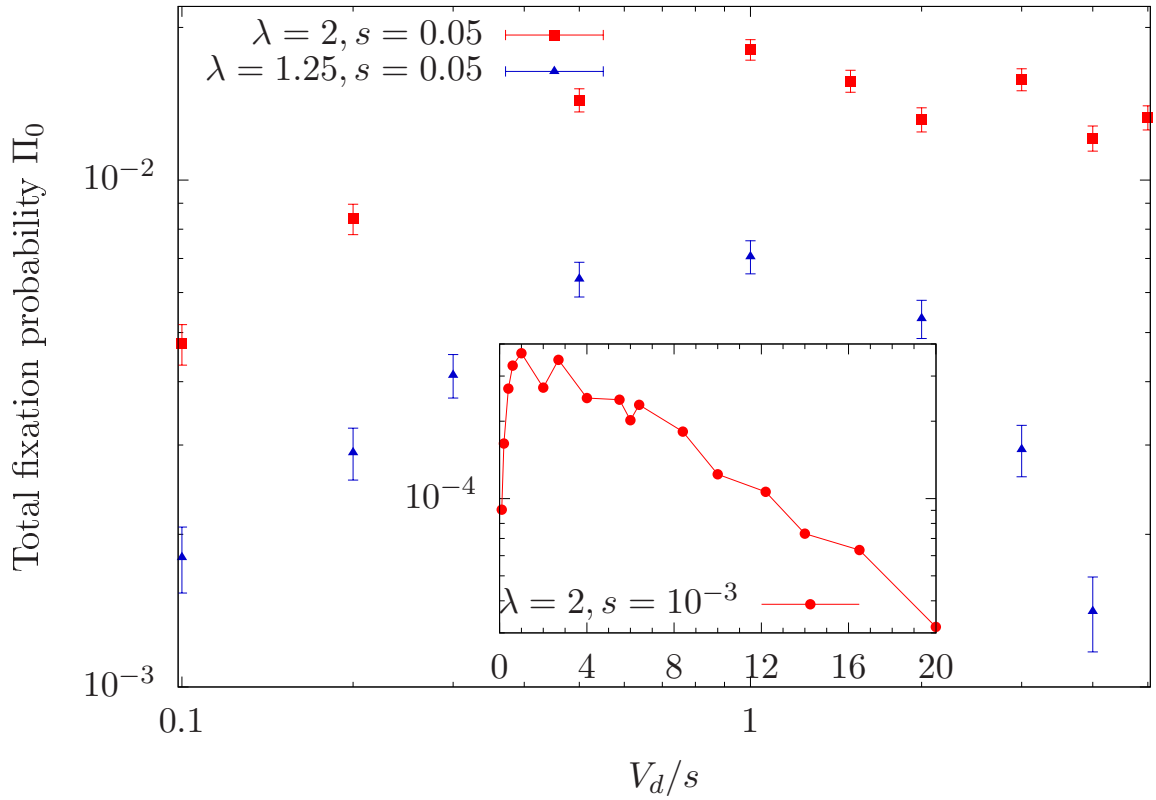


Fig. 3.2 The variation of $\Pi_0$ w.r.t. $V_d$ in Regimes I and III. Main figure: The simulation data (represented using the symbols) corresponding to Regimes I and III. The error bars indicate $\pm 2$ standard error (averaged over $10^5$ independent stochastic realizations). The population size is $N = 10,000$. Inset: Solution to the recurrence relation (3.3) using *Wolfram mathematica* 9.0.1.0 (represented using the circles) corresponding to Regimes I and III. The parameters are $s = 10^{-3}$ and $\lambda = 2$. In both the figures, $\frac{V_d - U_d}{s}$ can take non-integer values.

meaning of this is that with increase in the mutation rate, the background population gets spread out more. Correspondingly, the nonmutator is more likely to appear with more number of deleterious mutations. Hence, $\Pi_0 = \sum_k p_0(k)\pi_0(k)$ could be an increasing or decreasing function of $V_d$ depending on the values of the parameters $s, U_d$, and $V_d$ (see Figs. 3.2 and 3.3), similar to what has been observed by [13].

We have seen that $\pi_0(k)$ and $p_0(k)$ are respectively increasing and decreasing functions of $V_d/s$. This is clearly seen in Table 3.2. The first five rows show that with the rise in $V_d$ such that $k_{max}$ increases only by 1, one more fitness class becomes available to the nonmutator. At the same time, the mutator population spreads out more, and the nonmutator has less

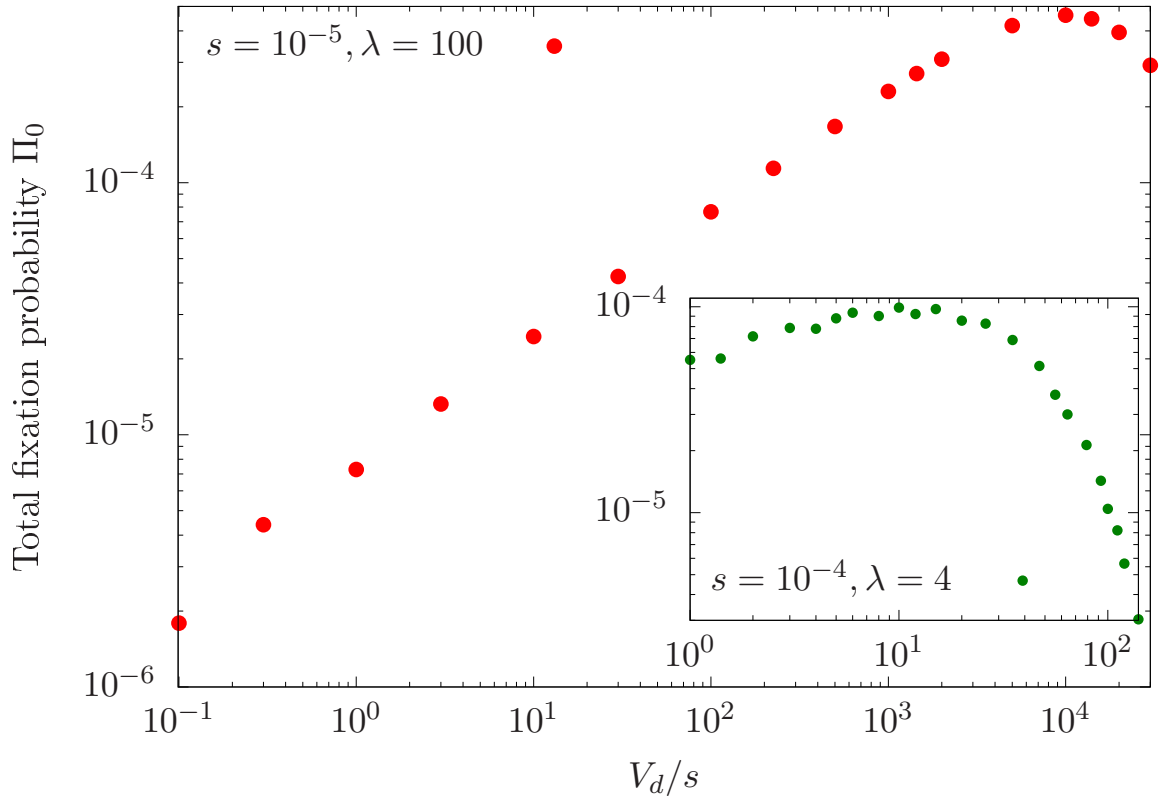


Fig. 3.3 The variation of $\Pi_0$ w.r.t. $V_d$ in Regimes I, II, and III. Main figure: Regimes I, II, and III. The parameters are $s = 10^{-5}$ and $\lambda = 100$. Inset: Regimes II and III. The parameters are $s = 10^{-4}$ and $\lambda = 16$. In both the figures, the solution to the recurrence relation (3.3) is obtained using *Wolfram mathematica* 9.0.1.0 (represented using the circles). Further, the exact values of $\Pi_0$ are obtained for the case in which $\frac{V_d - U_d}{s}$ can assume non-integer values.

chances of appearing in the high fitness classes. For small increments in $V_d$, the positive contribution from $\pi_0(k)$ to $\Pi_0$ exceeds the negative contribution from $p_0(k)$, by which $\Pi_0$ increases. When $V_d/s$ increases from 2 to 3 in Table 3.2, $\Pi_0$ increases by 24.7 per cent. However, for larger increments in $V_d$, the disadvantage conferred by the nonmutator due to fall in $p_0(k)$ exceeds the advantage due to rise in $\pi_0(k)$. Due to the functional forms taken by $\pi_0(k)$ and $p_0(k)$ for the parameters here, the reduction in $\Pi_0$ happens by a larger amount than the increment. For example, as $V_d/s$ increases from 3 to 4 in Table 3.2, $\Pi_0$ decreases by 27.2 per cent. Therefore, $\Pi_0$ decreases overall when $k_{max}$ increases by 1. This process repeats for every further increment in $k_{max}$ by 1. Instead of the mutator strength, when the

| Regime III: Variation of $\Pi_0$ with $V_d$ | | | | | | | | | | |
|---|---|---|---|---|---|---|---|---|---|---|
| $\frac{V_d}{s}$ | $\frac{V_d}{s}\left(1-\frac{1}{\lambda}\right)$ | $\pi_0(k)\times 10^3$ | | | | $p_0(k)\times 10^3$ | | | | $\Pi_0\times 10^4$ |
| | | $k=0$ | $k=1$ | $k=2$ | $k=3$ | $k=0$ | $k=1$ | $k=2$ | $k=3$ | Exact |
| 2.0 | 1.0 | 2.00 | 0.00 | | | 135 | 271 | | | 2.71 |
| 2.4 | 1.2 | 2.75 | 0.40 | | | 91 | 218 | | | 3.36 |
| 3.0 | 1.5 | 3.79 | 1.00 | | | 50 | 149 | | | 3.38 |
| 3.8 | 1.9 | 5.12 | 1.80 | | | 22 | 85 | | | 2.67 |
| 4.0 | 2.0 | 5.45 | 2.00 | 0.00 | | 18 | 73 | 147 | | 2.46 |
| 5.0 | 2.5 | 7.69 | 4.19 | 1.00 | | 7 | 34 | 84 | | 2.77 |
| 6.0 | 3.0 | 9.67 | 5.99 | 2.00 | 0.00 | 3 | 15 | 45 | 89 | 2.02 |

Table 3.2 The data correspond to $s = 10^{-3}$ and $\lambda = 2$ (these parameters are the same as those in the inset of Fig. 3.2). The integer value corresponding to the number in the second column gives $k_{max}$. Both $\pi_0(k)$ and $p_0(k)$ are scaled by $10^3$, while $\Pi_0$ values are scaled by $10^4$. $\pi_0(k)$ values are obtained numerically via solving (3.3), whereas $p_0(k)$ using (3.2). To get the exact values of $\Pi_0$ given in column 11, (3.3) and (2.3) have been numerically solved.

epistatic interactions between the fitness affecting mutations have been studied, a similar behavior has been observed [13].

### 3.3.2 When compensatory mutations are present

The compensatory mutations act against the deleterious mutations, trying to reduce their number in the genome, but at a lower rate [10, 27]. In a mutator population having the respective deleterious and compensatory mutation rates $V_d$ and $V_b$, when a nonmutator with the respective deleterious and compensatory mutation rates $U_d$ and $U_b$ is produced, the ratio $V_b/V_d = U_b/U_d$ remains the same. To solve the problem numerically, we take into account only the mutations from the nearest fitness classes. That is, both the mutator and the nonmutator cannot gain or lose more than one mutation per generation. An exact expression for the population fractions in this case has been obtained by [27]. The mean steady state fitness of the mutator population is given by $\overline{W} = e^{-s\bar{k}}$, where $\bar{k}$ is the average number of mutations carried by the mutator population [27]. Consequently, (3.3) takes the

**The effect of compensatory mutations for small values of $V_b/s$**

| $k_{max}$ | Description of the regime and reference to the corresponding figure | $\Pi/\Pi_0 - 1$ | | |
|---|---|---|---|---|
| | | sign | variation in magnitude as | |
| | | | $V_d \uparrow$ | $\lambda \uparrow$ |
| 0 | $\frac{V_d}{s} < 1$ (Regime I, case I) (Fig. 3.4) | − | ↓ | ↓ |
| | $\frac{V_d}{s} > 1$ (Regime I, case II) (Fig. 3.5) | + | ↑ | ↑ |
| ≥ 1 | $\frac{U_d}{s} < 1$ (Regime II) (Fig. 3.6) | + | | ↓ |
| | $\frac{U_d}{s} > 1$ (Regime III) (Figs. 3.7 ) | + | ↑ | ↓ |

Table 3.3 The summary of the results in Section 3.3.2. The sign of the value of $\frac{\Pi}{\Pi_0} - 1$ given in column 3 determines whether the nonmutators are getting enhanced (+) or suppressed (−) due to the compensatory mutations. The next two columns show the change in $|(\Pi/\Pi_0 - 1)|$ as $V_d$ and $\lambda$ are increased. The symbols ↑ and ↓ stand for increase and decrease, respectively.

form

$$1 - \pi(0) = e^{\left[-\frac{W(0)}{\overline{W}}((1-U_d)\pi(0)+U_d\pi(1))\right]}, \tag{3.6a}$$

$$1 - \pi(k) = e^{\left[-\frac{W(k)}{\overline{W}}(U_b\pi(k-1)+(1-U_d-U_b)\pi(k)+U_d\pi(k+1))\right]}, \tag{3.6b}$$

$$1 - \pi(L) = e^{\left[-\frac{W(L)}{\overline{W}}(U_b\pi(L-1)+(1-U_b)\pi(L))\right]}. \tag{3.6c}$$

Here, due to the presence of the compensatory mutations, irrespective of the fitness class in which the nonmutator appears, it has a non-zero fixation probability. Nevertheless, for large values of $k$, $\pi(k)$ will be a very small quantity. In order to find the numerical values of $\pi(k)$, the recurrence relation is truncated at a large value $k = L$. For arbitrary values of mutation rates and selection, (3.6) can be numerically solved using *mathematica*. The total fixation probability can be calculated using (2.3), where [27]

$$p(k) = \frac{(V_d/V_b)^{k/2}\ J_{k+\frac{(2-\beta_0)}{s/\sqrt{V_bV_d}}}\left(\frac{2}{s/\sqrt{V_bV_d}}\right)}{\sum_{m=0}^{\infty}(V_d/V_b)^{m/2}\ J_{m+\frac{(2-\beta_0)}{s/\sqrt{V_bV_d}}}\left(\frac{2}{s/\sqrt{V_bV_d}}\right)}. \tag{3.7}$$

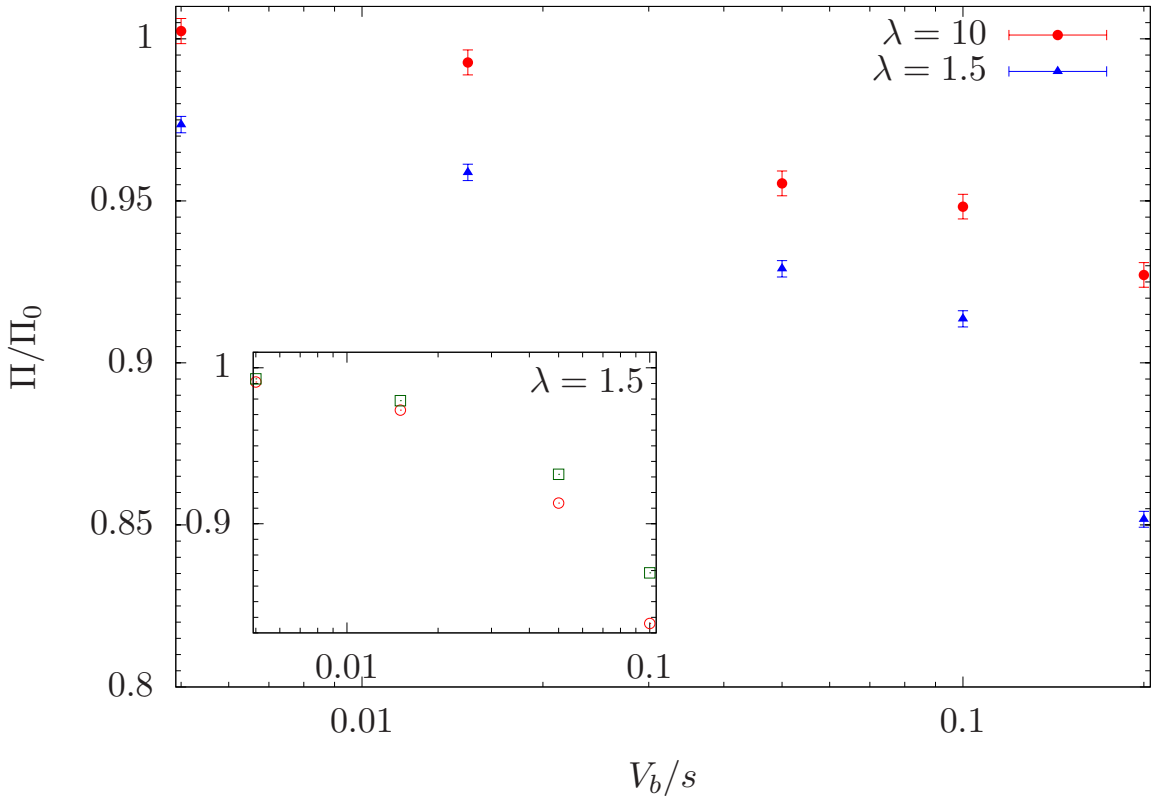


Fig. 3.4 The effect of compensatory mutations in Regime I, case I. Main figure: The simulation data with $10^5$ averaging. The error bars represent ±2 standard error. The parameters are $N = 5,000$, $s = 0.2$, and $V_d = 0.1$. Inset: The numerical solution to (3.6) for the parameters $s = 0.2$, $\lambda = 1.5$, with $V_d = 0.01$ (shown using the circles), and $V_d = 0.05$ (the squares).

Here, $J_{k+\frac{(2-\beta_0)}{s/\sqrt{V_b V_d}}}$ is the Bessel function of the first kind [66]. Further, $\beta_0$ is the minimum eigenvalue taken by $\beta$ in the solution to the expression [27]

$$J_{1+\frac{(2-\beta)}{s/\sqrt{V_b V_d}}}\left(\frac{2}{s/\sqrt{V_b V_d}}\right) - (2 - \sqrt{V_b/V_d} - \beta)\; J_{\frac{(2-\beta)}{s/\sqrt{V_b V_d}}}\left(\frac{2}{s/\sqrt{V_b V_d}}\right) = 0\,. \tag{3.8}$$

In the limit $\sqrt{V_b V_d}/s < 1$, the approximate expression [10, 27]

$$p(k) = p_0(k) + \frac{V_b}{s}\, p_1(k) = e^{-V_d/s}\,\frac{(V_d/s)^k}{k!}\left[1 + \frac{V_b V_d}{s^2}\,\ln\left(\frac{V_d}{sk}\right)\right] \quad \text{if} \quad k \gg 1 \tag{3.9}$$

is helpful in obtaining an analytical understanding here. The main results in this Section can be found in Table 3.3.

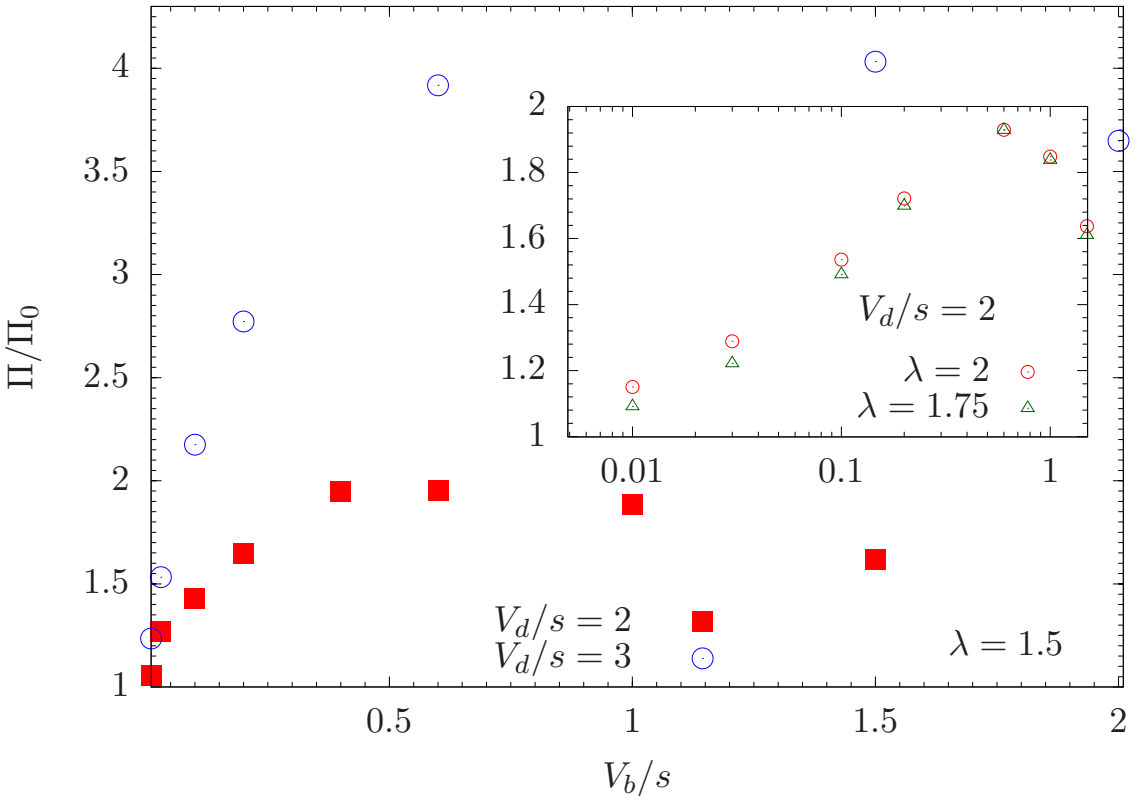


Fig. 3.5 The effect of compensatory mutations in Regime I, case II. Main figure: The simulation data is shown using the filled squares ($10^5$ averaging). The corresponding parameters are $N = 5{,}000$, $s = 0.05$, $V_d = 0.1$ and $\lambda = 1.5$. The open circles represent the numerical solution to (3.6) for the parameters $s = 0.05$, $V_d = 0.15$ and $\lambda = 1.5$. Inset: The open symbols represent the solution to (3.6). The parameters are $s = 0.05$, $V_d = 0.1$ with $\lambda = 1.75$ (triangles) and $\lambda = 2$ (circles).

#### 3.3.2.1 Regime I: $k_{max} = 0$

**Case I: Strong selection regime** ($V_d/s < 1$)

From Fig. 3.4, we see that the compensatory mutations suppress the fixation of the nonmutators, as observed in the previous Chapter [10]. The nonmutators having higher mutation rates (lower $\lambda$) suffer higher reductions in the fixation probability. The main figure of Fig. 3.4 captures this trend. When $s > V_d > U_d$, neither the mutator nor the nonmutator will be subject to the onslaught of detrimental mutations [67], and the population remains localized around class 0. The deleterious mutations try to reduce the fraction of mutators (nonmutators) present in the fitness class 0, while the compensatory mutations oppose it

at a rate $V_b$ ($U_b$) < $V_d$ ($U_d$). For a given background mutation rate $V_d$ and selection coefficient $s$, a nonmutator with a lower value of $\lambda$ will have a higher $U_d$ (and a higher $U_b$) value which is disadvantageous. This explains why $\Pi/\Pi_0$ displays the trend in the main figure of Fig. 3.4.

Note that the inset of Fig. 3.4 shows the variation of $\Pi/\Pi_0$ w.r.t. $s/V_d$. It can be observed that when $V_b$, $s$ and $\lambda$ are held constants, the compensatory mutations resist the nonmutator fixation more if the deleterious mutation rate of the background is low. This is because when $V_d$ is low relative to $V_b$, the compensatory mutations help the mutator population to withstand the build-up of detrimental mutations more.

**Case II: Weak selection regime** ($V_d/s > 1$)

In this regime, $\Pi/\Pi_0$ is a nonmonotonic function of $V_b$ (see Fig. 3.5) and an increasing function of $\lambda$. The compensatory mutations enable the fixation of nonmutators appearing in fitness classes $k > k_{max} = 0$. This causes a substantial relative increase in the total number of classes from which the fixation can happen with a non-negligible probability. Further, for $k < V_d/s$, each newly contributing fitness class will contribute to $\Pi$ by a factor proportional to $V_d/s$ owing to the form taken by $p(k)$. Hence, the total fixation probability increases by a very high amount in this case (since $V_d/s > 1$). This can be seen in Fig. 3.5. (Note that $\frac{\Pi}{\Pi_0}$ can be as large as 4.) Moreover, $\frac{\Pi}{\Pi_0}$ increases with $V_d/s$. This is obvious from the main figure of Fig. 3.5.

The inset of Fig. 3.5 captures an increasing trend of the ratio of the fixation probabilities $\frac{\Pi}{\Pi_0}$ w.r.t. $\lambda$. Since $U_d \geq s$, unlike the strong selection regime [67], the nonmutator can accumulate deleterious mutations. Because $U_d > U_b$ and $U_b/U_d$ being a constant, a lower value of the mutation rate of the nonmutator (higher value of $\lambda$) is more advantageous here. This physically explains the increasing behavior of $\frac{\Pi}{\Pi_0}$ with $\lambda$.

Since the compensatory mutation rate for the mutator population is greater than that of the nonmutators, we anticipate the mutators to be favored when $V_b$ is present. This means that $\frac{\Pi}{\Pi_0}$ is expected to decrease with $V_b$. Indeed, we see from Fig. 3.5 that $\frac{\Pi}{\Pi_0}$ decreases with $V_b$ following the an initial rise.

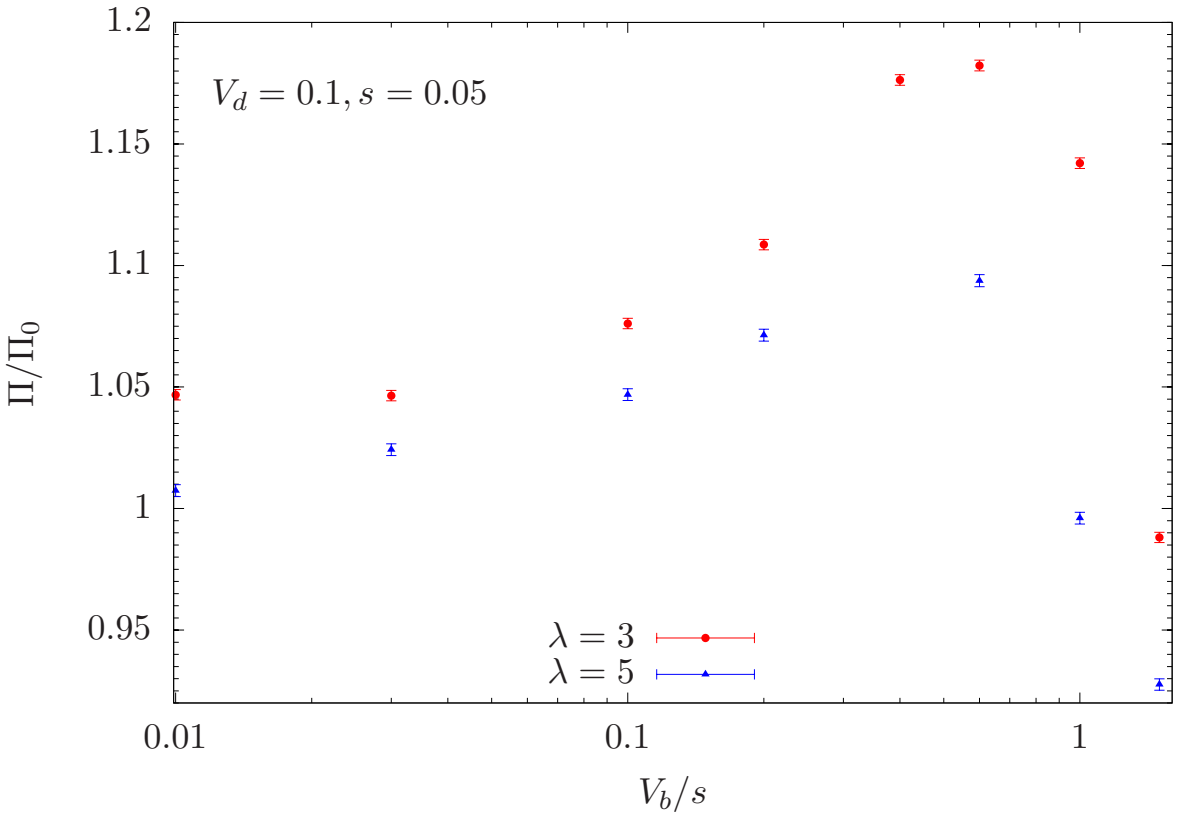


Fig. 3.6 The effect of compensatory mutations in Regime II. The simulation data is shown using the symbols ($10^5$ averaging). The error bars represent ±2 standard error. The parameters are $N = 5{,}000$, $s = 0.05$, $V_d = 0.1$ with $\lambda = 3$ (the circles) and $\lambda = 5$ (the triangles).

#### 3.3.2.2 Regime II: $k_{max} = \lfloor V_d/s \rfloor$ or $\lfloor V_d/s \rfloor - 1$

Here, even when the mutation rate of the nonmutator is neglected, it has been observed that $\Pi/\Pi_0$ exhibits a nonmonotonic behavior [10] w.r.t. the variation in $V_b$. When the nonmutator has a significantly high mutation rate, we want to know how the results are affected. From Fig. 3.6, we can clearly see that a nonmutator with a smaller value of $\lambda$ confers a higher advantage.

#### 3.3.2.3 Regime III: $k_{max} = \lfloor (V_d - U_d)/s \rfloor$

The most dominant "additional" contribution to $\Pi$ due to compensatory mutations comes from the factor $\frac{V_b}{s} \sum_k \pi_0(k)\ p_1(k)$, which is positive. Due to this, $\Pi/\Pi_0$ is an increasing function of $V_b/s$ for small values of $V_b/s$ as we can see from Fig. 3.7. Moreover, in this

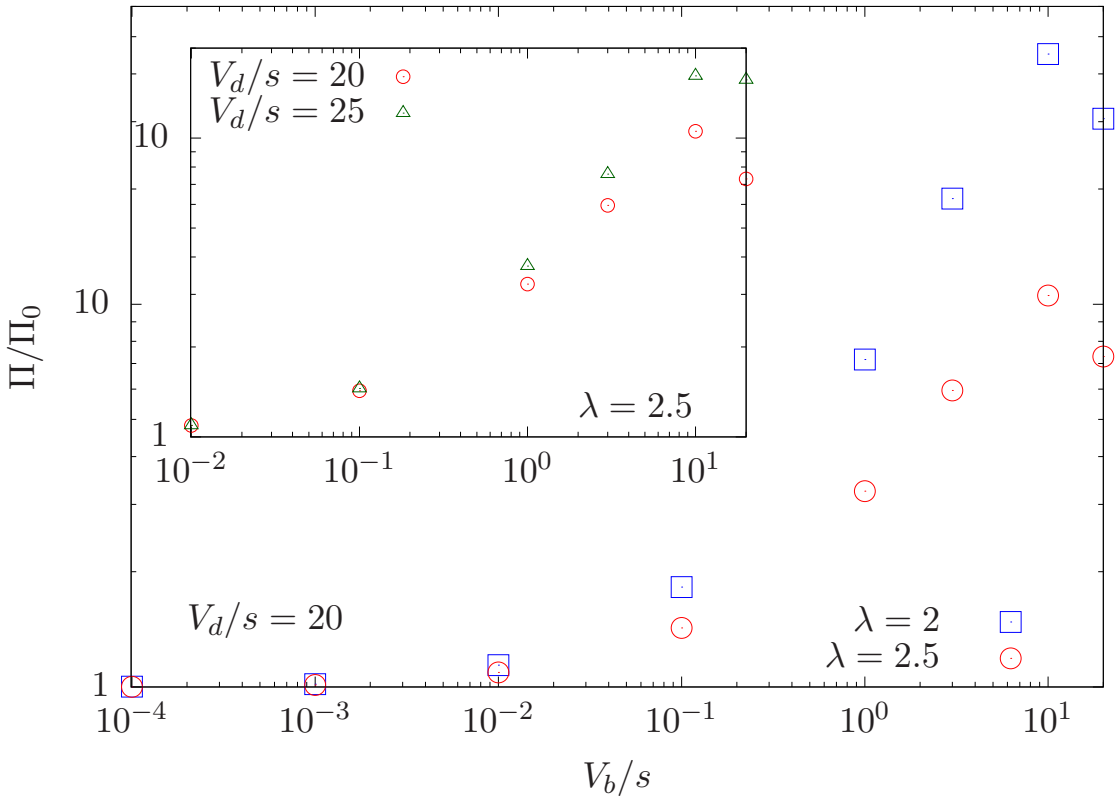


Fig. 3.7 The effect of compensatory mutations in Regime III. The symbols represent the numerical solution to (3.6) for $s = 5 \times 10^{-3}$ (for both the main figure and inset). Main figure: Variation of the advantage gained by the nonmutator w.r.t. $\lambda$ for $V_d/s = 20$. Inset: Variation of the advantage associated with the nonmutator w.r.t. $V_d$ for $\lambda = 2.5$.

regime, the compensatory mutations can magnify the fixation probability by an order of magnitude or more. The numerical solution to (3.6) for the parameters $V_d = 0.1$, $s = 5\times10^{-3}$, and $\lambda = 2$ yields $\pi(0) = 2.6\times10^{-2}$ and $p(0) = 5.6\times10^{-2}$ when $V_b/s = 10$, whereas $\pi_0(0) = 1.8\times 10^{-1}$ and $p_0(0) = 2.1\times10^{-9}$ in the absence of the compensatory mutations. Therefore, the huge increments in the population fractions corresponding to the small $k$ values account for the hikes in the fixation probabilities by substantial amounts.

The inset in Fig. 3.7 indicates that $\Pi/\Pi_0$ is an increasing function of $V_d$ similar to the trend in Case II in Section 3.3.2.1. The main figure in Fig. 3.7 shows that the relative increase $\Pi/\Pi_0$ in the fixation probability decreases with increase in $\lambda$.

In this regime also, as $V_b/s$ increases to large values, higher order terms contribute and $\Pi/\Pi_0$ exhibits a decreasing behavior, which is not unexpected (see Fig. 3.6 and Case II in Section 3.3.2.1 also).

## 3.4 Discussion

### 3.4.1 Summary of the results

A nonmutator appearing in an adapted mutator population confers a selective advantage and reaches fixation [6, 3]. We have learnt in the previous Chapter that when the fitness landscape is non-epistatic, the chances of fixation of the nonmutator increases with the background mutation rate, assuming the mutation rate of the nonmutator is negligibly small compared to the mutation rate of the mutator and the selection coefficient. However, in the present Chapter, we find that in the more realistic scenario in which the nonmutator can undergo mutations, the fixation probability $\Pi_0$ manifests a nonmonotonic behavior w.r.t. the increase in the mutation rate of the background population. When the difference $(V_d - U_d)$ between the mutation rates is less than the selective cost $s$ of a mutation, we see that for the ratio $V_d/s < (>)\ 1$, the value of $\Pi_0$ rises (drops) with increment in $V_d$ [12]. On the other hand, if $(V_d - U_d)$ exceeds $s$, $\Pi_0$ increases (falls) as a function of $V_d$ for $U_d/s < (>)$ $\lambda = V_d/U_d$ [12]. This behavior is a result of the fact that $\Pi_0 = \sum_k \pi_0(k)p_0(k)$, where $p_0(k)$ - the probability of the nonmutator to appear with $k$ mutations (which is the same as the fraction of the mutator population carrying $k$ mutations) - is a decreasing function of $V_d$, while $\pi_0(k)$ - the probability to attain fixation if it carries $k$ mutations - is an increasing function of $V_d$. For nonmutators with the mutation rates close to that of the mutator, we see that $\Pi_0$ behaves like a non-smooth function and declines in magnitude overall for $(V_d - U_d) > s$, when $V_d$ (see Fig. 3.2) is varied.

The compensatory mutations alleviate the accumulation of deleterious mutations. This means that the presence of compensatory mutations is expected to boost the mutator population and reduce $\Pi_0$. On the contrary, for the case $\lambda \to \infty$, it has been shown that the nonmutators will be benefited if $V_d > s$ [10]. In this Chapter, we examine the fate of non-

mutators when $\lambda$ is finite and the compensatory mutations can occur. We see that the advantage acquired by the nonmutator increases with the value of $V_d$. Moreover, this advantage increases with $\lambda$ in the regime $(V_d - U_d) < s$; $V_d > s$, while it drops as a function of $\lambda$ in the regime $(V_d - U_d) > s$. In the latter regime, we observe that for small values of $\lambda$, the compensatory mutations can enhance possibility of the nonmutator fixation by an order of magnitude or more. Given the very small likelihood of a nonmutator with a small value of $\lambda$ to take over the mutator population when only the deleterious mutations are present, the availability of compensatory mutations provides a possible mechanism (also, see Section 3.4.4) by which the mutation rate reduction can happen by small amounts.

### 3.4.2 Connection with real populations and biological relevance

The analysis in this Chapter focuses on the fixation of a single nonmutator. In addition to that, as we have elucidated in Section 3.2, we treat that the nonmutator appears only after the mutator population reaches a steady state. There are two limitations to this approach: 1) a nonmutator can appear before the mutator population attains the steady state and 2) not all the asexual populations are "large" enough to have a steady state. The detailed discussions on these shortcomings due to the assumptions in the model can be found in Section 3.4.5 as well as in the articles by [10] and [13] in which similar treatments have been made.

However, whether our theoretical predictions can be observed in real populations or not needs to be explored. For this purpose, we will investigate the values of the parameters such as $s$, $V_d$, $U_d$, and the population size $N$ in the case of the asexual microbe *E. coli* on which numerous evolution experiments have been performed. The value of the selection coefficient has been observed to vary from $10^{-3}$ [68] to $10^{-1}$ [69]. The mutation rate of the wild type *E. coli* strain is $2.7 \times 10^{-3}$ per genome per replication [26]. The mutation rate $V_d$ of the *E. coli* mutator strain can be as high as 40 [5] to 150 [6] times that of the wild type, though mutators of strength of the order $10^4$ are reported to have been observed [52]. In the experiment by [5], $N \sim 10^{10}$, whereas for the one by [6], $N \sim 10^7$ [54]. Note that the mutation rate of the nonmutator in the experiment by [6] has been estimated to be $40 - 60$

per cent of that of the mutator which corresponds to $\lambda \sim 2$, while in the case of a mutation reduction experiment on yeast [34], $\lambda \sim 4$. We have used the values of $s$, $V_d$, and $\lambda$ in the range $10^{-5} - 10^{-1}$, $10^{-6} - 10^{-1}$ per genome per generation, and $1.02 - 10^2$, respectively.

One important thing we need to confirm is the presence of a steady state. Based on the studies of [63] and [62], we take $N\ s\ e^{-V_d/s} \sim 10^2$ as the condition necessary to guarantee a steady state [13]. Using $N \sim 10^{10}$ and $s \sim 10^{-2}$, we see that the upperbound of $V_d/s \sim 14$. For this maximum value of $V_d/s$, it is possible to test all the results we have predicted. Note that for the parameters considered in the plots in Fig. 3.3, the population size needed for the existence of a steady state is too large in the biological limits.

To the best of our knowledge, the compensatory mutation rate has not been experimentally measured yet. Instead, measurements on the beneficial mutation rates are available. One such experiment by [57] on adapting *E. coli* populations has revealed that this rate can be as high as $\sim 10^{-5}$ per genome per generation (approximately 1 per cent of the deleterious mutation rate). Since this is an adapting population, this value could be an overestimate for the populations considered in this Chapter. Nevertheless, we use this value as an upperbound for the compensatory mutation rate. Moreover, because we are working with mutator populations, the elevated mutation rates are applicable to compensatory mutations as well. Therefore, when $V_d/s \gtrsim 10$, we set the maximum value of $V_b/s$ to be $\sim 10^{-1}$ corresponding to which the nonmutator fixation for small $\lambda$ values can be improved by $\sim 100$ per cent (see Fig. 3.7). The values of $V_b/s$ larger than $10^{-1}$ are extremely unlikely to be observed in biological populations.

### 3.4.3 Comparison with experiments

For a nonmutator produced at a constant rate $b$ in a large mutator population of size $N$, the fixation time [61] $T = (Nb\Pi)^{-1}$ [70, 10, 13], assuming $Nb \ll 1$. (To know more about the fixation time, refer to Section 4.4.4.) The fixation time has been measured in two recent mutation reduction experiments on *E. coli* [6] as well as *S. cerevisiae* [34]. According to the former experiment, $T$ ($\Pi$) is lowered (increased) as $U_d$ is increased (reduced), while as per the latter experiment, $T$ ($\Pi$) rises (falls) with the increment (decrement) in $U_d$. The behav-

ior of $T$ in the experiment by [6] is consistent with the analysis in this Chapter. On the other hand, assuming the background mutation rate remains a constant, the trend observed in the experiment by [34] cannot be explained on the basis of our study. However, it is not clear to us if the background mutation rates have been the same or not in this experiment. If the mutation rates of the resident populations are not the same for the two reductions reported by [34], it could be explained using our theory.

### 3.4.4 Comparison with previous theoretical studies

A previous study [13] (see Chapter 4) sheds light on the fact that even if the nonmutator does not undergo mutations ($\lambda = \infty$), $\Pi_0$ exhibits a nonmonotonic behavior (an initial increase followed by a decline) as a function of $V_d$, similar to that in Figs. 3.2 and 3.3, provided epistatic interactions are present and the value of the epistasis parameter is below a critical value. In addition to this, a preliminary numerical inspection in the same article suggests that for any value of $\lambda$, $\Pi_0$ can be a decreasing function of $V_d$ if the epistasis is below the corresponding critical value. The corollary of this finding is that irrespective of the value taken by $\lambda$, $\Pi_0$ can remain an increasing function of $V_d$ if the value of the epistasis parameter is above this limit. This is a possible mechanism which could operate against the resilience of high mutation rate populations to reduction in the mutation rate. However, for finite values of $\lambda$, the role of epistasis has to be investigated more in detail to unravel the exact functional dependence of the critical value of epistasis on parameters such as $s$, $V_d$, and $\lambda$ (see Section 3.4.5).

### 3.4.5 Conclusions and open questions

Our results indicate that the compensatory mutations and the mutation rate of the nonmutator can play a crucial role in the nonmutator fixation. As discussed in Section 3.4.4, the role of epistatic interactions on the fixation of a low mutation rate allele has been investigated [13] excluding these two factors. Given that the lowering of the mutation rate becomes highly unlikely in a high mutation rate background when the selection is weak,

and the compensatory mutations as well as a large value of the epistasis parameter [13] could help in mitigating the mutation rate, a complete study taking into account the effects of epistasis, compensatory mutations, and a non-zero mutation rate of the nonmutator can pave the way to a better understanding of the process of mutation rate reduction.

As we have explained in Section 3.4.2, there are limitations in the assumptions we have made in our models. These assumptions can be relaxed. The article by [32] studies the case in which the beneficial alleles appear at a constant rate in an asexual population undergoing deleterious mutations. Such an approach can be used in our model as well due to the selective advantage possessed by the nonmutator. However, when the selection is much greater than the mutation rates, this has already been done by [7]. The effect of finite population size on mutation rate evolution has been explored by [7], [22], and [10]. Nevertheless, using (2.1) and the results from the article by [27], a numerical evaluation of the fixation probability corresponding to a particular time $t$ could be possible. One could also attempt for analytical approximations in this case in a future study.

All the studies mentioned here except the one by [13] have examined the process of mutation rate reduction on a single-peaked multiplicative landscape. More complicated landscapes could be used to check the robustness of our results. Moreover, the physiological costs [58–60, 71, 2] associated with the decline in the mutation rates can be included in a further study to gain an insight into its effect on mutation rate evolution.

# Chapter 4

# Fixation of a nonmutator in the presence of epistasis

## 4.1 Introduction

In the last two Chapters, we have considered a simple non-epistatic fitness landscape in which the effect of each mutation is the same. In the current Chapter, we aim to understand the role of epistatic interactions between the fitness affecting mutations in the process of mutation rate reduction in a large adapted population [13]. Further, the influence of the joined action of the forces of mutation and selection in the presence of epistasis on the decline in mutation rate will be investigated in detail here [13].

All the theoretical studies on the evolution of mutation rate in adapted populations [72, 7, 73, 10] except the article by Jain and Nagar [49] have considered mutations to contribute independently to fitness, which is otherwise known as a non-epistatic fitness landscape. An epistatic landscape is a more general description of the actual biological scenario, since intergenetic interactions cannot be ignored. There have been numerous experiments demonstrating the presence of epistasis [74, 75, 24, 76–79]. The effect of epistasis on asexual populations has been explored theoretically as well [49, 63, 8, 80, 29, 62, 81, 82]. Among the theoretical studies on adapted populations with the inclusion of epistasis, Campos [80] has studied the process of fixation of a mutant with a direct selective advantage in a population

that is undergoing deleterious mutations at a constant rate, while Jain and Nagar [49] have explored the fixation of mutators. The focus in this Chapter is to understand the fixation of nonmutators in an adapted mutator population in the presence of epistatic interactions.

In the current study, we find that synergistic epistasis (two or more mutations interact with each other to produce larger decline in relative fitness) rises the fixation probability of a rare nonmutator, whereas antagonistic or diminishing epistasis (two or more mutations interact with each other to produce smaller decline in relative fitness) lowers it. When selection is much stronger compared to mutation rate, the fixation probability is independent of epistasis, and increases with mutation rate. This matches with the result in Chapter 2 [10] in the absence of epistasis. Below a particular value of antagonistic epistasis, we see that the fixation probability initially increases, and then decreases with mutation rate of the background. In the presence of synergistic interactions, as selection is varied, the fixation probability decreases overall, with damped oscillations. Our results can be merged with that of Kondrashov [63] to deduce that synergistic epistasis is doubly advantageous as it not only lowers the rate of accumulation of deleterious mutations, but also increases the chances of mutation rate reduction. On the other hand, antagonistic epistasis is doubly disadvantageous to an asexual population due to the faster rate of accumulation of harmful mutations [8], as well as the lower probability of mutation rate decline.

## 4.2 Models and methods

### 4.2.1 Details of stochastic simulations

We consider a large asexual population of haploid individuals of size $N$ on a fitness landscape [8]

$$W(k) = (1-s)^{k^{\alpha}}, \tag{4.1}$$

where $0 < s < 1$ is the selection coefficient and $\alpha > 0$ is the epistasis parameter. Here, $k$ is the number of deleterious mutations carried by the genome, represented using a binary sequence of length $L \to \infty$, of an individual. We also denote $k$ as the fitness class since the

fitness is decided by $k$. Antagonistic epistasis is modeled by $\alpha < 1$ and synergistic epistasis by $\alpha > 1$. $\alpha = 1$ implies no epistasis. Biologically, (4.1) represents a genome carrying infinite number of biallelic loci that are equivalent to each other, and the effect of a new mutation at any locus depends on the number of mutations already present in the genome. The probability that the genome of an individual accumulates $x$ number of deleterious mutations at the rate $V_d$ is Poisson distributed as given below.

$$M_{V_d}(k \to k+x) = e^{-V_d} \frac{(V_d)^x}{x!} . \tag{4.2}$$

The population evolves via standard Wright-Fisher (W-F) dynamics [62], where the population size is held constant in each non-overlapping generation. In the W-F process, corresponding to each individual, we randomly assign an individual in the previous generation as its parent. This undergoes mutation followed by reproduction with a probability proportional to its fitness.

Asexual populations can go extinct via the accumulation of deleterious mutations (see section 4.4.1), a process known as Muller's ratchet [47, 63]. Populations of large size with extremely small ratchet speed, that have been evolving for long timescales without changes in the environment can attain a steady state due to mutation-selection balance. For a population in steady state, the mean fitness and the population fractions corresponding to various genotypes remain time independent. In this study, it is assumed that the nonmutator with mutation rate $U_d = V_d/\lambda$, where $\lambda > 1$ is the strength of the mutator, appears when the mutator population is in steady state (see Chapter 3). The nonmutator also evolves via standard Wright-Fisher process, and (4.1) and (4.2) are applicable for it with $V_d$ being replaced by $U_d$. Here, we choose populations of size large enough to fulfill the criterion that the number of individuals carrying the minimum number of mutations (least loaded class) in steady state is at least 100 so that Muller's ratchet operates at a very small speed [63] (also, see Appendix B.5).

In simulations, we consider the population to be in steady state initially. This assumption is verified by ensuring that the population eventually reaches mutation-selection bal-

ance by observing single run plots corresponding to the given parameter set of $s$, $V_d$, and $\alpha$. Moreover, we confirm that the population fractions stabilize at values predicted by (B.5). Fig. 4.1 in the Appendix shows qualitative comparison of the fixation probability of a nonmutator created at time $t = 0$ in a population that is in steady state (filled symbols) with that of a nonmutator produced after a time interval of $10/s$ generations in a population which initially has no deleterious mutations (open symbols). In this Chapter, each simulation point (excluding the points in the single run plot Fig. 4.3) is averaged over $10^5$ independent stochastic runs. All simulations except those for Fig. 4.1 have assumed $N = 4{,}000$. Apart from Fig. B.2, only nonmutators with $\lambda = 100$ have been considered here. All the numerical calculations have been done using *Wolfram Mathematica* 9.0.1.0.

### 4.2.2 Analysis

Due to the lower rates of deleterious mutation accumulation and fitness decline, the nonmutator appearing in mutator background in an adapted population is effectively a beneficial allele. The fixation probability of such an allele can be studied using the branching process [9]. The details [32] are described below.

The extinction probability $\epsilon(k,t)$ of a nonmutator arising with $k$ deleterious mutations in generation $t$ in a very large population of mutators is given by

$$\epsilon(k,t) = \sum_{n=0}^{\infty} \psi_n(k,t) \left[ \sum_j M_{U_d}(k \to j)\, \epsilon(j, t+1) \right]^n . \tag{4.3}$$

The above equation assumes that the extinction probabilities are independent of each other. Here, $\psi_n(k,t)$ is the probability that the nonmutator will give rise to $n$ offspring in generation $t$. $M_{U_d}(k \to j)$ is the Poisson distributed probability of the nonmutator to mutate from class $k$ to $j > k$.

If the probability of reproduction of the nonmutator is assumed to be Poisson distributed, we get

$$\psi_n(k,t) = e^{-w(k,t)}\, \frac{w^n(k,t)}{n!} . \tag{4.4}$$

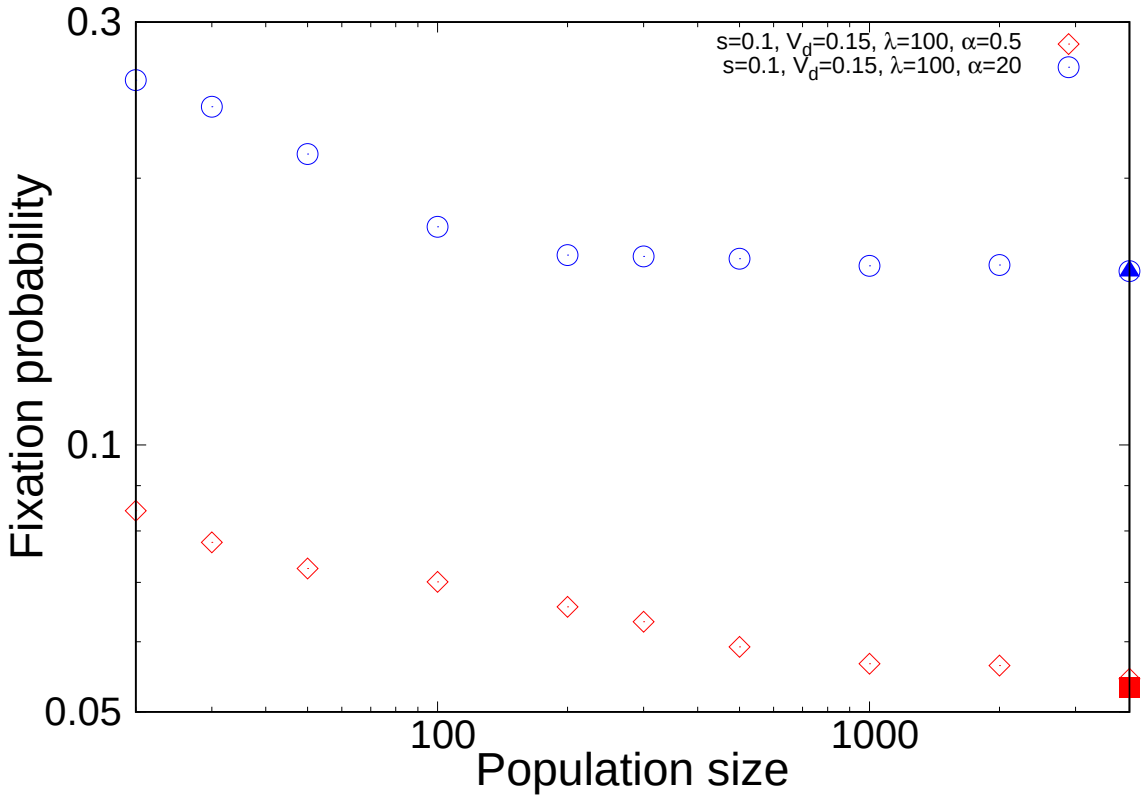


Fig. 4.1 Variation of the fixation probability with population size. A nonmutator is allowed to appear at time $t = 10/s$ in a population that is initially at its fittest genotype. For large values of $N$ (= 4,000), the result in this case (shown using the open symbols) is in good agreement with the fixation probability of a nonmutator arising in a population which is initially in steady state (filled symbols). The parameters are $s = 0.1$, $V_d = 0.15$, $\lambda = 100$ with $\alpha = 20$ (blue symbols), and $\alpha = 0.5$ (red symbols).

In this expression, the mean of the Poisson distribution equals the absolute fitness of the nonmutator, and hence we write

$$w(k,t) = \frac{W(k)}{\overline{W}(t)} \,. \tag{4.5}$$

Note that $\overline{W}(t) = \sum_{k=0}^{\infty} W(k)\ p(k,t)$ is the mean fitness of the background population with $p(k,t)$ being the fraction of population having $k$ deleterious mutations in generation $t$ (see Appendix B.1 for details on the expression $p(k)$ for population fraction in steady state). With the help of (4.4) and (4.5), we rewrite (4.3) as

$$\epsilon(k,t) = e^{-\frac{W(k)}{\overline{W}(t)}\left[1-\sum_j M_{U_d}(k\to j)\ \epsilon(j,t+1)\right]} \,. \tag{4.6}$$

The nonmutators are considered established if they do not go extinct. Due to the selective advantage possessed by the nonmutator, the establishment eventually leads to fixation, and these two are taken to be the same here. Hence, the fixation probability is $\pi(k,t) = 1-\epsilon(k,t)$. Therefore, from (4.6), it follows that

$$1-\pi(k,t) = e^{-\frac{W(k)}{\overline{W}(t)}\sum_i e^{-U_d}\ \frac{(U_d)^i}{i!}\ \pi(i+k,t+1)} \,, \tag{4.7}$$

since $\sum_{i=0}^{\infty} M_{U_d}(k\to i+k) = 1$. For a nonmutator that arises in the background population after the attainment of steady state, (4.7) becomes

$$1-\pi(k) = e^{-\frac{W(k)}{\overline{W}}\sum_i e^{-U_d}\ \frac{(U_d)^i}{i!}\ \pi(i+k)} \,. \tag{4.8}$$

We get the fixation probability of a nonmutator that is produced in a genetic background having $k$ number of deleterious mutations by solving (4.8). However, the mutator population is distributed across so many fitness classes, and the nonmutator can appear in any of these backgrounds. Hence, the total fixation probability can be calculated only by taking into account all the possible genetic backgrounds. The probability of the nonmutator to appear in fitness class $k$ is the same as the fraction $p(k)$ of the background population

in that class. This is an important concept which plays a major role in understanding the results. As explained above, the *total fixation probability* receives contributions from both the *fraction of background population* and the probability of *fixation*, and therefore, can be expressed as

$$\Pi = \sum_k p(k)\,\pi(k)\,. \tag{4.9}$$

The above expression is applicable for very large populations in which the effect of genetic drift can be neglected.

## 4.3 Results

As considered by [10], for strong mutators which have very high mutation rates ($\lambda \gg 1$) compared to the nonmutator [4, 36], we can neglect $U_d$ to write

$$1-\pi(k) = \exp\left[-\frac{W(k)}{\overline{W}}\pi(k)\right]\,. \tag{4.10}$$

If the nonmutator has negligible mutation rate, we can directly obtain (4.10) from (4.3) assuming steady state, since $\pi(k) = 1-\epsilon(k)$. Using (B.4), the average fitness of mutators in steady state is found to be $\overline{W} = (1-s)^{\overline{k^\alpha}} \approx e^{-V_d}$. This is otherwise the classical result obtained by [65] for the mean fitness of an asexual population. Following the approach of [10], taking logarithm on both sides of (4.10), and neglecting terms of order greater than 2 from the expansion $\ln(1-x) = -x - x^2/2 - ...$, we can solve the resulting quadratic equation to get

$$\pi(k) = \begin{cases} 2\left(\frac{W(k)}{\overline{W}} - 1\right) \;=\; 2s\left(\overline{k^\alpha} - k^\alpha\right) & \text{if } \; k < \lfloor (V_d/s)^{1/\alpha} \rfloor \\ 0 \;\text{ otherwise}\,. \end{cases} \tag{4.11}$$

Here, $\lfloor (V_d/s)^{1/\alpha} \rfloor$ is the largest integer corresponding to $(V_d/s)^{1/\alpha}$, and $\overline{k^\alpha}$ is given by (B.4). We see that with rise in the background mutation rate $V_d$, $\pi(k)$ increases, which is rather expected. The intuitive meaning of (4.11) is that the effective selective advantage of a nonmutator carrying $k$ mutations, appearing in the background having mean fitness $e^{-s\overline{k^\alpha}}$ is

| **Class 0 mutator frequency** $p(0)$ | | |
|---|---|---|
| | $\left(\frac{V_d}{s}\right) > 1$ | $\left(\frac{V_d}{s}\right) < 1$ |
| $\alpha \leq 1$ | $p(0) = (2\pi)^{\frac{\alpha-1}{2}} \frac{\sqrt{\alpha}\left(\frac{V_d}{s}\right)^{\frac{\alpha-1}{2\alpha}}}{e^{\alpha\left(\frac{V_d}{s}\right)^{1/\alpha}}}$ | $p(0) = \left(1 - \frac{V_d}{s}\right)$ if $\alpha \ll 1$ |
| $\alpha > 1$ | $p(0) = \left(1 + \frac{V_d}{s} + \frac{(V_d/s)^2}{2^\alpha}\right)^{-1}$ if $\alpha > \frac{\ln(V_d/s)}{\ln 2}$ | $p(0) = \left(1 + \frac{V_d}{s} + \frac{(V_d/s)^2}{2^\alpha}\right)^{-1}$ |
| $\alpha = 2$ | $p(0) = \left[I_0\left(2\sqrt{\frac{V_d}{s}}\right)\right]^{-1}$ | $p(0) = \left[I_0\left(2\sqrt{\frac{V_d}{s}}\right)\right]^{-1}$ |

Table 4.1 The above expressions are derived in Appendices B.1 and B.2. Expressions in the last row are exact, while the other ones are approximations. The symbols $V_d$, $s$ and $\alpha$ respectively represent the mutation rate of the background population, selection coefficient and epistasis parameter.

$s(\overline{k^\alpha} - k^\alpha)$, and its fixation probability is twice that. The latter statement follows from the single locus model [44, 45].

Plugging (B.5) and (4.11) in (4.9), and performing the resulting sum give rise to

$$\Pi = \frac{2V_d\,(V_d/s)^{\lfloor (V_d/s)^{1/\alpha} \rfloor}}{\left(\lfloor (V_d/s)^{1/\alpha} \rfloor !\right)^\alpha}\, p(0)\,. \tag{4.12}$$

The derivations for the frequency $p(0)$ of the background population with zero deleterious mutation are given in Appendices B.1 and B.2, and the final expressions are summarized in Table 4.1. Based on whether the selection is strong ($V_d/s < 1$) or weak ($V_d/s > 1$) and the epistasis is antagonistic ($\alpha < 1$) or synergistic ($\alpha > 1$), there are four regimes for $\Pi$.

### 4.3.1 Variation of fixation probability with epistasis parameter

#### 4.3.1.1 Weak selection; antagonistic epistasis ($V_d/s > 1$, $\alpha \leq 1$)

For large $(V_d/s)^{1/\alpha}$, with the help of Stirling's approximation $x! \approx \sqrt{2\pi x}\,(x/e)^x$, we obtain

$$\Pi = \frac{2V_d\,(V_d/s)^{(1-\alpha)V_d/s}\, e^{V_d\alpha/s}}{(2\pi V_d/s)^{\alpha/2}}\, p(0)\,. \tag{4.13}$$

Using the result from Table 4.1, we get

$$\Pi = V_d \sqrt{\frac{2\alpha}{\pi}} \left(\frac{s}{V_d}\right)^{\frac{1}{2\alpha}} . \tag{4.14}$$

Expression (4.14) yields the known result [10] for $\alpha = 1$. It is evident that $\Pi \propto V_d^{1-\frac{1}{2\alpha}}$, implying the total fixation probability to be an increasing function of the background mutation rate for $\alpha > 0.5$ and decreasing function for $\alpha < 0.5$, as shown in Fig. 4.2. The value of $\alpha$ at which this transition happens is denoted as $\alpha_c$, the critical value of the epistasis parameter. Corresponding to $\alpha = \alpha_c$, (4.14) gives $\Pi = \frac{s}{\sqrt{\pi}}$. As the mutation rate of a population increases, we expect it to have higher probability to reduce its mutation rate. However, if $\alpha < 0.5$, we see that the higher the mutation rate of a population, the lower is the probability that its mutation rate will decrease. The physical interpretation of this surprising trend is explained in the following paragraph.

Combining (B.9) and (B.12) enables us to write

$$p(k) = \frac{e^{\frac{-\alpha\left(k-(V_d/s)^{1/\alpha}\right)^2}{2(V_d/s)^{1/\alpha}}}}{\sqrt{2\pi\,\frac{(V_d/s)^{1/\alpha}}{\alpha}}} . \tag{4.15}$$

This clearly states that the background population frequency $p(k)$, which is also equal to the probability of the nonmutator to appear with $k$ deleterious mutations, is a Gaussian distribution with mean $(V_d/s)^{1/\alpha}$ and variance $\alpha^{-1}(V_d/s)^{1/\alpha}$. Therefore, in the regime $\alpha < 1$ and $(V_d/s) > 1$, the mutator population will be more spread out for larger values of $V_d$ and smaller values of $\alpha$.

As $V_d$ increases, it is more likely that the nonmutator will appear with higher number of deleterious mutations, which is disadvantageous to the invader population. However, as we saw in (4.11), once the nonmutator appears with a particular number of mutations, its fixation probability $\pi(k)$ increases with $V_d$. This is an advantageous factor associated with $V_d$. Competition between the advantageous and disadvantageous effects of $V_d$ on the nonmutator decides the behavior of its total fixation probability as a function of $\alpha$. As $\alpha$

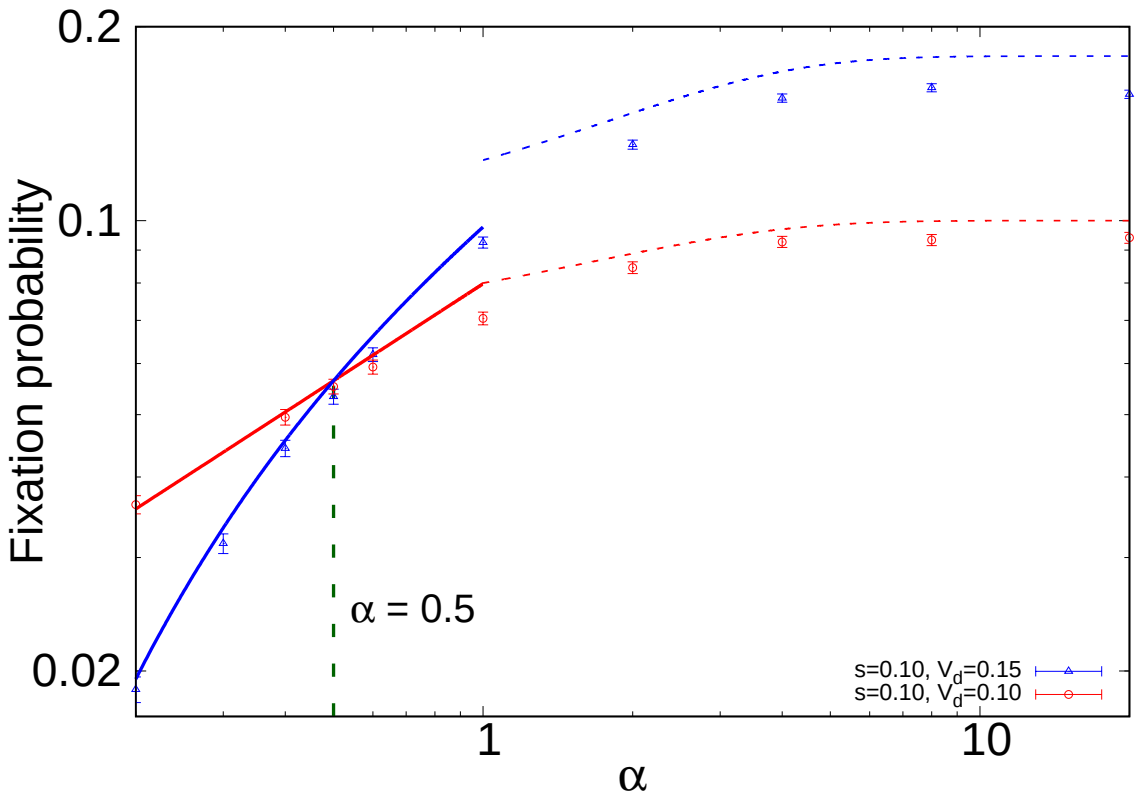


Fig. 4.2 Weak selection with antagonistic and synergistic epistasis. The symbols represent simulation data (red circles for $s = 0.1$, $V_d = 0.1$, and $\lambda = 100$; blue triangles for $s = 0.1$, $V_d = 0.15$, and $\lambda = 100$). Each simulation point is averaged over $10^5$ independent stochastic runs. The error bars stand for $\pm 2$ standard error [14]. The corresponding solid curves indicate (4.14), and the dashed curves represent (4.16). The green vertical broken line is drawn at $\alpha = 0.5$.

falls below 0.5, the disadvantage experienced by the lower mutation rate allele due to its low fitness dominates its advantage of arising in a background that has high mutation rate.

Fig. 4.2, 4.5, and 4.6 show that the trend predicted by (4.14) is observed in finite size populations. Further, in the parameter regime used in the plot, (4.14) is a good approximation for the total fixation probability of a lower mutation rate individual in the strong mutator background.

It has to be noted that the result $\alpha_c = 0.5$ is valid only for the strong mutator background. A discussion on $\alpha_c$ for the case in which the mutation rates of the nonmutator and mutator are comparable (weak mutator background) can be found in Appendix B.6.

#### 4.3.1.2 Weak selection; synergistic epistasis ($V_d/s > 1$, $\alpha > 1$)

We have an analytical expression for $p(0)$ only for the limiting case $\alpha > \frac{\ln(V_d/s)}{\ln 2}$ ($(V_d/s)^{1/\alpha} < 2$), which is given in Table 4.1. The mutation rates of asexual microbes such as *E. coli* and *S. cerevisiae* are measured to be of the order of $10^{-3}$ per genome per generation [26]. The value of selection coefficient for *E. coli* is found to vary from $10^{-3}$ [68] to $10^{-1}$ [69]. Even for the maximum value of $(V_d/s)$ in this case, which is 100, $\alpha \geq 6.7$ ensures that only the first two classes contribute to $\Pi$. In fact, even if $(V_d/s) \sim 10^6$, which could be biologically improbable, $\alpha \geq 20$ guarantees that $\pi(k) = 0$ for $k > 1$. This physically corresponds to two or more mutations interacting with each other to produce lethal effects on the genome. This is illustrated in Fig. 4.3 in the Appendix. Therefore, it follows from (4.12) that

$$\Pi = \frac{2V_d\, V_d/s}{\left(1 + \frac{V_d}{s} + \frac{(V_d/s)^2}{2^\alpha}\right)} \quad \text{if} \quad \alpha > \frac{\ln(V_d/s)}{\ln 2}\,. \tag{4.16}$$

Here, the $\alpha$ dependence of $\Pi$ comes from $p(0)$. For $\alpha \gg \frac{\ln(V_d/s)}{\ln 2}$, epistasis affects neither the fixation probability $\pi(k)$ nor the fraction of background population $p(k)$ of the first two fitness classes. Unsurprisingly, it can be seen that $\Pi$ rises with increase in $\alpha$ initially and reaches its maximum value $2V_d\ (V_d/s)\left(1 + \frac{V_d}{s}\right)^{-1}$, which is independent of $\alpha$. This is captured in Fig. 4.2 (also, see Appendix B.4 where the discrepancy between the results from simulations and analytics has been discussed). It is important to note that if the condition $\alpha > \frac{\ln(V_d/s)}{\ln 2}$ is not satisfied, the nonmutator can arise in fitness classes having low fitness. Owing to this, (4.16) overestimates the actual value of $\Pi$.

Note that for $(V_d/s) \gg 1$ and $\alpha \gg \frac{\ln(V_d/s)}{\ln 2}$, (4.16) simplifies to the known result for fixation probability $\Pi = 2V_d$ [10] of a nonmutator on a non-epistatic fitness landscape, when the selective effects are strong with respect to mutation rate. From (B.5) and (B.13), we see that synergistic epistasis with $\alpha \gg \frac{\ln(V_d/s)}{\ln 2}$ causes the background population to be concentrated around fitness class 1, and therefore, $p(1) \approx 1$ for $(V_d/s) \gg 1$. The fixation probability of a nonmutator with a single deleterious mutation is $\pi(1) \approx 2V_d$ from (4.11) when $(V_d/s) \gg 1$. Thus, both $p(1)$ and $\pi(1)$ give the same results as $p(0)$ and $\pi(0)$, respectively when selection is very strong and epistasis is either absent [10] or synergistic (see section 4.3.1.4).

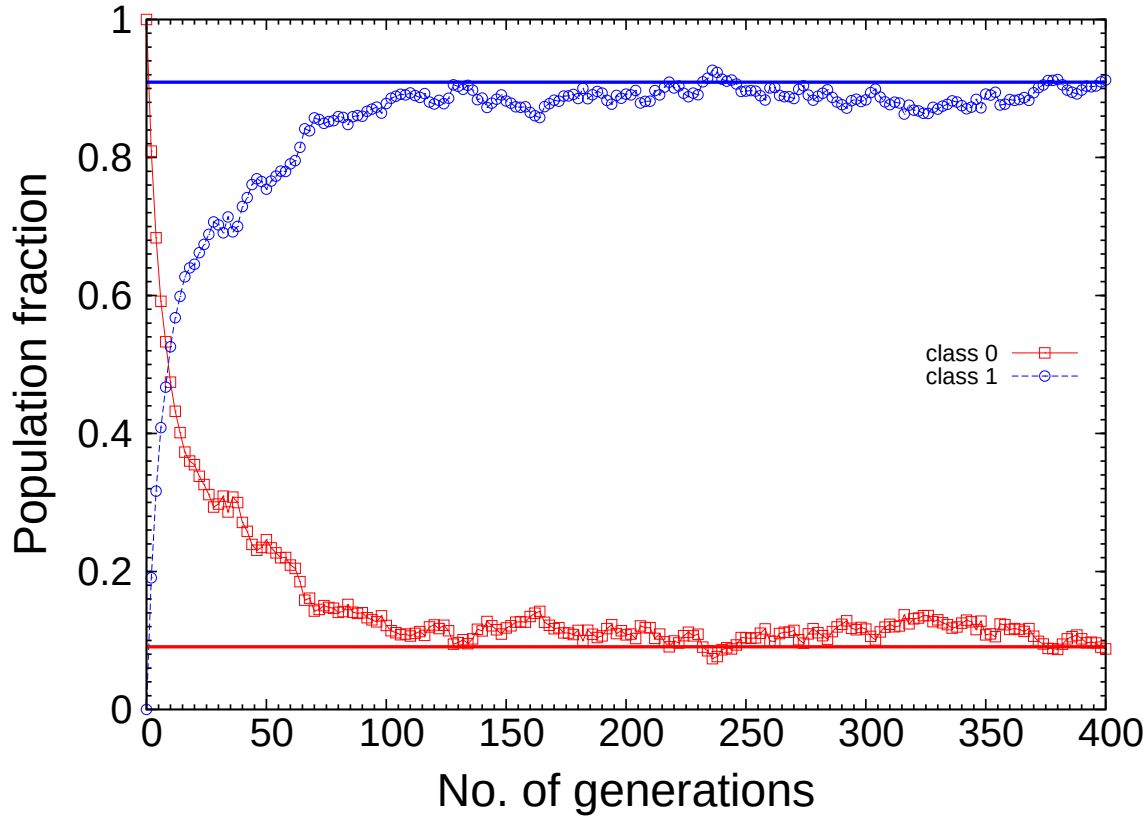


Fig. 4.3 Weak selection; synergistic epistasis. Single run plot of population fractions. It can be seen that the population will be localized in the first two fitness classes. The parameters are $\alpha = 16$, $V_d = 0.1$, $s = 0.01$, and $N = 4,000$. The solid horizontal lines show the steady state population fractions as calculated using (B.6). At $t = 0$, the population has no deleterious mutations. One can see that the population fractions from simulation approach the steady state values as time increases.

Effectively, the fitness class 1 for $\alpha \gg \frac{\ln(V_d/s)}{\ln 2}$ and $(V_d/s) \gg 1$ "replaces" fitness class 0 for $(V_d/s) \ll 1$ and $\alpha \geq 1$. Fig. 4.7 shows variation of (4.16) with $s$.

#### 4.3.1.3 Strong selection; antagonistic epistasis ($V_d/s < 1$, $\alpha < 1$)

As $(V_d/s) < 1$, $\lfloor (V_d/s)^{1/\alpha} \rfloor = 0$, and hence the fixation probability receives contribution only from class 0. Using the result from Table 4.1 in (4.12), we obtain

$$\Pi = 2V_d\,(1 - V_d/s) \;\text{ if }\; \alpha \ll 1\,. \tag{4.17}$$

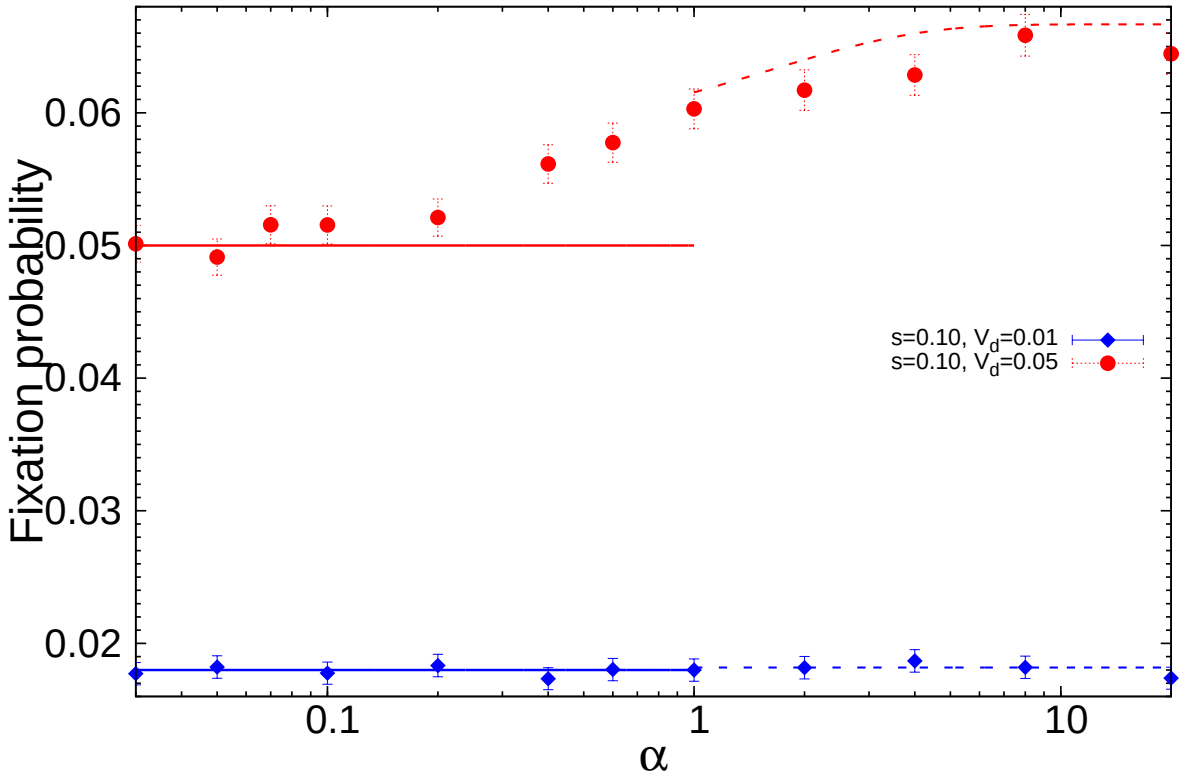


Fig. 4.4 Strong selection with antagonistic and synergistic epistasis. The symbols represent simulation data (red circles for $s = 0.1$ and $V_d = 0.05$; blue diamonds for $s = 0.1$ and $V_d = 0.01$). $\lambda = 100$ for both the cases. Each simulation point is averaged over $10^5$ independent stochastic realizations. The error bars represent $\pm 2$ standard error. The solid lines correspond to (4.17), and the broken curves represent (4.18).

Fig. 4.4, 4.5 and 4.6 show the validity of (4.17) by comparing against finite population simulations. For $(V_d/s)$ values comparable to 1, if the condition $\alpha \ll 1$ is not fulfilled, the expression for $p(0)$ is not valid (see Table B.1, and Case III in Appendix B.2). From Fig. 4.5 and 4.6, we can infer that for $(V_d/s) \gtrsim 0.5$, $\Pi$ varies with $\alpha$. For $(V_d/s) \ll 1$, $\Pi$ is independent of $\alpha$.

#### 4.3.1.4 Strong selection; synergistic epistasis ($V_d/s < 1$, $\alpha > 1$)

Since $\lfloor (V_d/s)^{1/\alpha} \rfloor = 0$, the use of the result from Table 4.1 in (4.12) yields

$$\Pi = \frac{2V_d}{\left(1 + \frac{V_d}{s} + \frac{(V_d/s)^2}{2^\alpha}\right)}. \tag{4.18}$$

As in the case of (4.16), with increase in $\alpha$, the dependence of $\Pi$ on epistasis will vanish, and (4.18) will approach the constant value $2V_d\left(1+\frac{V_d}{s}\right)^{-1}$. Fig. 4.4 and 4.7 show the comparison of (4.18) with finite population simulations (a discussion on the discrepancy between the results from simulations and analytics can be found in Appendix B.4). Table 4.2 gives summary of all the results from section 3.3.

It is obvious that, for $(V_d/s) \ll 1$, (4.17) and (4.18) approach the known result for fixation probability $\Pi = 2V_d$ [10] in the absence of epistasis ($\alpha = 1$). This can also be obtained using a single locus model, since the population consists only of class 0 individuals, and the selective advantage of nonmutators is the difference in the class 0 frequencies. As the class 0 individuals remain unaffected by epistasis for very strong selection, $\Pi$, which receives contribution only from class 0, is independent of $\alpha$.

### 4.3.2 Variation of fixation probability with mutation rate

#### 4.3.2.1 Strong selection; antagonistic epistasis ($V_d/s < 1$, $\alpha < 1$)

When we vary $V_d$ keeping $s$ to be the same, for $(V_d/s) < 1$, only the class 0 individuals decide $\Pi$. For $(V_d/s) \ll 1$, $p(0) \approx 1$ (see Table 4.1). This means that a mutation is very costly, due to which any individual carrying it will not survive. As the number of mutators in class 0 decreases with the rise in $V_d$, a reduction in the mutation rate will be highly favored. Thus, $\Pi$ increases with $V_d$. For $(V_d/s) \gtrsim 0.5$, $\Pi$ depends on epistasis (Fig. 4.5 and 4.6), though the dependence is not analytically captured. This is because $p(0)$ depends on $\alpha$. An increase (decrease) in $V_d$ ($\alpha$) leads to decrease in $p(0)$ (see Table B.1 and Fig. B.1), as the background population spreads out more. On the other hand, $\pi(0) = 2V_d$. This results in $\Pi = \pi(0)p(0)$

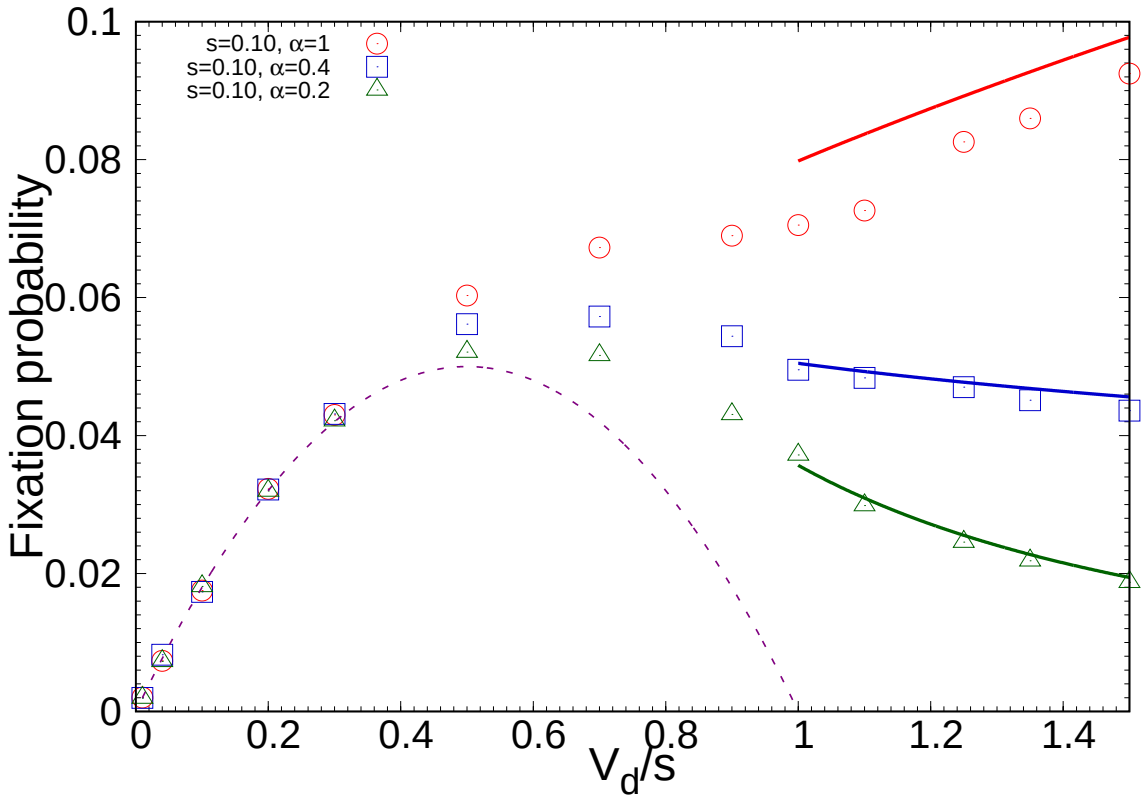


Fig. 4.5 Antagonistic epistasis with strong and weak selection. Variation of $\Pi$ with $V_d$. The symbols represent simulation data (red circles for $\alpha = 1$, blue squares for $\alpha = 0.4$, and green triangles for $\alpha = 0.2$). Each point is averaged over $10^5$ independent stochastic runs. The other parameters are $s = 0.1$ and $\lambda = 100$. The solid curves correspond to (4.14), and the broken curve represents (4.17). Clearly, (4.17) deviates from simulation results as $(V_d/s) \rightarrow 1$.

showing $\alpha$ dependent behavior for $1 > (V_d/s) \gtrsim 0.5$ similar to that in the regime $(V_d/s) > 1$, $\alpha < 1$.

#### 4.3.2.2 Weak selection; antagonistic epistasis ($V_d/s > 1$, $\alpha < 1$)

As discussed in section 4.3.1.1, the total fixation probability in the regime $(V_d/s) > 1$ is a multilocus problem. For antagonistic epistasis, the nonmutator has higher chances of appearing in a lower fit background for larger values of $V_d$. When $\alpha < 0.5$, this disadvantage cannot be compensated by its benefit associated with being created in a higher mutation rate background. Due to this, $\Pi$ falls as a function of $V_d$. These two factors together give rise

to a nonmonotonic behavior of $\Pi$ with respect to $V_d$ for $\alpha < 0.5$, as shown in Fig. 4.5. If $1 \geq \alpha > 0.5$, we see that the advantage conferred by the nonmutator owing to being produced in a high mutation rate background dominates its drawback and therefore, $\Pi$ increases with $V_d$. Thus, $\Pi$ is a monotonically increasing function of $V_d$ for $1 \geq \alpha > 0.5$ (see Fig. 4.5).

#### 4.3.2.3 Synergistic epistasis ($\alpha > 1$)

For synergistic epistasis, $\Pi$ rises with $V_d$ for both weak selection (see Fig. 4.2) and strong selection (see (4.18)). For $\alpha \gg \frac{\ln(V_d/s)}{\ln 2}$, $\Pi$ is a linearly increasing function of $V_d$ for both $(V_d/s) \gg 1$ and $(V_d/s) \ll 1$.

#### 4.3.2.4 Effect of very large or small $(V_d/s)$ when $s$ is held constant

As $V_d$ increases to very large values relative to selection, for $\alpha <$ (>) $\alpha_c$, $\Pi$ approaches 0 (1). Note that $\Pi$ can never exceed 1. When $V_d$ is decreased to very small values compared to $s$, $\Pi$ falls towards 0 irrespective of $\alpha$. This is obvious because the lower the mutation rate of the mutator is, the smaller the advantage associated with the reduction of mutation rate.

### 4.3.3 Variation of fixation probability with selection

#### 4.3.3.1 Antagonistic epistasis ($\alpha < 1$)

The selection coefficient decides the effect of a mutation. Since the expression (4.17) for $(V_d/s) < 1$ and $\alpha < 1$ is inadequate to capture the $\alpha$ dependence, the simulation data corresponding to two $\alpha$ values have been plotted for that regime in Fig. 4.6. Qualitatively, one can conclude that $\Pi$ increases with $s$. When $s$ is large, the nonmutator has a higher advantage by virtue of the higher deleterious effect of a mutation. For $(V_d/s) \ll 1$, it is possible to understand from (4.17) that $\Pi$ becomes independent of $s$, since it is determined only by the individuals that do not undergo mutation. In the weak selection regime, better understanding is possible with the help of (4.14), which is plotted in Fig. 4.6 for $\alpha = 0.6$. When $\alpha = 0.2$, for the given set of parameters and population size ($N = 4,000$), a steady state does

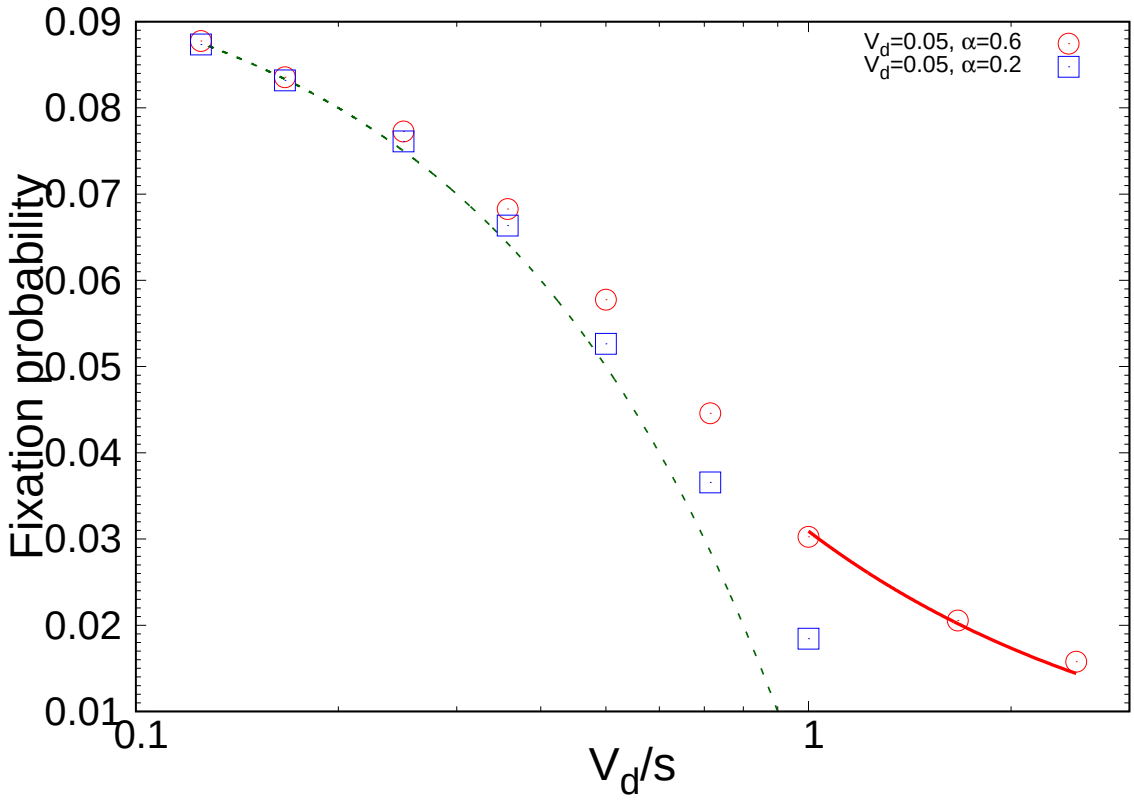


Fig. 4.6 Antagonistic epistasis with weak and strong selection. Variation of $\Pi$ with $s$. The symbols show simulation data (average over $10^5$ replicas). Here, $\alpha = 0.6$ (red circles) and 0.2 (blue squares). The other parameters are $V_d = 0.05$ and $\lambda = 100$. The red solid curve is (4.14), and the green broken curve is (4.17).

not exist in the weak selection regime. Hence, the corresponding data is not shown in Fig. 4.6.

#### 4.3.3.2 Synergistic epistasis ($\alpha > 1$)

For synergistic epistasis, in the special case of $\alpha = 2$, an exact solution exists for $p(0)$. With the help of the result in Table 4.1, (4.12) becomes

$$\Pi = \frac{2V_d \left(\frac{V_d}{s}\right)^{\lfloor\sqrt{(V_d/s)}\rfloor}}{\left(\lfloor\sqrt{(V_d/s)}\rfloor!\right)^2 I_0\left(2\sqrt{\frac{V_d}{s}}\right)}, \tag{4.19}$$

which is valid for any value of $(V_d/s)$. Corresponding to $(V_d/s) < 1$, $\lfloor\sqrt{(V_d/s)}\rfloor = 0$, by which (4.19) takes the form

$$\Pi = \frac{2V_d}{I_0\left(2\sqrt{\frac{V_d}{s}}\right)} \text{ if } (V_d/s) < 1\,. \tag{4.20}$$

Fig. 4.7 shows the comparison of (4.19) with simulation data, which is represented using the blue open triangles. For the values of $s$ corresponding to which a population of size $N = 4{,}000$ do not have steady state, the numerical solutions of (4.8) and (4.9) using *Wolfram Mathematica* 9.0.1.0 are shown using the filled circles in the main figure in Fig. 4.7. Since we assumed $U_d = 0$ and used the approximation (4.11), (4.19) overestimates the exact numerical solution by a small amount. The comparison of (4.19) with the exact solution using (4.8) and (4.9) is given in the last two columns of Table B.2. The detailed explanation for the surprising trend in Fig. 4.7 is given in Appendix B.3.

#### 4.3.3.3 Effect of very large or small $(V_d/s)$ when $V_d$ is kept the same

We know from sections 4.3.1.3 and 4.3.1.4 that when $(V_d/s) \ll 1$, $\Pi$ assumes the value $2V_d$ regardless of $\alpha$. Expressions (4.20) and (B.19) also justify this claim, as the denominators of them approach 1 for $(V_d/s) \ll 1$. When selection is reduced to much lower values compared to mutation rate, $\Pi \to 0$. This can be seen from (4.14) for $\alpha \leq 1$, and Fig. 4.7 for $\alpha = 2$. This is because there will not be any significant difference between mutators and nonmutators when the selective effects are negligibly small.

## 4.4 Discussion

### 4.4.1 Summary of results and connection with real populations

In an asexual adapted population, it is known that [62] in the presence of synergistic epistasis, a higher proportion of individuals will carry less mutations, while in the presence of antagonistic epistasis, the fraction of individuals containing less mutations will be very low. In this Chapter, it is found that antagonistic epistasis lowers the fixation probability of a

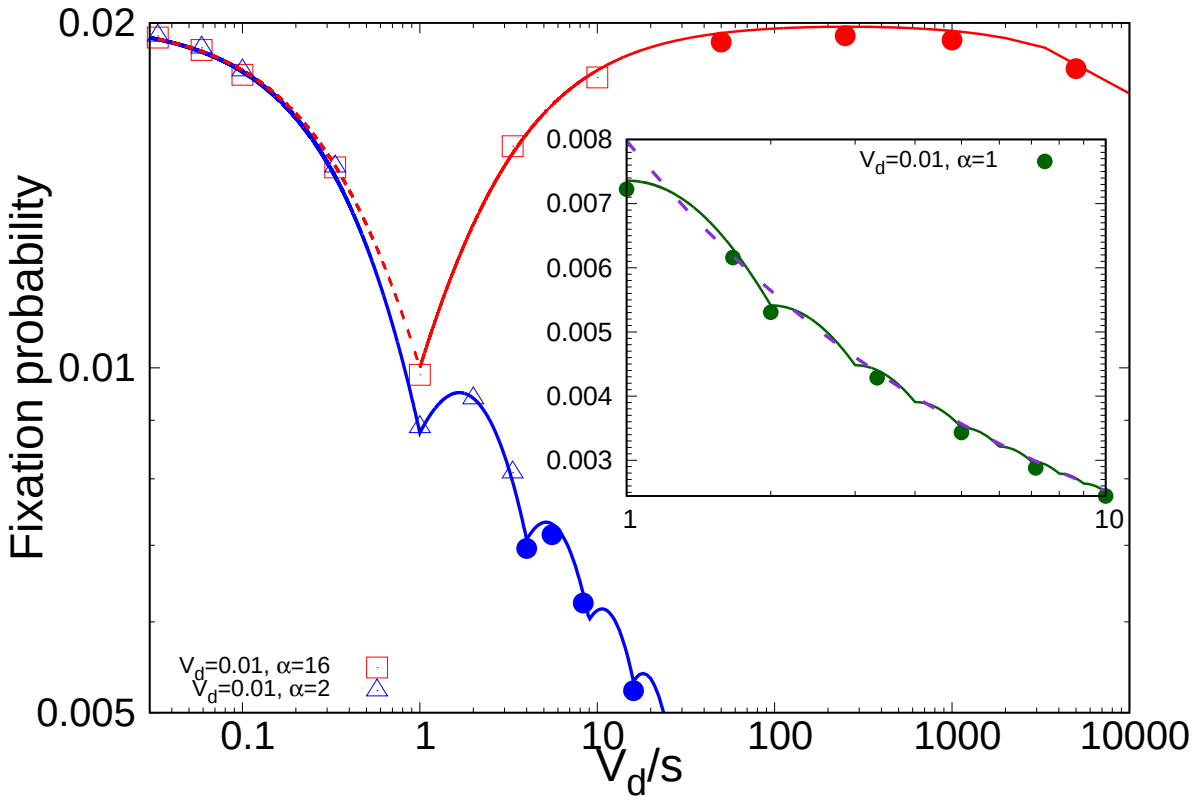


Fig. 4.7 Synergistic epistasis with strong and weak selection. Variation of Π with $s$. The open symbols show simulation data (averaged over $10^5$ independent realizations). The filled circles represent the numerical solutions of (4.8) and (4.9). The parameters are $\alpha = 16$ (red squares), 2 (blue triangles), and 1 (green circles) with $V_d = 0.01$ and $\lambda = 100$. The red curves plotted with the data respectively indicate (4.16) and (4.18) in the weak and strong selection regimes. The blue and green (inset) solid curves are (4.19) and (B.19), respectively. The broken violet line in the inset represents the simplified expression (4.14).

**Analytical expressions for $\Pi$**

| | $(V_d/s) \geq 1$ (Fig. 4.2) | $(V_d/s) < 1$ (Fig. 4.4) |
|---|---|---|
| $\alpha \leq 1$ (Fig. 4.5 & 4.6) | $\Pi = V_d \sqrt{\frac{2\alpha}{\pi}} \left(\frac{s}{V_d}\right)^{\frac{1}{2\alpha}}$ | $\Pi = 2V_d\,(1 - V_d/s)$ if $\alpha \ll 1$ |
| $\alpha > 1$ (Fig. 4.7) | $\Pi = \frac{2V_d\ V_d/s}{\left(1+\frac{V_d}{s}+\frac{(V_d/s)^2}{2^\alpha}\right)}$ if $\alpha > \frac{\ln(V_d/s)}{\ln 2}$ | $\Pi = \frac{2V_d}{\left(1+\frac{V_d}{s}+\frac{(V_d/s)^2}{2^\alpha}\right)}$ |
| $\alpha = 2$ (Fig. 4.7) | $\Pi = \frac{2V_d \left(\frac{V_d}{s}\right)^{\lfloor\sqrt{(V_d/s)}\rfloor}}{\left(\lfloor\sqrt{(V_d/s)}\rfloor!\right)^2 I_0\left(2\sqrt{\frac{V_d}{s}}\right)}$ | $\Pi = \frac{2V_d}{I_0\left(2\sqrt{\frac{V_d}{s}}\right)}$ |

Table 4.2 The figure denoted in bracket in any row (column) indicates that the validity of the next two expressions given in the same row (column) is shown in that figure. All expressions in the last column (strong selection regime) involve nonmutators created only in class 0. Even though the expressions in the second row can be used for $\alpha = 2$, the equations in the last row are more accurate.

lower mutation rate allele, thereby opposing the decline in mutation rate, while synergistic epistasis favors the reduction in mutation rate. Using a model similar to the one in this Chapter, [63] hypothesized that asexual populations could resist mutation accumulation in the presence of synergistic interactions. However, the model here assumes the population size to be a constant in every generation, while the size of an actual population fluctuates stochastically. A theoretical study in which the population size was allowed to vary with time [83] revealed that the extinction time of asexuals by virtue of onslaught of detrimental mutations vary depending on the values of parameters such as mutation rate, selection, etc. Since epistasis influences mutation rate reduction, results in this Chapter can be connected to the analysis of [83] to unravel the role of epistasis on the extinction time of asexuals. However, real populations can have compensatory or back mutations (see two different models that incorporate compensatory mutations - [84, 10]) acting against the influx of deleterious mutations, which were neglected by all the above studies. In order to understand the fate of

real asexual populations, the current study has to be extended by including more realistic considerations as discussed above.

It is observed in this study that there exists a critical value $\alpha_c$ of epistasis below which the probability of reduction of mutation rate in an infinite population shows negative correlation with its mutation rate. For strong mutators, $\alpha_c$ is found to be at 0.5 using analytical arguments (see Appendices B.4 and B.6). Though the mutation rate reduction happens with a non-zero probability, which is characteristic of any beneficial mutation, the decline in mutation rate becomes more unlikely when $\alpha < \alpha_c$. For $\alpha < \alpha_c$, the fixation probability of a nonmutator decreases with $V_d$ in the weak selection regime, as the lower mutation rate allele now appears with large number of mutations and finds it difficult to outcompete the resident population. On the other hand, $\Pi$ increases with $V_d$ in the strong selection regime because of the nonmutator arising in class 0 benefiting from the reduction of mutational load by a larger amount. (A discussion on $\alpha_c$ in the weak mutator background is given in Appendix B.6.)

In the presence of synergistic interactions, $\Pi$ initially remains constant at the value $2V_d$ followed by a reduction, as $s$ is reduced in the strong selection regime. In the weak selection regime, as $s$ drops, $\Pi$ manifests a nonmonotonic behavior for every $n^{-\alpha}\ V_d < s < (n+1)^{-\alpha}\ V_d$, where $n = 1,2,3,...$, but experiences eventual decay. This is shown in Fig. 4.7.

### 4.4.2 Limitations of the models and future goals

One major assumption which we have made in this Chapter is that the population attains steady state after a large number of generations. However, populations of small size (see section 4.2.1 and Appendix B.5) do not have steady state, and hence the results presented here are not applicable to them. It is possible to evaluate the total fixation probabilities of nonmutators in such populations using (4.7) and (B.1). The total fixation probability will depend on the time of arrival of the nonmutator. This has been studied by [7] for a non-epistatic landscape, when the selective effects are very strong. It is an open question for the epistatic landscape, and is not done here. The analysis in this Chapter is a special case of this problem.

However, Fig. 4.1 in the Appendix helps to have a qualitative understanding of the effect of variation of $N$. For each value of $N$ in the figure, the nonmutator appears after $10/s$ generations. It is noticeable that large populations are more effective in withstanding the accumulation of harmful mutations. Small populations that are incapable of resisting the build-up of deleterious mutations and decline of mean fitness will be benefited more from the reduction in mutation rate. As a result, when $N$ increases, the fixation probability decreases and approaches the constant value predicted by (4.9). Articles like [11, 7, 49, 22, 10], etc. give insights into the role of population size on mutation rate evolution.

It is noteworthy that the model in this Chapter examines the fixation probability of a single nonmutator appearing in the mutator population as described using (4.3). Its fixation is decided by whether the lineage of this particular nonmutator takes over the population or not. In reality, there can be multiple nonmutators emerging in the population. The article by [32] includes the study of fixation probability of beneficial alleles arising at a constant rate. The same approach can be used to model the fate of multiple nonmutators arising in the adapted mutator population, since the nonmutator is effectively beneficial.

Actual biological populations may not have all the mutations having the same selective effects. There are models in which the selection coefficient is chosen from a distribution. However, the robustness of the results presented here could be tested using other fitness functions. There have been works taking into account the possible physiological costs associated with lowering the mutation rates [58–60, 71, 2]. The effect of this factor could be explored.

### 4.4.3 Choice of parameters and biological relevance

Maisnier-Patin et al. [24] experimentally confirmed that in *Salmonella typhimurium*, for various values of the mutation rates, the fitness effect of the mutations resembles the function (4.1) with $\alpha = 0.46$. Synergistic epistasis has been observed in experiments [74, 75]. In *Drosophila melanogaster*, the logarithm of relative productivity of genotypes was measured to be proportional to negative of the number of mutant regions carried by them [75]. This is similar to the fitness function (4.1) with the corresponding $\alpha$ being 2. In previous theo-

retical studies, the chosen values for $\alpha$ range from 0.02 [82] to 5 [80], whereas $\alpha$ has been varied from 0.03 to 20 in the simulations in this Chapter. The strength $\lambda$ of the mutator can be as large as 1000 [52] to as small as around 2 [34, 6]. In this study, $\lambda$ values ranging from 1.25 to 10,000 (see Appendix B.6) are used. For *E. coli* populations, $s$ is observed to be in the range $10^{-3}$ [68] $- 10^{-1}$ [69], while $V_d \sim 10^{-3}$ per genome per generation [26]. This Chapter includes values of $s$ and the absolute values of mutation rate (for both mutators and nonmutators) in the range $10^{-5} - 10^{-1}$ and $10^{-4} - 10^{-1}$ per genome per generation, respectively. In the experiment by Maisnier-Patin et al. [24], $V_d$ was varied from $4 \times 10^{-4}$ to 0.31 per genome per replication, and $s$ was measured to be $4.1 \times 10^{-2}$.

With the help of information about the parameters $s$, $V_d$ and $\alpha$ from the experiment by Maisnier-Patin et al. [24], it follows from (B.6) that $p(0)$ lies between 0.99 and $7.3 \times 10^{-18}$ corresponding to the lower and upper limits of $V_d$. By including the selection coefficient, the condition proposed by Kondrashov [63] can be modified to write $N_m p(0) s \sim 10^2$, where $N_m$ is the minimum value of $N$ so as to have a steady state (see Appendix B.5). Hence, for the experiment by Maisnier-Patin et al. [24], $N_m$ varies from $3 \times 10^3$ to $3 \times 10^{20}$. Nevertheless, the population size in this case was $10^8$. For this value of $N$, a steady state is possible for $V_d \leq 0.16$. Therefore, to the best of our knowledge, *Salmonella typhimurium* is the only model organism which can be used to test the results in this Chapter, as it is the only asexual for which $\alpha$ has been measured.

### 4.4.4 Fixation time and comparison with experiments

The time required for the fixation of a nonmutator is given by the inverse of the rate at which nonmutators that are certain to get fixed are created [70]. (The details of the fixation time can be found in [61].) The rate of creation of nonmutators that are expected to reach fixation is the product of their rate of production and fixation probability. Thus, for a large population, the fixation time [10] is $T = (Nb\Pi)^{-1}$, where $b$ is the rate at which the mutation that produces the lower mutation rate allele happens, provided $Nb \ll 1$.

Table 2 of [6] gives the mutation rate corresponding to 3 genotypes and their respective times of origin. Assuming the time of origin corresponds to the time when a genotype was

significantly high in proportion in order to get detected, we see that the time for reduction of mutation rate is inversely proportional to magnitude of the reduction. However, the experiment of [34] indicates that this reduction time is higher for a higher magnitude of decline in the mutation rate. The opposite trends observed in the above two experiments can be explained if epistasis is assumed to be present, as the fixation probability can be either an increasing or decreasing function of mutation rate depending on the epistasis parameter.

### 4.4.5 Comparison with previous theoretical works

It is known that the fixation probability of an allele with effective selective advantage $S$ in a finite population of size $N$ is $\Pi(N) = (1-e^{-2S})/(1-e^{-2SN})$ [28]. In this model, for infinite population size, $\Pi = 2S$, as discussed in [10]. That is, the fixation probability of a beneficial allele in an infinite population is twice its net selective advantage. For a harmful allele, $S$ is negative, and hence, its fixation probability (time) falls (increases) exponentially with $N$ [50, 51].

Fixation of mutators in an asexual nonmutator population is effectively the same as fixation of a harmful allele if the fitness affecting beneficial mutations are excluded. For this problem, [49] studied the fixation time of mutators, and the time was found to increase exponentially ($e^{2N\sqrt{\frac{2\alpha(\lambda-1)}{\pi}}\, s^{\frac{1}{\alpha}} \left(\frac{V_d}{\lambda}\right)^{2-\frac{1}{\alpha}}}$ for weak selection, and $e^{2NV_d\,(1-1/\lambda)}$ for strong selection). It is important to be noted that we study only the strong mutator case ($\lambda \gg 1$). From the above mentioned result of [49], we can obtain the effective selective disadvantage conferred by the mutator (which is also the same as $(\Pi/2)$) to be $\sqrt{\frac{2\alpha\lambda}{\pi}}\, s^{\frac{1}{2\alpha}} \left(\frac{V_d}{\lambda}\right)^{1-\frac{1}{2\alpha}}$ for weak selection. This has similar dependence on $V_d$ as (4.14), though the mutator strength does not enter our expression. For $\alpha = 1$, these two solutions differ only by a factor 2. Nevertheless, in the strong selection regime, the net selective disadvantage of the mutator is simply $V_d(1-1/\lambda)$, which exactly matches with our result. In the case of the work of [49], there is a continuous production of mutators from nonmutators owing to which mutators sweep to fixation in a finite population. For a population of large size, the corresponding steady

state fitness is $e^{-V_d}$. In this Chapter, we analyze a mutator population that is in steady state initially with mean fitness $e^{-V_d}$. The nonmutator allele can appear in a background carrying $k$ mutations, and reach fixation to form a distribution of nonmutators with mean fitness $(1-s)^{k^\alpha} e^{-V_d/\lambda}$. Though the initial state of the problem addressed in this Chapter is the same as the final state of the problem considered by [49], the reverse is not true. In the special case of strong selection, these two works study "complementary" processes.

# Chapter 5

# Summary

Here, we summarize the main points discussed in the thesis and provide future prospects for research. The evolutionary aspects of the phenomenon of the reduction in mutation rate are very less theoretically probed. In this thesis, we have focused on the influence of the forces of genetic drift, mutation, and selection on the evolution of low mutation rates in adapted populations.

In Chapter 2, we consider the very simple case in which the mutations do not interact with each other and the nonmutator competes for fixation in a background that has a significantly high mutation rate than that of the invader. The important findings from this Chapter are the following [10]:

1. A nonmutator is more likely to fix when the deleterious mutation rate of the mutator population is high.

2. As the rate of compensatory mutations increases, the fixation probability of a nonmutator decreases if the selection coefficient is large, while it exhibits a surprising nonmonotonic behavior if the selection is mild.

3. Connecting the results obtained for the fixation probability with a drift-barrier hypothesis [11, 7], we show that the lower bound of mutation rate is inversely proportional to the population size for strong selective effects [7], while it decays at a much faster rate if selection is weak.

In Chapter 3, we analyze the extension of the case studied in Chapter 2, in which the nonmutator can have a mutation rate comparable to that of the resident population [12].

1. The probability of fixation of a nonmutator rises or falls as a function of the mutation rate of the mutator depending on the values of the mutation rates and selection.

2. The analysis for strong mutators with compensatory mutations in nonmutators shows that the effect in [10] is not general.

In the previous two Chapters, we have studied the simple non-epistatic fitness landscape. Unlike before, in Chapter 4, we aim to understand the role of epistatic interactions between the fitness affecting mutations in the process of evolution of low mutation rates. The main observations from this Chapter are listed below [13]:

1. The likelihood of the nonmutator to reach fixation increases as the epistasis parameter (strength of the interactions) increases.

2. The presence of a critical value of epistasis parameter has been discovered, below which the fixation probability behaves nonmonotonically with variation in mutation rate of the background population.

3. For synergistic epistasis, when the selection is varied, the fixation probability reduces overall, with damped oscillations.

It would be interesting to examine the effect of compensatory mutations on an epistatic fitness landscape. Further, the robustness of our results could be tested using different fitness functions or when the selective cost of each mutation is chosen from a distribution. Throughout the thesis, we have studied a haploid asexual population. However, there have been experiments on mutation rate evolution on diploid populations as well as in the presence of recombination [3]. Such realistic considerations could be taken into account.

# References


[1] A. H. Sturtevant. Essays on evolution. I. On the effects of selection on the mutation rate. *Q. Rev. Biol.*, 12:464–476, 1937.

[2] C. F. Baer, M. M. Miyamoto, and D. R. Denver. Mutation rate variation in multicellular eukaryotes. *Nat. Rev. Genet.*, 8:619–631, 2007.

[3] Y. Raynes and P. Sniegowski. Experimental evolution and the dynamics of genomic mutation rate modifiers. *Heredity*, 113:375–380, 2014.

[4] P. D. Sniegowski, P. J. Gerrish, and R. Lenski. Evolution of high mutation rates in experimental populations of *E. coli*. *Nature*, 387:703–705, 1997.

[5] L. Notley-McRobb, S. Seeto, and T. Ferenci. Enrichment and elimination of mutY mutators in *Escherichia coli* populations. *Genetics*, 162:1055–1062, 2002.

[6] S. Wielgoss, J. E. Barrick, O. Tenaillon, M. J. Wiser, W. J. Dittmar, S. Cruveiller, B. Chane-Woon-Ming, R. E. Lenski, and D. Schneider. Mutation rate dynamics in a bacterial population reflect tension between adaptation and genetic load. *Proc. Natl. Acad. Sci. U.S.A.*, 110:222–227, 2013.

[7] M. Lynch. The lower bound to the evolution of mutation rates. *Genome Evol. Biol.*, 3:1107–1118, 2011.

[8] T. Wiehe. Model dependency of error thresholds: the role of fitness functions and contrasts between the finite and infinite sites model. *Genet. Res. Camb.*, 69:127–136, 1997.

[9] Z. Patwa and L. Wahl. The fixation probability of beneficial mutations. *J. R. Soc. Interface*, 5:1279–1289, 2008.

[10] A. James and K. Jain. Fixation probability of rare nonmutator and evolution of mutation rates. *Ecol. Evol.*, 6:755–764, 2016.

[11] M. Lynch. Evolution of the mutation rate. *Trends in Genetics*, 26:345–352, 2010.

[12] K. Jain and A. James. Fixation probability of a nonmutator in a large population of asexual mutators. *In preparation*, 2017.

[13] A. James. Role of epistasis on the fixation probability of a non-mutator in an adapted asexual population. *J. Theor. Biol.*, 407:225–237, 2016.

[14] G. Cumming, F. Fidler, and D. L. Vaux. Error bars in experimental biology. *J. Cell. Biol.*, 177:7–11, 2007.

[15] B. Charlesworth and D. Charlesworth. *Elements of evolutionary genetics*. Roberts and Company Publishers, 2010.

[16] D. L. Hartl and A. G. Clark. *Principles of Population Genetics*. Sinauer Associates, Inc., 1997.

[17] J. Wakeley. The limits of theoretical population genetics. *Genetics*, 169:1–7, 2005.

[18] S. John. *Evolution of large populations under the joint action of deleterious and beneficial mutations*. Ph. D. thesis, JNCASR, Bangalore, 2016.

[19] S. P. Otto and T. Day. *A Biologist's Guide to Mathematical Modeling in Ecology and Evolution*. Princeton University Press, 2007.

[20] R. A. Fisher. *The genetical theory of natural selection*. Oxford University Press, 1930.

[21] J. W. Drake. A constant rate of spontaneous mutation in dna-based microbes. *Proc. Natl. Acad. Sci. U.S.A.*, 88:7160–64, 1991.

[22] W. Sung, M. S. Ackerman, S. F. Miller, T. G. Doak, and M. Lynch. Drift-barrier hypothesis and mutation-rate evolution. *Proc. Natl. Acad. Sci. U.S.A.*, 109:18488–18492, 2012.

[23] J. A. G. M. de Visser and J. Krug. Empirical fitness landscapes and the predictability of evolution. *Nat. Rev. Genet.*, 15:480–490, 2014.

[24] S. Maisnier-Patin, J.R. Roth, A. Fredriksson, T. Thomas Nyström, O.G. Berg, and D.I. Andersson. Genomic buffering mitigates the effects of deleterious mutations in bacteria. *Nat. Genet.*, 37:1376 – 1379, 2005.

[25] N. H. Barton, D. E. G. Briggs, J. A. Eisen, D. B. Goldstein, and N. H. Patel. *Evolution*. Cold Spring Harb., 2007.

[26] J. W. Drake, B. Charlesworth, D. Charlesworth, and J. F. Crow. Rates of spontaneous mutation. *Genetics*, 148:1667–86, 1998.

[27] K. Jain and S. John. Deterministic evolution of an asexual population under the action of beneficial and deleterious mutations on additive fitness landscapes. *Theor. Pop. Biol.*, 112:117–125, 2016.

[28] M. Kimura. On the probability of fixation of mutant genes in a population. *Genetics*, 47:713–719, 1962.

[29] K. Jain and J. Krug. Adaptation in simple and complex fitness landscapes. In U. Bastolla, M. Porto, H.E. Roman, and M. Vendruscolo, editors, *Structural Approaches to Sequence Evolution: Molecules, Networks and Populations*, pages 299–340. Springer, Berlin, 2007.

[30] T. E. Harris. *The theory of branching processes*. Springer-Verlag, 1964.

[31] L. J. S. Allen. *An Introduction to Stochastic Processes with Applications to Biology*. Pearson Education, Inc., New Jersey, 2003.

[32] T. Johnson and N. H. Barton. The effect of deleterious alleles on adaptation in asexual populations. *Genetics*, 162:395–411, 2002.

[33] W. Tröbner and R. Piechocki. Selection against hypermutability in *Escherichia coli* during long-term evolution. *Mol. Gen. Genet.*, 198:177–178, 1984.

[34] M. J. McDonald, Y. Y. Hsieh, Y. H. Yu, S. L. Chang, and J. Y. Leu. The evolution of low mutation rates in experimental mutator populations of *Saccharomyces cerevisiae*. *Current Biology*, 22:1235–40, 2012.

[35] T. Taddei, M. Radman, J. Maynard-Smith, B. Toupance, P. H. Gouyon, and B. Godelle. Role of mutator alleles in adaptive evolution. *Nature*, 387:700–702, 1997.

[36] A. Oliver, R. Cantón, P. Campo, F. Baquero, and J. Blázquez. High frequency of hypermutable *Pseudomonas aeruginosa* in cystic fibrosis lung infection. *Science*, 288:1251–1253, 2000.

[37] M. Eigen. Selforganization of matter and evolution of biological macromolecules. *Naturwissenchaften*, 58:465 – 523, 1971.

[38] J. Maynard-Smith and J. Haigh. Hitchhiking effect of a favourable gene. *Genet. Res.*, 23:23–35, 1974.

[39] U. Liberman and M.W. Feldman. A general reduction principle for genetic modifiers of recombination. *Theor. Pop. Biol.*, 30:341–371, 1986.

[40] M. C. Turrientes, F. Baquero, B. Levin, J. L. Martinez, A. Ripoll, J. M. González-Alba, R. Tobes, M. Manrique, M. R. Baquero, M. J. Rodriguez-Dominguez, R. Cantón, and Galńa J. C. Normal mutation rate variants arise in a mutator (mut s) *Escherichia coli* population. *PLoS ONE*, 8:e72963, 2013.

[41] J.-B. Andre and B Godelle. The evolution of mutation rate in finite asexual populations. *Genetics*, 172:611–626, 2006.

[42] C. S. Wylie, C. M. Ghim, D. Kessler, and H. Levine. The fixation probability of rare mutators in finite asexual populations. *Genetics*, 181:1595–1612, 2009.

[43] M. M. Desai and D. S. Fisher. The balance between mutators and nonmutators in asexual populations. *Genetics*, 188:997–1014, 2011.

[44] R. A. Fisher. On the dominance ratio. *Proc. Roy. Soc. Edinburgh*, 52:399–433, 1922.

[45] J. B. S. Haldane. A mathematical theory of natural and artificial selection. v. *Proc. Camb. Philos. Soc.*, 23:838–844, 1927.

[46] M. Kimura and T. Maruyama. The mutational load with epistatic gene interactions in fitness. *Genetics*, 54:1337–1351, 1966.

[47] J. Haigh. The accumulation of deleterious genes in a population - Muller's ratchet. *Theor. Pop. Biol.*, 14:251–267, 1978.

[48] T. Johnson. The approach to mutation — selection balance in an infinite asexual population, and the evolution of mutation rates. *Proc. Royal Society B*, 266:2389, 1999.

[49] K. Jain and A. Nagar. Fixation of mutators in asexual populations: the role of genetic drift and epistasis. *Evolution*, 67:1143, 2013.

[50] M. Kimura. Average time until fixation of a mutant allele in a finite population under continued mutation pressure: Studies by analytical, numerical, and pseudo-sampling methods. *Proc. Natl. Acad. Sci. USA*, 77:522–526, 1980.

[51] M. Assaf and M Mobilia. Fixation of a deleterious allele under mutation pressure and finite selection intensity. *J. Theor. Biol.*, 275:93–103, 2011.

[52] J. Miller. Spontaneous mutators in bacteria: Insights into pathways of mutagenesis and repair. *Annu. Rev. Microbiol*, 50:625–643, 1996.

[53] L. Boe, M. Danielsen, S. Knudsen, J. B. Petersen, J. Maymann, and P. R. Jensen. The frequency of mutators in populations of Escherichia coli. *Mut. Res.*, 448:47–55, 2000.

[54] L. Wahl, P. Gerrish, and I. Saika-Voivod. Evaluating the impact of population bottlenecks in experimental evolution. *Genetics*, 162:961–971, 2002.

[55] P. J. Gerrish and R. E. Lenski. The fate of competing beneficial mutations in an asexual populations. *Genetica*, 102:127–144, 1998.

[56] B. H. Good and M. M. Desai. Evolution of mutation rates in rapidly adapting asexual populations. *Genetics*, 204:1249–1266, 2016.

[57] L. Perfeito, L. Fernandes, C. Mota, and I. Gordo. Adaptive mutations in bacteria: high rate and small effects. *Science*, 317:813–815, 2007.

[58] M. Kimura. On the evolutionary adjustment of spontaneous mutation rates. *Genet. Res.*, 9:23–34, 1967.

[59] A. Kondrashov. Contamination of the genome by very slightly deleterious mutations: why have we not died 100 times over? *J. Theor. Biol.*, 175:583–594, 1995.

[60] K.J. Dawson. Evolutionarily stable mutation rates. *J. Theor. Biol.*, 194:143–157, 1998.

[61] W. J. Ewens. *Mathematical Population Genetics I. Theoretical Introduction*. Springer, 2004.

[62] K. Jain. Loss of least-loaded class in asexual populations due to drift and epistasis. *Genetics*, 179:2125–2134, 2008.

[63] A.S. Kondrashov. Muller's ratchet under epistatic selection. *Genetics*, 136:1469–1473, 1994.

[64] P. G. Higgs. Error thresholds and stationary mutant distributions in multi-locus diploid genetic models. *Genet. Res. Camb.*, 63:63–78, 1994.

[65] J. B. S. Haldane. The effect of variation on fitness. *Am. Naturalist*, 71:337–349, 1937.

[66] M. Abramowitz and I. A. Stegun. *Handbook of Mathematical Functions with Formulas, Graphs, and Mathematical Tables*. Dover, New York, 1964.

[67] S. Seetharaman and K. Jain. Adaptive walks and distribution of beneficial fitness effects. *Evolution*, 68-4:965–975, 2013.

[68] R. Gallet, T. F. Cooper, S. F. Elena, and T. Lenormand. Measuring selection coefficients below $10^{-3}$: methods, questions and prospects. *Genetics*, 190:175–186, 2012.

[69] R. E. Lenski, M. R. Rose, S. C. Simpson, and S. C. Tadler. Long-term experimental evolution in *Escherichia coli*. i. adaptation and divergence during 2,000 generations. *Am. Nat.*, 138:1315–1341, 1991.

[70] D. M. Weinreich, and L. Chao. Rapid evolutionary escape by large populations from local fitness peaks is likely in nature. *Evolution*, 59(6):1175–82, 2005.

[71] T. Johnson. Beneficial mutations, hitchhiking and the evolution of mutation rates in sexual populations. *Genetics*, 51:1621–1631, 1999.

[72] A. Nagar and K. Jain. Exact phase diagram of quasispecies model with mutation rate modifier. *Phys. Rev. Lett.*, 102:038101, 2009.

[73] R.J. Söderberg and O.G. Berg. Kick-starting the ratchet: The fate of mutators in an asexual population. *Genetics*, 187:1129–1137, 2011.

[74] T. Mukai. The genetic structure of natural populations of *Drosophila melanogaster*. VII. Synergistic interaction of spontaneous mutant polygenes controlling viability. *Genetics*, 61:749–761, 1969.

[75] M. C. Whitlock and D. Bourguet. Factors affecting the genetic load in *Drosophila*: synergistic epistasis and correlations among fitness components. *Evolution*, 54:1654–60, 2000.

[76] S. Kryazhimskiy, G. Tkacik, and J. B. Plotkin. The dynamics of adaptation on correlated fitness landscapes. *Proc. Natl. Acad. Sci. USA*, 106:18638–18643, 2009.

[77] H. Chou, H. Chiu, N. F. Delaney, D. Segre, and C. J. Marx. Diminishing returns epistasis among beneficial mutations decelerates adaptation. *Science*, 332:1190–1192, 2011.

[78] A.I. Khan, D. M. Dinh, D. Schneider, R.E. Lenski, and T.F. Cooper. Negative epistasis between beneficial mutations in an evolving bacterial population. *Science*, 332:1193, 2011.

[79] J. Plucain, T. Hindre, M. Le Gac, O. Tenaillon, S. Cruveiller, C. Medigue, N. Leiby, W. R. Harcombe, C. J. Marx, R. E. Lenski, and D. Schneider. Epistasis and allele specificity in the emergence of a stable polymorphism in *Escherichia coli*. *Science*, 343:1366–1369, 2014.

[80] P. R. A. Campos. Fixation of beneficial mutations in the presence of epistatic interactions. *Bull. Math. Biol.*, 66:473–486, 2004.

[81] K. Jain. Time to fixation in the presence of recombination. *Theor. Pop. Biol.*, 77:23, 2010.

[82] M. R. Fumagalli, M. Osella, P. Thomen, F. Heslot, and M. C. Lagomarsino. Speed of evolution in large asexual populations with diminishing returns. *J. Theor. Biol.*, 365:23–31, 2015.

[83] W. Gabriel, M. Lynch, and R. Bürger. Muller's ratchet and mutational meltdowns. *Evolution*, 47:1744–1757, 1993.

[84] S. John and K. Jain. Effect of drift, selection and recombination on the equilibrium frequency of deleterious mutations. *J. Theor. Biol.*, 365:238–246, 2015.

# Appendix A

## A.1 Mutator frequency when compensatory mutations are included

For small selection coefficient and mutation rates, the mutator frequency $p(k,t)$ obeys the following continuous time equations:

$$\begin{aligned}\frac{\partial p(0,t)}{\partial t} &= -V_d\, p(0,t) + V_b p(1,t) + s\bar{k} p(0,t) \\ \frac{\partial p(k,t)}{\partial t} &= -V\, p(k,t) + V_d\, p(k-1,t) + V_b p(k+1,t) - s(k-\bar{k}(t))p(k,t)\ ,\end{aligned} \tag{A.1}$$

where $V = V_d + V_b$ and $\bar{k}(t) = \sum_{k=0}^{\infty} k\ p(k,t)$. In the stationary state, the LHS is zero and the frequencies are time-independent. On dividing both sides of the above equations by $s$, we find that the stationary frequency $p(k)$ depends on the ratios $V_b/s$ and $V_d/s$. We first expand the fraction $p(k)$ in a power series about $V_b/s = 0$ as

$$p(k) = \sum_{n=0}^{\infty} \left(\frac{V_b}{s}\right)^n\ p_n(k)\ , \tag{A.2}$$

where $p_n(k)$ is proportional to the $n$th derivative of $p(k)$ with respect to $V_b/s$ evaluated at $V_b = 0$. The lowest order term $p_0(k)$ is the solution of the steady state of (A.1) in the absence of compensatory mutations, and is known to be a Poisson distribution with mean $\bar{k}_0 = V_d/s$ [47]:

$$p_0(k) = e^{-\bar{k}_0}\ \frac{\bar{k}_0^k}{k!}\ ,\ k = 0, 1, \ldots \tag{A.3}$$

To find the solution with nonzero $V_b$, we first set the LHS of (A.1) equal to zero, and substitute (A.2) in these equations. On neglecting the terms of order $(V_b/s)^2$ and higher, we obtain the following equations for $p_1(k)$:

$$\bar{k}_1 p_0(0) = -p_0(1) \tag{A.4}$$

$$\bar{k}_0 p_1(k-1) - k p_1(k) + \bar{k}_1 p_0(k) = p_0(k) - p_0(k+1)\ ,\ k = 1,2,... \tag{A.5}$$

where $\bar{k}_1 = \sum_{k=0}^{\infty} k p_1(k)$. Equation (A.4) above immediately yields $\bar{k}_1 = -\bar{k}_0$. Thus, as expected, the effect of compensatory mutations is to decrease the deleterious mutations in a population. Using this result in (A.5), after some simple algebra, we get the following one-term recursion equation for $p_1(k)\ ,\ k \geq 1$:

$$p_1(k) = \frac{\bar{k}_0}{k}\ p_1(k-1) - \left(\frac{1}{k} + \frac{\bar{k}_0}{k+1}\right)\ p_0(k)\ , \tag{A.6}$$

which can be iterated easily to give

$$p_1(k) = \frac{\bar{k}_0^k}{k!}\ p_1(0) - p_0(k)\ \left[\bar{k}_0(H_{k+1} - 1) + H_k\right]\ , \tag{A.7}$$

where the harmonic number $H_k = \sum_{i=1}^{k} i^{-1}$ and the fraction $p_1(0)$ is determined using the normalisation condition, viz., $\sum_{k=0}^{\infty} p(k) = 1$. Since the fraction $p_0(k)$ already satisfies this condition, we have the constraint $\sum_{k=0}^{\infty} p_1(k) = 0$, on using which, $p_1(0)$ can be found. For large $k$, using $H_k \approx \ln k$ in (A.7), we obtain the expression (2.10).

## A.2 Fixation probability in the absence of compensatory mutations

To find the total fixation probability given by (2.3), we use the expression (2.5) for the fixation probability and (A.3) for the mutator fraction $p_0(k)$ which is a Poisson distribution with mean $\bar{k}_0$. When $\bar{k}_0 \ll 1$, we have $\Pi_0 \approx p_0(0)\pi_0(0) = 2V_d$. But for $\bar{k}_0 \gg 1$, on summing over the mutator backgrounds in which a nonmutator can arise, we obtain the total fixation

probability to be

$$\Pi_0 = \sum_{k=0}^{\lfloor \bar{k}_0 \rfloor} p_0(k)\pi_0(k) = 2s\,\frac{e^{-\lfloor \bar{k}_0 \rfloor}\,\lfloor \bar{k}_0 \rfloor^{\lfloor \bar{k}_0 \rfloor+1}}{\lfloor \bar{k}_0 \rfloor!}\,. \tag{A.8}$$

On using the Stirling's formula $x! \approx \sqrt{2\pi x}(x/e)^x$ for large $x$ in the last expression, we immediately obtain (2.6). Another way of seeing the result in the large $\bar{k}_0$ regime is by approximating the Poisson-distributed $p_0(k)$ by a Gaussian with mean and variance equal to $\bar{k}_0$ and thus obtain

$$\Pi_0 \sim 2s\int_{\bar{k}_0-\sqrt{\bar{k}_0}}^{\bar{k}_0} dk(\bar{k}_0-k)\,\frac{1}{\sqrt{\bar{k}_0}}\,e^{-\frac{(k-\bar{k}_0)^2}{2\bar{k}_0}} \sim 2s\sqrt{\bar{k}_0}\int_0^1 dx\; xe^{-x^2} \tag{A.9}$$

where we have used the fact that the mutator frequency is substantial in the fitness classes lying within a distance $\sqrt{\bar{k}_0}$ of the mean.

## A.3 Fixation probability when compensatory mutations are included

Inserting $\Pi = \Pi_0 + (V_b/s)\Pi_1$ and $\overline{W} = \overline{W}_0 + (V_b/s)\overline{W}_1$ in (2.2), and using the exact equation for $\pi_0(k)$, we get a rather involved expression for $\pi_1(k)$ given by

$$\pi_1(k) = -\frac{\overline{W}_1}{\overline{W}_0}\,\frac{W(k)\pi_0(k)(1-\pi_0(k))}{\overline{W}_0 - W(k)(1-\pi_0(k))}\,. \tag{A.10}$$

Since all the parameters are smaller than one, we work with the approximate expression (2.5) for the probability $\pi_0(k)$ and arrive at (2.9).

We now calculate the contribution $\Pi_1$ given by (2.8) when $\bar{k}_0 \gg 1$ using the expression (2.9) for $\pi_1(k)$ and the frequency $p_1(k)$ in (2.10). We have

$$\Pi_1 = -2s\bar{k}_0(1-\sum_{k=\lfloor \bar{k}_0 \rfloor}^{\infty} p_0(k)) + 2s\sum_{k=0}^{\infty}(\bar{k}_0-k)p_1(k) - \sum_{k=\lfloor \bar{k}_0 \rfloor}^{\infty} p_1(k)\pi_0(k) \tag{A.11}$$

$$= 2s\bar{k}_0\sum_{k=\lfloor \bar{k}_0 \rfloor}^{\infty} p_0(k) - 2\sum_{k=\lfloor \bar{k}_0 \rfloor}^{\infty}(\bar{k}_0-k)\;sp_1(k)\,, \tag{A.12}$$

where we have assumed that $V_b, V_d, s$ are small, but $V_b/s$ and $V_d/s$ are finite. The last expression is obtained on using the normalisation condition $\sum_{k=0}^{\infty} p_1(k) = 0$ and the expression for the average $\bar{k}_1$. For large $\bar{k}_0$, we approximate the Poisson distribution $p_0(k)$ by a Gaussian as

$$p_0(k) \approx \frac{1}{\sqrt{2\pi\bar{k}_0}}\, e^{-\frac{(k-\bar{k}_0)^2}{2\bar{k}_0}} \left(1 - \frac{k-\bar{k}_0}{2\bar{k}_0} + \mathcal{O}(\bar{k}_0^{-2})\right). \tag{A.13}$$

Approximating the sums in (A.12) by integrals, we finally have

$$\frac{\Pi_1}{s} \approx \left[\bar{k}_0 - \sqrt{\frac{\bar{k}_0}{2\pi}}\right] - \frac{2\bar{k}_0}{\sqrt{\pi}} \int_0^{\infty} dz \frac{e^{-z^2}}{1 + z\sqrt{\frac{2}{\bar{k}_0}}} \approx \sqrt{\frac{\bar{k}_0}{2\pi}}\,, \tag{A.14}$$

where we have carried out an integration by parts in the second integral on the RHS and neglected subleading terms in $\bar{k}_0$.

# Appendix B

## B.1 Frequency of mutator population

Similar to (A.1) in Appendix A.1, when $s$ and $V_d$ are small, the population fraction of mutators carrying $k$ mutations in generation $t$ can be expressed using the equation

$$\frac{\partial p(k,t)}{\partial t} = V_d[\bar{p}(k-1,t) - \bar{p}(k,t)] - s[k^\alpha - \overline{k^\alpha}(t)]p(k,t)\,, \tag{B.1}$$

where

$$\overline{k^\alpha}(t) = \sum_{k=0}^{\infty} (k)^\alpha\, p(k,t) \tag{B.2}$$

and $p(-1,t) = 0$. Note that the difference between (B.1) and (A.1) is that (A.1) is for a non-epistatic fitness landscpae ($\alpha = 1$ in (B.1)), but in the presence of compensatory mutations. When the population is in steady state, (B.1) and (B.2) become time independent, and we get

$$V_d[\bar{p}(k-1) - \bar{p}(k)] - s[k^\alpha - \overline{k^\alpha}]p(k) = 0\,. \tag{B.3}$$

Solving (B.3) for $k = 0$ yields expression for negative of the mean Wrightian fitness (logarithm of the Malthusian fitness given by (4.1)) of the population per selection coefficient

$$\overline{k^\alpha} = V_d/s\,. \tag{B.4}$$

This can be substituted back in (B.3) and iterated to get [62]

$$p(k) = \frac{(V_d/s)^k}{(k!)^\alpha} p(0)\ . \tag{B.5}$$

The normalization condition $\sum_{k=0}^{\infty} p(k) = 1$ gives [62]

$$p(0) = \left[ \sum_{k=0}^{\infty} (V_d/s)^k \, (k!)^{-\alpha} \right]^{-1} . \tag{B.6}$$

The exact solutions to the above expression are possible only for $\alpha = 1$ (non-epistatic case) [46, 47] and $\alpha = 2$ [62].

$$p(0) = \begin{cases} e^{-V_d/s} & \text{if } \ \alpha = 1 \\ \left[ I_0\left(2\sqrt{\frac{V_d}{s}}\right) \right]^{-1} & \text{if } \ \alpha = 2. \end{cases} \tag{B.7}$$

$I_0\left(2\sqrt{\frac{V_d}{s}}\right)$ is the modified Bessel function of the first kind of order 0. (Refer to [66] to know more about this function.) It is a monotonically increasing function of $(V_d/s)$, so that $p(0)$ decreases with increase in $(V_d/s)$. For any value of $\alpha$ except 1 and 2, approximations are needed to solve (B.6).

## B.2 Approximate expressions for the class zero mutator frequency

By taking the ratio $p(k)/p(k-1)$ in (B.5), we can see that the maximum of $p(k)$ is at $k_m = (V_d/s)^{1/\alpha}$.

Case I: $V_d/s > 1$, $\alpha \leq 1$

For $\alpha \leq 1$, when selection is weaker than mutation rate, $(V_d/s)^{1/\alpha} > 1$. Correspondingly, the distribution of mutators can be approximated by a Gaussian. As a first step, upon using Stirling's approximation $k! \approx \sqrt{2\pi k}\,(k/e)^k$ in (B.5), we obtain

$$p(k) = \frac{(V_d/s)^k \ e^{k\alpha}}{\left(\sqrt{2\pi k}\ k^k\right)^\alpha} \ p(0)\ . \tag{B.8}$$

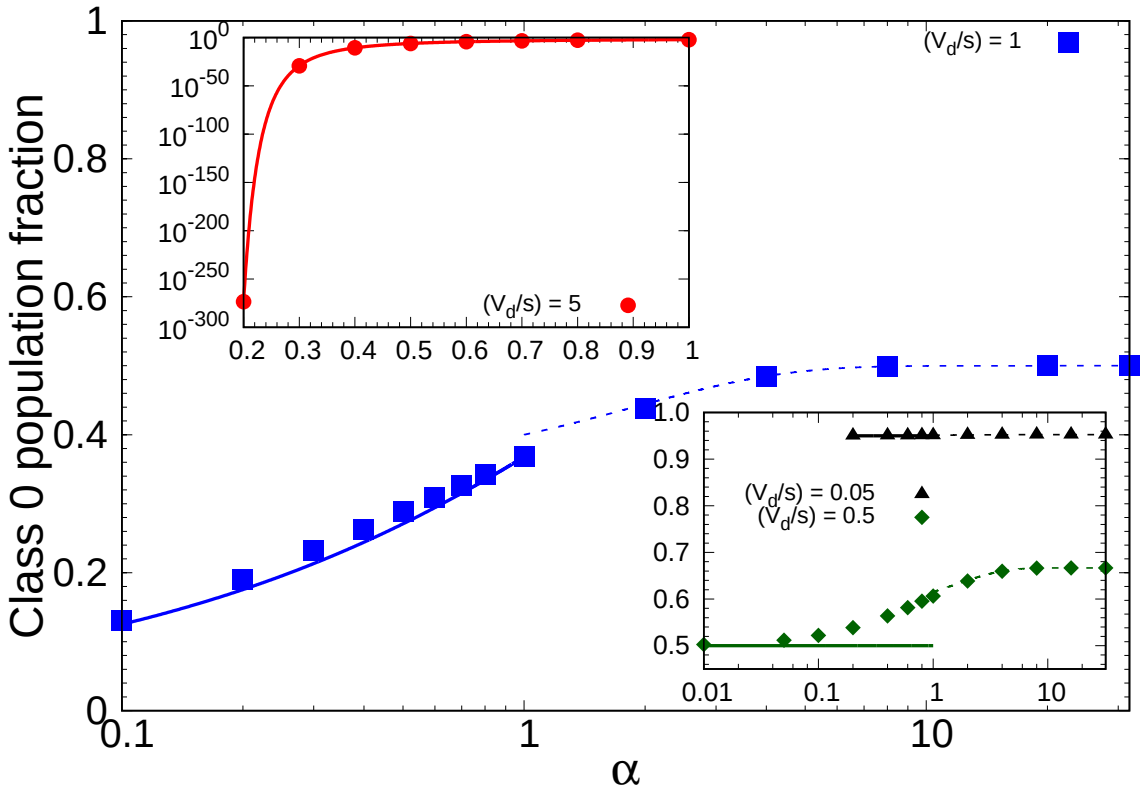


Fig. B.1 Class 0 mutator fractions. For the main figure and the insets, the symbols represent the numerically evaluated values of the full sum in (B.6). Main figure: Weak selection with antagonistic and synergistic epistasis. Solid and broken curves are expressions (B.12) and (B.13), respectively for $(V_d/s) = 1$ (blue squares). Left top inset: Weak selection; antagonistic epistasis. The red solid curve is (B.12) for $(V_d/s) = 5$. Right bottom inset: Strong selection with antagonistic and synergistic epistasis. The solid and broken curves show (B.14) and (B.15), respectively for $(V_d/s) = 0.05$ (black triangles) and $(V_d/s) = 0.5$ (green diamonds).

Now, converting (B.8) to an exponential and then expanding around its maximum $(V_d/s)^{1/\alpha}$ using Taylor series gives

$$p(k) = \frac{e^{\alpha(V_d/s)^{1/\alpha}}}{\left(2\pi(V_d/s)^{1/\alpha}\right)^{\alpha/2}} \; e^{\frac{-\alpha\left(k-(V_d/s)^{1/\alpha}\right)^2}{2(V_d/s)^{1/\alpha}}} \; p(0) \; . \tag{B.9}$$

By replacing the sum in (B.6) by an integral and using (B.9), we get

$$p(0) = \left( \frac{e^{\alpha(V_d/s)^{1/\alpha}}}{\left(\sqrt{2\pi(V_d/s)^{1/\alpha}}\right)^{\alpha}} \left[ \int_{x=0}^{(V_d/s)^{1/\alpha}} e^{-\frac{\alpha x^2}{2(V_d/s)^{1/\alpha}}} dx + \int_{x=0}^{\infty} e^{-\frac{\alpha x^2}{2(V_d/s)^{1/\alpha}}} dx \right] \right)^{-1} . \tag{B.10}$$

Performing the integral in (B.10) yields

$$p(0) = \left( \frac{e^{\alpha(V_d/s)^{1/\alpha}}}{\left(\sqrt{2\pi(V_d/s)^{1/\alpha}}\right)^{\alpha}} \sqrt{\frac{\pi(V_d/s)^{1/\alpha}}{2\alpha}} \left[ 1 + erf\left( \sqrt{\frac{\alpha(V_d/s)^{1/\alpha}}{2}} \right) \right] \right)^{-1} . \tag{B.11}$$

For large values of $x$, we have the expansion $erf(x) \approx 1 - \frac{e^{-x^2}}{x\sqrt{\pi}} \approx 1$. By using this, we can simplify (B.11) to write

$$p(0) = (2\pi)^{\frac{\alpha-1}{2}} e^{-\alpha(V_d/s)^{1/\alpha}} \alpha^{1/2} (V_d/s)^{\frac{\alpha-1}{2\alpha}} \; . \tag{B.12}$$

Note that (B.12) reproduces the known result $p(0) = e^{-V_d/s}$ for $\alpha = 1$. Fig. B.1 shows a comparison of (B.12) with (B.6). The inset at the left top clearly indicates that (B.12) very well captures the exact sum even for extremely small values of $p(0)$.

Case II: $V_d/s > 1$, $\alpha > 1$

In this case, the Gaussian approximation does not hold good. An approximate solution is possible for the limit case $(V_d/s)^{1/\alpha} < 2$. When $(V_d/s)^{1/\alpha} < 2$, the mutator frequency peaks around 1 (also, see section 4.3.1.2), and contributions to $p(k)$ from classes with $k > 1$ are negligibly small. Nevertheless, in order to obtain a very accurate estimate of $p(0)$, terms up

to second order can be retained. Effectively, we get

$$p(0) \approx \frac{1}{1 + V_d/s + \frac{(V_d/s)^2}{2^\alpha}} \quad \text{if} \quad \alpha > \frac{\ln(V_d/s)}{\ln 2} \,. \tag{B.13}$$

As $\alpha$ increases, $p(0)$ rises to the constant value $(1 + V_d/s)^{-1}$, which is the upper bound of $p(0)$. Fig. B.1 shows that (B.13) matches well with (B.6) for large values of $\alpha$. For values of $\alpha$ that are not very large, other classes also contribute. As a result, $p(0)$ will be smaller than what is predicted by (B.13).

Case III: $V_d/s < 1$, $\alpha < 1$

When $V_d/s < 1$, $p(k)$ in (B.5) is a monotonically decreasing function of $k$. In the limiting case $\alpha \to 0$, (B.6) becomes

$$p(0) \approx \left[ \sum_{k=0}^{\infty} (V_d/s)^k \right]^{-1} = (1 - V_d/s), \quad \text{if} \quad \alpha \ll 1 \,. \tag{B.14}$$

However, (B.14) only provides the lower bound of $p(0)$ in the presence of antagonistic epistasis when the selection is strong. When both $(V_d/s)$ and $\alpha$ are not very small compared to 1, this expression is not accurate to obtain the exact values of $p(0)$ (see Table B.1). The right bottom inset of Fig. B.1 shows that $p(0)$ predicted by (B.6) decreases to (B.14) for very small values of $\alpha$. It can be seen that $p(0)$ depends on $\alpha$ if the numerical value of $(V_d/s)$ is close to 1. Expression (B.14) does not capture this dependence. When $(V_d/s) \ll 1$, $p(0)$ becomes independent of $\alpha$. Moreover, Table B.1 and Fig. B.1 indicate that corresponding to the same value of $\alpha$, as the value of $(V_d/s)$ increases, $p(0)$ decreases.

Note that when $\alpha = 0$, it follows from (4.1) that all the individuals carrying non-zero mutations have the same fitness $(1 - s)$. Thus, in practice, the population has only two classes differing in fitness by $s$, with mutation rate from class 0 to 1 being $V_d$. For this, the steady state solution for population fraction in class 0 yields (B.14).

Case IV: $V_d/s < 1$, $\alpha > 1$

| Comparison of (B.14) with (B.6) | | | |
|---|---|---|---|
| $\alpha$ | $V_d/s$ | $p(0)$ (exact) | $(1-V_d/s)$ |
| 1 | 0.9 | 0.407 | 0.1 |
| $10^{-1}$ | 0.9 | 0.196 | 0.1 |
| $10^{-2}$ | 0.9 | 0.115 | 0.1 |
| $10^{-3}$ | 0.9 | 0.102 | 0.1 |
| 1 | 0.5 | 0.607 | 0.5 |
| $10^{-1}$ | 0.5 | 0.522 | 0.5 |
| $10^{-2}$ | 0.5 | 0.503 | 0.5 |
| 1 | 0.2 | 0.819 | 0.8 |
| $10^{-1}$ | 0.2 | 0.803 | 0.8 |
| 1 | 0.1 | 0.905 | 0.9 |

Table B.1 Evaluation of $p(0)$ (exact) is done using (B.6). For small $(V_d/s)$ values, (B.14) and (B.6) show a good agreement. For larger $(V_d/s)$, these two solutions match only for $\alpha \ll 1$.

Like Case II studied here, the class 0 mutator fraction increases with $\alpha$.

$$p(0) \approx \frac{1}{1+V_d/s+\frac{(V_d/s)^2}{2^\alpha}} \quad \text{if} \quad \alpha > 1\,. \tag{B.15}$$

From the right bottom inset of Fig. B.1, we can see that $p(0)$ predicted by (B.6) increases to $(1+V_d/s)^{-1}$ for large values of $\alpha$. When $(V_d/s) \ll 1$, (B.14) and (B.15) give almost the same result close to 1 for $p(0)$, indicating the fact that the fraction of individuals with zero deleterious mutations in the population is unaffected by epistasis when the selective effects are very strong. Since the population is localized around class 0, the frequency of individuals in other fitness classes will be insignificant. Note that when $(V_d/s)$ is not very small compared to 1, $p(0)$ depends on $\alpha$.

Results of this section are summarized in Table 4.1.

## B.3 Explanation for the trend in Fig. 4.7

Table B.2 gives the numerical values of $\pi(k)$ using (4.8), and $p(k)$ for different values of $s$. When $s$ is reduced, $\pi(0)$ remains roughly the same, while $p(0)$ decreases. This explains why

$\Pi = \pi(0)p(0)$ falls as a function of $s$ in the strong selection regime. For $k > 0$, for a given value of $k$, $\pi(k) = 2(V_d - sk^\alpha)$ (see (4.11)) increases with decrease in $s$. From Appendix B.2, we understand that the distribution $p(k)$ peaks around $k_m = (V_d/s)^{1/\alpha}$. Column 2 of Table B.2 shows this value. The integer part $\lfloor k_m \rfloor$ of the corresponding number gives the maximum value of the fitness class that contributes to $\Pi$. In the weak selection regime, when $s$ is lowered keeping $\lfloor k_m \rfloor$ to be the same, we see from Table B.2 that $p(k_m)$ remains almost the same, while $p(k)$ decreases for all $k < k_m$. Hence, the net effect on $\Pi$ due to decrease in $s$ is not a straightforward problem. To have a better understanding at least for $1 \leq (V_d/s)^{1/\alpha} < 2$ ($\lfloor k_m \rfloor = 1$), we can make use of (4.16). The argument used in understanding the case $\lfloor k_m \rfloor = 1$ can be extrapolated to the general case $\lfloor k_m \rfloor = n$, where $n$ takes only positive integer values.

By taking the first derivative of $\Pi$ in (4.16) with regard to $s$, we can see that $\Pi$ peaks at a particular value of selection

$$s^* = 2^{-\alpha/2} V_d \,. \tag{B.16}$$

Note that for $\alpha = 2$, (B.16) yields $s^* = 5 \times 10^{-3}$ ($V_d/s^* = 2$), which approximately matches with the simulation data (blue triangles) shown in Fig. 4.7, whereas for $\alpha = 16$ (shown using the red squares), $s^* = 3.9 \times 10^{-5}$ ($V_d/s^* = 256$). The latter point also agrees with the data plotted in Fig. 4.7. The red curves for the weak and strong selection regimes are (4.16) and (4.18), respectively. $\Pi$ increases with decrease in $s$ for $V_d < s \leq s^*$. Further decrement in $s$ reduces $\Pi$ for $s^* < s \leq 2^{-\alpha} V_d$. When $s$ is lowered from $n^{-\alpha}\ V_d$ to $(n+1)^{-\alpha}\ V_d$, where $n = 1, 2, 3, \ldots$ (see Table B.2), $\lfloor k_m \rfloor$ increases by 1. Consequently, frequencies $p(k)$ of classes having high $\pi(k)$ values decrease. For $k > 1$, $\pi(k)$ declines rapidly with $k$. This can be explicitly seen in the last row in Table B.2, for which the selection is very small. Therefore, each time $\lfloor k_m \rfloor$ increases by 1 due to decrement in $s$, $\Pi$ increases initially, followed by a faster decay. As a result, whenever $(V_d/s) = n^\alpha$ with $n$ being any non-zero value of $\lfloor k_m \rfloor$, $\Pi$ assumes its local minimum values, as we see in Fig. 4.7.

In the weak selection regime, for $\alpha > 1$, $\Pi$ undergoes damped oscillations and decreases overall. We will examine the properties of its local maxima or peaks. The relative increase

in $\Pi$ corresponding to $s^*$ (first peak) can be measured as

$$\frac{\Delta\Pi(s^*)}{\Pi(s)|_{V_d}} = \frac{\Pi(s)|_{s^*} - \Pi(s)|_{V_d}}{\Pi(s)|_{V_d}} . \tag{B.17}$$

Substituting (B.16) in (4.16), we get

$$\Pi(s)|_{s^*} = \frac{2V_d\, 2^{\alpha/2}}{2+2^{\alpha/2}} . \tag{B.18}$$

For $\alpha = 16$, (B.18) yields $\Pi(s, \alpha = 16)|_{s^*} = 2V_d$, and (4.16) leads to $\Pi(s, \alpha = 16)|_{V_d} = V_d$. Indeed, these two match with the observed values in Fig. 4.7. Thus, we estimate the value of the relative increase in $\Pi$ corresponding to $s^*$ to be 100 percent for $\alpha = 16$ using (B.17). This result is applicable for any large value of $\alpha$ for which $2^{\alpha/2} \gg 2$. For $\alpha = 2$, (B.16) can be substituted back in the exact expression (4.19) to obtain $\Pi(s, \alpha = 2)|_{s^*} = 0.94V_d$. At $s = V_d$, using (4.19), $\Pi(s, \alpha = 2)|_{V_d} = 0.88V_d$. These two results also are in good agreement with what is observed in Fig. 4.7. The resulting relative increase in $\Pi$ for $\alpha = 2$ corresponding to $s^*$ is 6.8 percent. It is evident that with reduction in $\alpha$, the first peak gets smaller. Moreover, Fig. 4.7 suggests that for the same value of $\alpha$, the peaks associated with further reductions in $s$ ($\lfloor k_m \rfloor > 1$) become less significant.

For $\alpha \leq 1$, the approximation $\lfloor k_m \rfloor = k_m$ was made in order to get the simple analytical expression (4.14). At least for $\alpha = 1$, for which an exact formula for $p(0)$ is available, the presence of non-monotonicity in the weak selection regime can be tested. Using (B.7) in (4.12), we can write

$$\Pi = \frac{2V_d \left(\frac{V_d}{s}\right)^{\lfloor (V_d/s) \rfloor}}{(\lfloor (V_d/s) \rfloor !)}\, e^{-V_d/s} . \tag{B.19}$$

In the weak selection regime, when $\lfloor V_d/s \rfloor = n$, this can be rewritten as $\Pi = 2V_d\,(V_d/s)^n\, e^{-V_d/s}/(n!)$. By differentiating $\Pi$ with respect to $s$, one can see that $\Pi$ peaks at $s = n^{-1}V_d$. However, in this section, we have already seen that the local minima of $\Pi$ occur at $s = n^{-1}V_d$. This reflects the fact that there is no nonmonotonicity for $\alpha = 1$. The inset of Fig. 4.7 shows (B.19) using dark green lines, and the filled circles are the numerical solutions of $\Pi$ using (4.8) and (4.9). The broken violet line is the approximate expression (4.14) for $\alpha = 1$. For antagonistic

| **Synergistic epistasis: Variation of $\Pi$ with selection** | | | | | | | | | | | |
|---|---|---|---|---|---|---|---|---|---|---|---|
| $\left(\frac{s}{V_d}\right)$ | $\left(\frac{V_d}{s}\right)^{\frac{1}{\alpha}}$ | $\pi(k)\times 10^2$ | | | | $p(0)$ | $p(1)$ | $p(2)$ | $p(3)$ | $\Pi\times 10^3$ | |
| | | $k=0$ | $k=1$ | $k=2$ | $k=3$ | | | | | Exact | Eqn. (4.19) |
| 10.0 | 0.32 | 1.96 | | | | 0.91 | | | | 17.8 | 18.1 |
| 3.00 | 0.58 | 1.96 | | | | 0.73 | | | | 14.4 | 14.7 |
| 1.00 | 1.00 | 1.96 | 0.00 | | | 0.44 | 0.44 | | | 8.6 | 8.8 |
| 0.90 | 1.05 | 1.97 | 0.17 | | | 0.41 | 0.45 | | | 8.8 | 9.0 |
| 0.50 | 1.41 | 1.97 | 0.97 | | | 0.24 | 0.47 | | | 9.2 | 9.4 |
| 0.25 | 2.00 | 1.98 | 1.47 | 0.00 | | 0.09 | 0.35 | 0.35 | | 7.0 | 7.1 |
| 0.20 | 2.24 | 1.98 | 1.57 | 0.38 | | 0.06 | 0.29 | 0.37 | | 7.2 | 7.3 |
| 0.14 | 2.67 | 1.98 | 1.70 | 0.86 | | 0.03 | 0.19 | 0.34 | | 6.7 | 6.9 |
| 0.10 | 3.16 | 1.98 | 1.78 | 1.12 | 0.18 | 0.01 | 0.11 | 0.28 | 0.31 | 6.0 | 6.1 |

Table B.2 The data corresponds to $V_d = 0.01$ and $\alpha = 2$. The integer value corresponding to the number in the second column gives the number of classes that contribute to $\Pi$. $\pi(k)$ and $\Pi$ are scaled by $10^2$ and $10^3$, respectively. $\pi(k)$ values are obtained numerically via solving (4.8), while $p(k)$ using (B.7). To get the exact values of $\Pi$ given in column 11, (4.8) and (4.9) have been numerically solved.

epistasis, from the simulation data in Figures 4.5 and 4.6, we do not see any nonmonotonic trend in the weak selection regime unlike Fig. 4.7. Note that for the set of parameters used in these two figures, $\lfloor (V_d/s)^{1/\alpha} \rfloor$ can be as large as 7.

## B.4 Regarding the discrepancy between the analytical and simulation results

To have a steady state, the size of a population needs to be of the order of 100 $(p(0))^{-1}$ [63]. Table B.3 gives $p(0)$ values by solving (B.12) corresponding to two $(V_d/s)$ values, changing $\alpha$. For large $(V_d/s)$ and small $\alpha$, we find that the size required for the attainment of steady state is too large for most of the biological populations. Hence, populations of lower size will accumulate deleterious mutations and go extinct (see section 4.4.1). By comparing columns 4 and 5, it can be seen that as $\alpha$ decreases, (4.14) deviates from the exact solution of $\Pi$ obtained using (4.8) and (4.9). This is because the approximation (4.11) does not hold good for the fitness classes close to $\lfloor (V_d/s)^{1/\alpha} \rfloor$, which contribute more to $\Pi$ due to the form (4.15) taken by the mutator frequency. Moreover, for a particular value of $\alpha$, the deviation

| **Weak selection; antagonistic epistasis: Comparison of (4.14) with the exact numerical solution for Π** | | | | |
|---|---|---|---|---|
| $\alpha$ | $V_d/s$ | $p(0)$ | Exact value of Π using (4.8) and (4.9) | Π using (4.14) |
| 0.5 | 5 | $7.44\times10^{-7}$ | $1.03\times10^{-2}$ | $1.19\times10^{-2}$ |
| 0.45 | 5 | $1.56\times10^{-8}$ | $8.00\times10^{-3}$ | $8.96\times10^{-3}$ |
| 0.4 | 5 | $2.12\times10^{-11}$ | $5.84\times10^{-3}$ | $6.75\times10^{-3}$ |
| 0.3 | 5 | $6.24\times10^{-30}$ | $2.13\times10^{-3}$ | $2.99\times10^{-3}$ |
| 0.2 | 1.5 | $2.09\times10^{-2}$ | $3.81\times10^{-3}$ | $3.89\times10^{-3}$ |
| 0.15 | 1.5 | $5.99\times10^{-3}$ | $2.23\times10^{-3}$ | $2.40\times10^{-3}$ |
| 0.1 | 1.5 | $6.98\times10^{-5}$ | $7.62\times10^{-4}$ | $9.97\times10^{-4}$ |

Table B.3 Here, $p(0)$ is evaluated using (B.12). The value of $s$ is chosen to be 0.02 for the two values of $(V_d/s)$ used.

is less if the value of $(V_d/s)$ is small. Nevertheless, populations of size in the biological limit having larger values of $(V_d/s)$ and smaller values of $\alpha$ do not have steady state. Hence, (4.14) is applicable to most of the real populations except those with both $(V_d/s) \sim 1$ and antagonistic epistasis with very small $\alpha$ values. However, a better approximation to $\pi(k)$ is needed to yield more accurate results for Π when $(V_d/s) \gg 1$ and $\alpha \ll 1$.

One more thing to note is that $\alpha_c = 0.5$ is obtained using (4.14). This tells us that the "true" value of $\alpha_c$ could be slightly different from 0.5, as (4.14) deviates from the exact results. The best estimate of $\alpha_c$ is given in Appendix B.6.

To derive (4.11), we assumed that $\pi(k) \ll 1$ and neglected cubic and higher order terms. When $V_d \gtrsim 0.1$, $\pi(k)$ values will differ from what we obtain using (4.11). Due to the same reason, there is discrepancy between (4.16) and (4.18), as well as the simulation data in Figures 4.2 and 4.4, respectively. The same expressions match well with the simulation points for $V_d = 10^{-2}$ as shown in Fig. 4.7 and using the blue diamonds in Fig. 4.4. Corresponding to the point $\alpha = 20$, Table B.4 provides a comparison of (4.16) and (4.18), and the simulation results in Figures 4.2 and 4.4, respectively. In fact, (4.14) also deviates from the simulation results for large $V_d$ values. This is clear in the case of the red circles corresponding to $\alpha = 1$ and the blue squares corresponding to $\alpha = 0.4$ in Fig. 4.5, and in Fig. 4.2, where $log$ scale is

| Synergistic epistasis: Comparison of simulation data in Figures 4.2 and 4.4 with analytical results | | | |
|---|---|---|---|
| $V_d$ | $\overline{\Pi}_{sim}$ (standard error) | $\Pi_{num}$ | $\Pi_{analytic}$ |
| 0.15 | $1.571 \times 10^{-1}$ $(1.15 \times 10^{-3})$ | $1.553 \times 10^{-1}$ | $1.80 \times 10^{-1}$ |
| 0.10 | $9.406 \times 10^{-2}$ $(9.231 \times 10^{-4})$ | $9.12 \times 10^{-2}$ | $1.00 \times 10^{-1}$ |
| 0.05 | $6.445 \times 10^{-2}$ $(7.765 \times 10^{-4})$ | $6.33 \times 10^{-2}$ | $6.67 \times 10^{-2}$ |
| 0.01 | $1.738 \times 10^{-2}$ $(4.133 \times 10^{-4})$ | $1.785 \times 10^{-2}$ | $1.82 \times 10^{-2}$ |

Table B.4 The parameters used here are $\alpha = 20$, $s = 0.1$, and $N = 4000$. Note that $\Pi_{analytic}$ is given by (4.16) for weak selection, which is applicable to the $V_d$ values in the first two rows. $\Pi_{analytic}$ is obtained using (4.18) for strong selection, applicable to the $V_d$ values in the last two rows. $\Pi_{num}$ is obtained by solving (4.8) and (4.9).

used to plot the data. Moreover, based on the discussion in Appendix B.3, it is worth noting that (4.12) is the more accurate form of (4.14), but the latter is more simplified.

The analytical expression (4.17) for the strong selection; antagonistic epistasis regime (section 4.3.1.3) is valid only for $\alpha \ll 1$. A more precise formula for $p(0)$ in this case can help us to analytically understand the variation of $\Pi$ with $\alpha$, and the nonmonotonic behavior in Fig. 4.5. Further, (4.16) and (4.18) are not exact expressions. A more accurate expression for $p(0)$ in the presence of synergistic epistasis will pave the way for better analytical understanding.

## B.5 Regarding steady state

The argument of [63] on the minimum population size necessary to ensure steady state includes only the population fraction corresponding to the least loaded class (see section 4.2.1). A further detailed analysis by [62] shows that the ratchet time is actually proportional to the number of individuals in the least loaded class times the selection coefficient. A very high ratchet time corresponds to very a slowly operating ratchet. For smaller values of selection coefficient, the deviation from the results of [63] becomes clearer. Nevertheless, for the parameters used in this Chapter, there will not be any significant difference from the above theory, since smaller values of selection have been used only for synergistic epistasis.

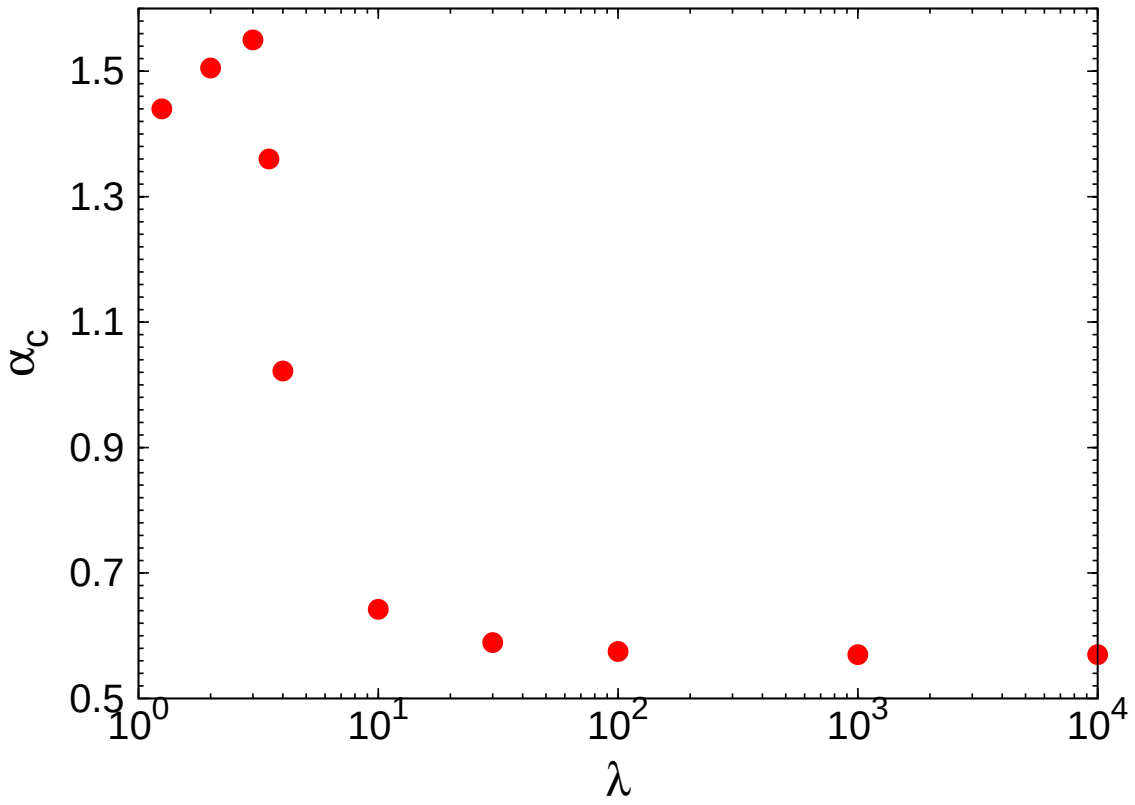


Fig. B.2 Variation of $\alpha_c$ with the strength $\lambda$ of the mutator. The points (red filled circles) are obtained using numerical solution of (4.8) and (4.9). For all these points, $s = 0.1$.

## B.6 Critical value of epistasis for the weak mutator background

Weak mutator refers to the case when the mutation rate of the nonmutator is comparable ($\lambda \sim 1$) with that of the mutator. In two recent mutation reduction experiments [34, 6], weak mutators with $\lambda$ as low as 2 have been observed. By solving (4.8) and (4.9) using *Wolfram Mathematica* 9.0.1.0, we obtain $\Pi$ as a function of $\alpha$ for a given value of $\lambda$. By comparing these $\Pi$ values up to three significant figures for two different values of $V_d$, we estimate $\alpha_c$ corresponding to each $\lambda$. With the variation in mutator strength, $\alpha_c$ changes. This is plotted in Fig. B.2. For strong mutators, the exact numerical analysis suggests that $\alpha_c$ approaches its minimum value 0.57, as $\lambda \to \infty$. This is contrary to the analytical result $\alpha_c = 0.5$ using (4.14). Therefore, even though (4.14) is helpful in demonstrating the presence of $\alpha_c$ (see section 4.3.1.1), this expression is not very accurate in determining $\alpha_c$ precisely. This is

| **Simulation results for weak mutators** | | | | | | | |
|---|---|---|---|---|---|---|---|
| $\lambda$ | $V_d$ | $\alpha$ | $\overline{\Pi}_{sim}$ $(SE \times 10^4)$ | $\overline{\Pi}_{sim}$ $(SE \times 10^4)$ | $\alpha$ | $V_d$ | $\lambda$ |
| | | 1.7 | 0.04164 (6.317) | 0.04159 (6.314) | 1.7 | | |
| 2 | 0.15 | **1.6** | 0.04023 (6.214) | 0.04025 (6.215) | **1.6** | 0.10 | 2 |
| | | 1.5 | 0.03866 (6.096) | 0.04048 (6.232) | 1.5 | | |
| | | 1.0 | 0.05411 (7.154) | 0.05253 (7.055) | 1.0 | | |
| 4 | 0.15 | **0.9** | 0.05140 (6.983) | 0.05106 (6.961) | **0.9** | 0.10 | 4 |
| | | 0.8 | 0.04659 (6.665) | 0.04931 (6.847) | 0.8 | | |
| | | 0.6 | 0.06195 (7.623) | 0.05926 (7.466) | 0.6 | | |
| 100 | 0.15 | **0.5** | 0.05332 (7.105) | 0.05527 (7.226) | **0.5** | 0.10 | 100 |
| | | 0.4 | 0.04432 (6.508) | 0.04953 (6.861) | 0.4 | | |

Table B.5 Example of values for $\Pi$ for two different values of $V_d$, and $\alpha_c$ is obtained as the value of $\alpha$ for which the difference between the two $\Pi$ values is the minimum. The $\alpha_c$ value corresponding to each $\lambda$ is indicated in bold. The simulation parameters are $s = 0.1$, $N = 4000$, and each simulation point is averaged over $10^5$ independent stochastic realizations. The standard error ($SE$) value given in each row is the actual value multiplied by $10^4$. The best estimates of $\alpha_c$ using *Mathematica* (see Appendix B.6 and Fig. B.2) are 1.505, 1.022 and 0.575 for $\lambda = 2$, 4 and 100, respectively.

because of the two approximations (B.12) and (4.11) involved in the derivation of (4.14) (see Appendix B.4 as well). As $\lambda$ falls towards 3, $\alpha_c$ rises to its upper limit 1.55. A further reduction in $\lambda$ results in decrease in $\alpha_c$.

The interpretation for the initial increase of $\alpha_c$ with decrease in $\lambda$ is as follows: A significantly high deleterious mutation rate reduces the fixation probability of nonmutator, since it is a disadvantageous factor. Thus, a nonmutator produced in a weak mutator background that is less spread out, and that created in a strong mutator background which is more spread out can have the same fixation probabilities. The former and latter respectively correspond to larger and smaller values of $\alpha$. Therefore, the critical value $\alpha_c$ of the epistasis parameter rises as the strength of the mutator decreases. However, the decline of $\alpha_c$ with $\lambda$ for $\lambda < 3$ is counterintuitive. The explanation for this interesting trend requires a detailed analysis. A study of the weak mutator case is beyond the scope of this project and will be left for a separate work. The results presented regarding weak mutators is meant to give directions for future work. Solving (4.8) without neglecting $U_d$ will be useful in obtaining analytical expressions in this case.

Table B.5 gives the data from finite $N$ simulations for three values of $\lambda$. Using this, a crude estimate of $\alpha_c$ has been made corresponding to each $\lambda$. The errors associated with $\alpha_c$ are not given, since the error calculation is not straightforward here. Nevertheless, we see a clear variation with respect to $\lambda$, similar to what we see from the exact numerical solution.